Title
STRANGE-PARTICLE PRODUCTION IN n+d INTERACTIONS AT 2.7 TO 4.2 GeV/c

Author
Hoch, Paul Lawrence.

Publication Date
1972-10-01

STRANGE-PARTICLE PRODUCTION IN $\pi^+ d$ INTERACTIONS AT 2.7 TO 4.2 GeV/c

Paul Lawrence Hoch
(Ph. D. Thesis, Part 1)

October 16, 1972

Prepared for the U.S. Atomic Energy Commission under Contract W-7405-ENG-48

DISCLAIMER

STRANGE-PARTICLE PRODUCTION IN π^+d INTERACTIONS AT 2.7 TO 4.2 GeV/c

CONTENTS

Chapter 3 of this thesis, with Appendix D, has been printed as Lawrence Berkeley Laboratory Report LBL-1052; Chapter 4 is LBL-1053. The remaining sections are in this report (LBL-1051). Each of the 3 LBL reports has a separate Table of Contents.

STRANGE-PARTICLE PRODUCTION IN π^+d INTERACTIONS AT 2.7 TO 4.2 GeV/c

CONTENTS (Part 1 - LBL-1051)

STRANGE-PARTICLE PRODUCTION IN π^+d INTERACTIONS AT 2.7 TO 4.2 GeV/c

Paul L. Hoch

Lawrence Berkeley Laboratory
University of California

ABSTRACT

We report on strange-particle production in a π^+d exposure of the 72-inch bubble chamber. The total exposure size was ≈22 events/μb at 2.7 to 4.2 GeV/c. A conventional Bevatron π^+ beam was used; the importance of the proton contamination (10 to 25%) is discussed. The film was scanned for all Λ and K^o topologies; after a thorough measuring and remeasuring process a final sample of 18362 events was obtained.

Each event was assigned to the most likely final-state hypothesis on the basis of the badness function, a modification of the χ^2 with parameters depending on the production constraint class of each fit. These parameters were chosen after examination of the missing mass, decay angles, and similar distributions. The motivation for this method, and the quality of the final separation, are discussed.

A standard fitting program was used, treating an invisible spectator proton as quasi-measured. The usual fiducial cuts and weights were applied. Various properties of the spectator-momentum distributions are discussed. Tallies and approximate cross sections are presented for each final state.

CHAPTER 1. INTRODUCTION

This thesis reports on an exposure of the deuterium-filled 72-inch bubble chamber to a beam of π^+ mesons at incident momenta of 2.7 to 4.2 GeV/c. Events with a visible decay of a K^o or Λ are discussed here.

Production of non-strange particles in this exposure has been studied by our collaborators at Purdue and Illinois.[1] (Theses have been written there by R. J. Miller,[2] John Campbell,[3] and Howard Gordon.[4]) Just after this experiment was performed at the Bevatron in 1966, we ran a companion experiment with lower incident momentum (1.1 to 2.4 GeV/c); essentially the same data processing was used. Reports on strange-particle production[5] (including a thesis by Don Davies[6]) and on non-strange-particle production[7] (including theses by Jerry Danburg,[8] Bob Rader,[9] and Jerry Manning[9A]) have already been compeleted.

This experiment (known as Pi66A) was designed to complement Pi63, a previous LBL exposure of π^-p in the 3 to 4 GeV/c range. To the extent that π^+n interactions can be inferred from π^+d events where there is a "spectator" proton, Pi66 included many reactions which are charge-symmetric to those in Pi63. In many cases the π^+d exposure merely provides additional events for channels that were studied in π^-p; however, certain final states which are unanalysable missing-mass hypotheses in π^-p are constrained fits in π^+d. A specific purpose of this exposure was to study one such case: In his report on Pi63, Dick Hess suggested a search for the $K_sK_s\pi^o$ decay mode of the D and E mesons in π^+d around 2.6 GeV/c;[10] the senior physicists from Pi63 proposed and directed the Pi66 exposure. (Our inconclusive results on D and E production are presented in Appendix A.)

The physics results reported in this thesis comprise two unconnected studies, both of which use data from other experiments in addition to our π^+d exposure. Chapter 3 presents data on $\pi^+n \rightarrow K^oY^{*+}$ and on various other decuplet-baryon production reactions, none of which can proceed by the exchange of a single known meson. A "forbidden" forward peak is observed nonetheless both in our data and in that of other LBL experiments. This chapter also includes an extensive review of proposed explanations for this kind of forbidden peaking.

In Chapter 4 we report an attempt to measure the electromagnetic mass difference between the charged and neutral $K^*(890)$. This analysis is based on the use of data for charge-symmetric π^+n and π^-p reactions.

Our experimental procedures are explained in Chapter 2. One of the main purposes of this thesis is to document our work well enough to make the data accessible to other experimenters. (See Appendix C for details on what is available.) Chapter 2 has been written with this goal in mind. A major section of Chapter 2 concerns the methods we used to assign ambiguous events to appropriate final states. A limited analysis of our data as a whole (e.g., final-state cross sections) is also presented; we note, however, that most of the final states were subjected only to a hasty and unreported survey.

CHAPTER 2. EXPERIMENTAL PROCEDURES AND UNUSUAL PRACTICES

INTRODUCTION

The first part of this chapter describes the procedures involved in obtaining and processing the film and preparing a sample of good events with all successful final-state fits. The remaining sections cover the assignment of each event to a single final state and present some general results.

This chapter has several different purposes. One is to explain what we did to our data for anyone who is primarily interested in the results reported in subsequent chapters. Since the processing described here was not done with those specific studies in mind, and since they are based on data from other experiments also, those readers may wish to turn directly to Chapters 3 and 4; references back to this chapter are provided. Alternatively, the reader may skip to the summary in the last section of this chapter.

A second goal is to provide an exposition of some of our procedures which were non-standard or otherwise interesting; such material might be of use to the reader who is working on a deuterium bubble chamber experiment himself. (We have also included references to some techniques which we considered but did not use.) Since we include less discussion of procedures that are documented elsewhere, the balance of this chapter does not really reflect the relative importance of the various steps in the data handling. (Special emphasis is placed on the choice of final-state hypotheses, Section 2.8.)

A third purpose is to provide a reference work for anyone who happens to be using our data in the future. [Details that would interest only such a reader are generally enclosed in brackets, like this.]

2.1 BEAM PROPERTIES

This exposure utilized a single-stage separated beam at the Bevatron. A schematic diagram[11] and detailed descriptions[12] of this beam have been presented elsewhere.

The major problem encountered during the experimental run (which took place in March through August of 1966) was maintaining the vertical separation of pions from protons. We were limited by the maximum field that could be applied to the electrostatic separators, and by the total distance between the Bevatron wall

and the building housing the deuterium-filled 72-inch bubble chamber. A path-tracking program was used to decide on the optimum configuration and settings of the quadrupoles and bending magnets. (The resulting proton contamination is discussed in Section 2.3.)

Counters were used to suppress the triggering of the cameras unless the appropriate number of tracks (roughly 5 to 15) had entered the chamber. With this many tracks diverging from an imperfect focus, there will be overlapping of beam tracks both with secondary tracks and with each other. This leads to problems in measurement, especially on semi-automatic devices such as the Spiral Reader. Therefore a "stepper" magnet was used to shift the beam laterally each time a beam particle entered the chamber, thus producing well separated and roughly parallel beam tracks. This device consisted of a series of 16 small magnets which were triggered sequentially by counters monitoring the beam.

We treat the known central value of the beam momentum distribution as a second measurement of the beam-track momentum, with an error corresponding to the width of the distribution. Since the beam momentum is greater than that of each final-state track, and hence generally less well measured, this procedure is quite useful. This "beam averaging" is especially valuable when the measured part of the beam track is short, as was the case with the events we measured on the Spiral Reader. (If the two measurements differed by more than 3 standard deviations, the event was rejected.)

The average beam momenta used for most of the processing were taken from the distribution of measured momenta. These values were checked against the fitted beam-track momentum distribution from events with a fit with 4 production constraints. [In the companion low-momentum $\pi^+ d$ exposure, Pi66B, it was found that errors in the original beam-average momenta found in this manner produced effects large enough to justify refitting all the events with improved values.[13] In this experiment, only the events at the highest momentum, 4.2 GeV/c, were reprocessed.] The final beam momenta [at the center of the chamber, as put into the fitting program] and the widths used in the beam averaging are given in Table 2.1 for each of the 4 nominal momentum settings. [The rolls of film at 3.1 and 4.2 GeV/c were divided into two subintervals. These values are consistent with those found independently by our collaborators at Purdue[14,15] (2.7 and 3.7 GeV/c) and at Illinois[16] (4.2 GeV/c).]

The effective c.m. energy spectrum produced by these beam momenta and the Fermi motion within the deuterons is discussed in Section 2.10.

$P_{nominal}$ (GeV/c)	P_{beam} (MeV/c)	dP_{beam} (MeV/c)
2.7	2700	35
3.1	3068	60
	3070	60
3.7	3717	60
4.2	4190	70
	4232	60

Beam Momenta

Table 2.1

2.2 EXPOSURE SIZE

We took about 100,000 frames at each of the four momentum settings (2.7, 3.1, 3.7, and 4.2 GeV/c). The path length (exposure size) at each beam momentum has been estimated directly, following the procedure set forth in an unpublished memo by Janos Kirz.[17] The results are given in Table 2.2; the details follow here.

In a special scan of every fifth frame of several rolls of film at each momentum, we counted the number of incoming tracks, the number leaving the side of the chamber without interacting, and the number of interacting tracks. To allow a determination of the total cross section and that for evident strange-particle decays (vees), in every 25th frame we recorded the interactions of each topology (and, as a check, the number of noninteracting tracks leaving the chamber).

The observed value for N_i, the number of interacting tracks, is corrected to account for a loss of (10 ± 10)% of the events with 1 or 2 prongs (charged tracks). (Half of this correction is for an observed depletion in the forward direction, and half for the low scan efficiency for these topologies at all scattering angles. For details of this estimate, see Ref. 17.)

N_s, the number of tracks leaving the side, is counted directly. N_e, the number exiting, is then $N_{in}-N_s-N_i^{corr}$. The path length in the scanned frames is simply

$$L = N_e s_e + N_s s_s + N_i^{corr} s_i ,$$

where s is the average length of each kind of track.

The fiducial volume for scanning spans 150 cm of the length of the chamber.[18] We take s_e to be 150 cm, corrected at each momentum for the fact that the tracks enter the chamber at a slight angle. (The correction for curvature is negligible at these momenta.) Some uncertainty about what to use for s_e is introduced by the possible variation of the effective scanning fiducial volume with topology or between the general scan and this special scan. We estimate an error in s_e of ±2.0 cm, which is comparable to the statistical error in N_e.

In the low-momentum exposure (Pi66B), s_s was measured and found to be typically 130 cm, varying with momentum from 106 cm to 140 cm, with an error of 5%.[19] Since there are few leaving tracks at the momenta of this experiment, a

P_{beam} (GeV/c)	2.7	3.1	3.7	4.2
s_e (cm)	150.1 ± 2.0	152.1 ± 2.0	150.4 ± 2.0	150.5 ± 2.0
*$N_{Incoming}$	16899	17662	13571	15735
*N_s (leaving sides)	1910	67	65	111
*$N_{Interacting}$ (Corr.)	4832 ± 246	5292 ± 258	3870 ± 200	4405 ± 221
From data for every 25th frame:				
$N_{1-2\ prongs}$	515	549	401	419
$N_{Other\ Interactions}$	381	447	362	399
$N_{Incoming}$	3334	3528	2832	3088
*L in scan (10^6 cm)	2.11 ± 0.05	2.26 ± 0.04	1.73 ± 0.03	2.01 ± 0.04
# Rolls (this scan)[a]	10	10	9	10
# Rolls, Total	124	157	129	152
L (Total) (10^6 cm)	131.1 ± 3.3	177.3 ± 3.3	124.1 ± 2.4	153.1 ± 2.9
L (Total) (ev/μb)	4.99 ± 0.14	6.76 ± 0.15	4.73 ± 0.11	5.83 ± 0.13

*: These quantities are for every 5th frame. (See text.)

(a): The average number of frames per roll is 730.

Results of Special Scan for Path Length

Table 2.2

precise measurement of s_s is not needed. We have used s_s = 130 cm ± 15%.

Obviously, $s_i \approx s_e/2$, since only a small fraction of the beam interacts within the chamber. More precisely,

$$s_i = s_e\{(s_o/s_e) + 1/[1 - \exp(s_e/s_o)]\}$$

where s_o is the interaction length.[20] Since the total cross section for $\pi^+ d$ at these momenta is about 60 mb, s_o = 16 ft and we get $s_i = (0.47 \pm 0.01)s_e$.

At this point we emphasize that many factors must be taken into account before the path length values of Table 2.2 can be used to determine cross sections. This path length is for the entire beam, not just the pionic component. The "events/μb" figure refers to events produced with the primary vertex within the scanning volume. The number of events in any final state must be corrected for scanning inefficiency, fitting failures, non-visible decay modes of the Λ and K^o, cuts on beam direction and momentum tighter than those in the scan, and fiducial cutoffs on the location of secondary vertices. To get πN (rather than πd) cross-sections, proper note must be taken of various nontrivial features of the spectator model. We note that the reported path length at each momentum setting covers a substantial range in effective c.m. energies. (Material relevant to these corrections is discussed in subsequent sections; rough cross sections are given in Section 2.9.)

[Our path-length results can be reconciled with independent determinations by Campbell and Gordon. Campbell has reported a cross-section scale factor of (0.235 μb/event ±4%) at 2.7 GeV/c, and (0.431 μb/event ±2%) at 3.7 GeV/c.[21] These results agree with mine within a couple of percent, if we take note of the fact that he used a smaller fiducial length (about 133 rather than 150 cm, before correction and attenuation) and that he observed beam tracks at a rate about 5% less than mine. (This may well result from a tighter cut on beam track momentum during the scan.)]

[At 4.2 GeV/c, Gordon has reported L = (3.52 ± 0.10) ev/μb.[22] However, this number is for the π^+ fraction of the beam (which he determined to be 71%) and for a smaller fiducial length (133 cm rather than 150 cm).[23] Thus, it corresponds to 5.59 ev/μb total path length in my fiducial volume. The discrepancy with my result (5.83 ± 0.13 ev/μb) is primarily due to the fact that Gordon counted about 8% fewer beam tracks per frame.]

Finally, we note that the errors in Table 2.2 reflect only the indicated uncertainties in the values of s, and the statistical errors in the N's. [The fluctuations in the number of beam tracks per frame, and in the number of good

frames per roll, were not examined, but the use of every fifth frame of several rolls in the special scan should have eliminated the effects of such fluctuations.] No better error estimate is needed.

Observed Total Cross Section

We can easily calculate the total cross section observed in the special scan just described, by scaling the corrected number of interactions up to the entire film sample and dividing by the path length. The result is given in Table 2.3, along with the known total π^+d cross sections.[24]

The small differences here can easily be accounted for by proton and muon contamination in the beam, as shown in Table 2.4. There we have given the known total pd cross section;[25] of course the muons do not interact strongly with the deuterons. We have indicated the cross-section discrepancy and the minimum contamination which will explain it. (For example, if the muon fraction α_μ is 0, the proton fraction α_p is given by $\alpha_p = [\sigma(\text{obs})-\sigma(\pi^+d)]/[\sigma(pd)-\sigma(\pi^+d)]$.) Since the π^+d cross section is intermediate between the μ^+d and pd ones, the differences can also be explained by the presence of both contaminants rather than just one. Thus, even if the errors in our observed cross sections were much smaller, those measurements would not give us any real handle on the contamination. We do note, however, that the minimum required contamination is indeed less than the independent estimates in the next section.

2.3 BEAM CONTAMINATION

The presence of protons and muons in the beam must be considered for two reasons:

(1) Given a pure and complete sample of a certain pion-induced final state, to convert from the number of events to the cross section one must know the path length of the pion part of the beam.

(2) Proton-induced events may go preferentially into certain final states and/or kinematic regions.

Since we cannot expect to get a pure and complete sample of most final states, the error in pion pathlength would not be expected to dominate calculated cross sections. To avoid the second class of problems would require a detailed understanding of the consequences of fitting proton-induced events only to pion hypotheses. We do not even understand the cross-contamination of pion-induced

$P_{nominal}$ (GeV/c)	Total Cross Sections (mb) Observed	π^+d (Ref. 24)
2.7	59.2 ± 3.2	61.5 ± 0.2
3.1	61.4 ± 3.1	59.2 ± 0.2
3.7	61.2 ± 3.2	56.5 ± 0.2
4.2	56.3 ± 2.9	55.1 ± 0.2

Total Cross Sections

Table 2.3

$P_{nominal}$ (GeV/c)	σ(pd) (mb)	σ(obs)−$\sigma(\pi^+d)$ (mb)	Minimum Contamination (muon and proton percent)
2.7	83.94 ± 0.05	−2.3 ± 3.2	α_p=0, α_μ=(4 ± 5)%
3.1	83.30 ± 0.05	+2.2 ± 3.1	α_μ=0, α_p=(9 ± 13)%
3.7	81.42 ± 0.05	+4.7 ± 3.2	α_μ=0, α_p=(19 ± 13)%
4.2	80.52 ± 0.05	+1.2 ± 2.9	α_μ=0, α_p=(5 ± 11)%

Minimum Contamination from Cross Sections

Table 2.4

events very well (as is discussed in Section 2.8). Thus, a rough estimate of the proton fraction in the beam will be adequate for our purposes.

Figure 2.1 consists of typical plots showing the π^+–p separation at the four momentum settings of our beam. On the y–axis the counting rate recorded close to the bubble–chamber entrance is plotted logarithmically; on the x–axis we plot the setting for the current in the spectrometer S_2 which was used for steering the beam. (The units are of no significance.) The peak on the left corresponds to pions, and that on the right to protons. A very high estimate for the fraction of protons around the pion peak is the ratio of the valley between the peaks to the height of the pion peak, denoted by "V/P"; a low estimate is obtained by extending the proton peak downwards, as indicated by the dotted lines, and comparing with the peak height; this ratio is denoted by "B/P". The points denoted by "x" were taken with the target (where the π^+ beam is produced) moved out of the way and provide a lower limit for the background under the peak; the "target out" counts are probably protons (scattered from the primary beam or produced by the high neutron flux from the Bevatron). Note that the proton peak is a few times as high as the pion peak at the low momenta, and an order of magnitude larger at the upper settings. Since the currents in the spectrometer and the other steering elements were not controlled precisely enough to keep us on the pion peak, the separation was a rather delicate problem.

As confirmation that the ratios V/P and B/P probably bracket the actual beam contamination, we may examine similar curves from a thesis by David Brown on a π^+p experiment at the Bevatron which used components of our beam in a quite similar arrangement.[26] For his separation curve at 4 GeV/c, V/P and B/P are ≈45% and ≈20% respectively. Brown also had Čerenkov counters in the beam, from which he determined the proton fraction to be ≈30%.

We take a value between these two ratios as our estimate of the proton fraction: that is, (10 ± 5)% at 3 GeV/c (the two lower beam settings) and (25 ± 10)% at 4 GeV/c.

It should be noted that curves like Fig. 2.1 were taken during the experiment to determine the proper current setting for the spectrometer and to compensate for drift. We certainly were not running under optimum conditions – that is, at the pion peak – at all times. In addition, we made occasional modifications in the collimator which cut out the protons, and elsewhere in the beam, which may have affected the scattering of protons into the chamber. Thus,

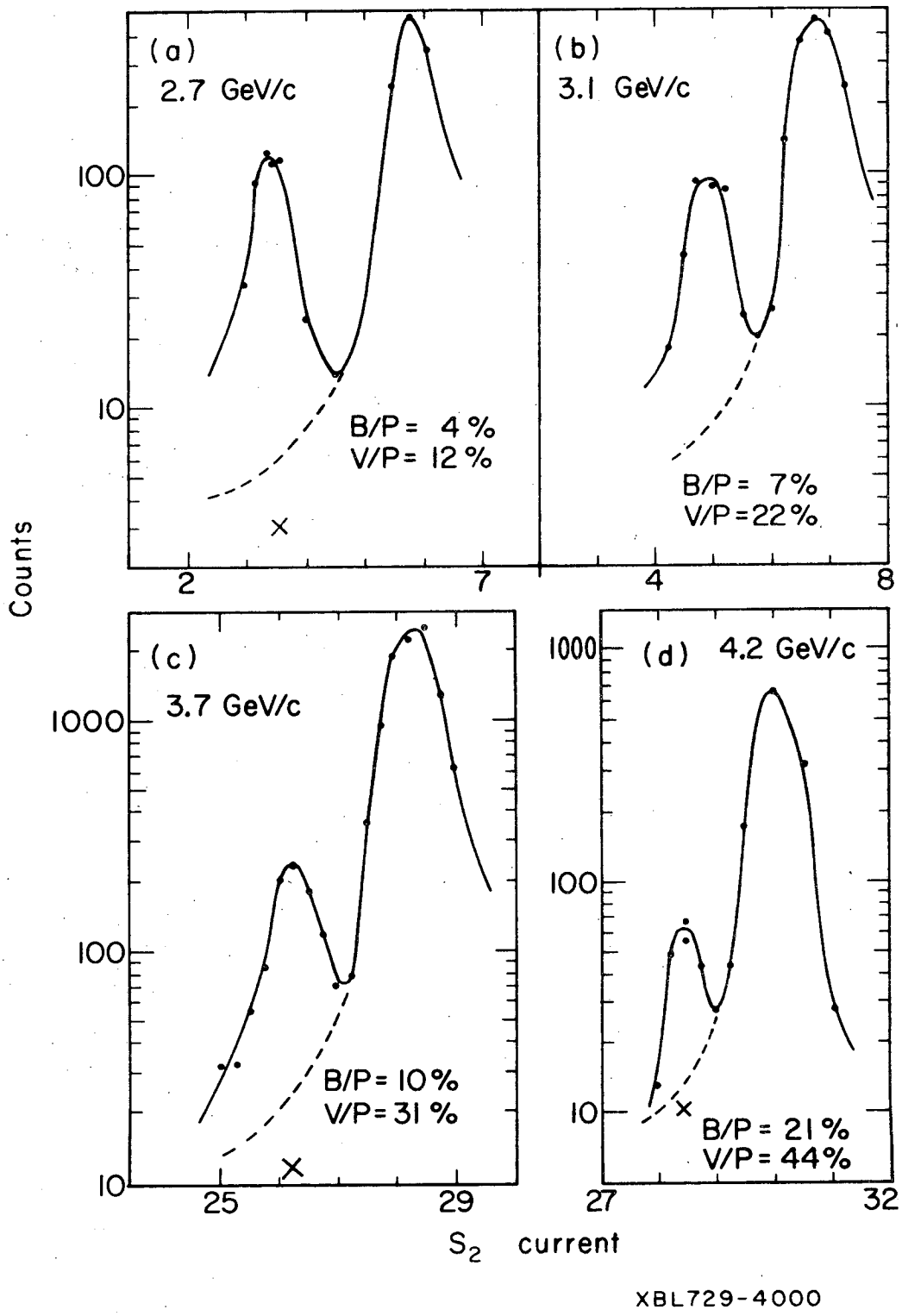
(a)
2.7 GeV/c
B/P= 4%
V/P= 12%
(b)
3.1 GeV/c
B/P= 7%
V/P=22%
(c)
3.7 GeV/c
B/P= 10%
V/P=31%
(d) 4.2 GeV/c
B/P= 21%
V/P= 44%
Counts
S_2 current
XBL729-4000

Fig. 2.1

the above-quoted proton fraction is a rather crude estimate.

[Our collaborators at Illinois made an independent determination of the contamination by counting δ-rays. Noting that protons at 4.2 GeV/c produce only δ-rays with momentum less than 20 MeV/c, Gordon compared the distribution of higher-momentum δ-rays with the expected one. This led him to an estimate of (14 ± 3)% proton contamination.[27]]

[Lichtman, who studied the 2.7 GeV/c film at Purdue, has suggested an evaluation of the proton fraction based on reflections of the reaction $pn \rightarrow p\Delta^0$, the cross-section for which can be estimated. A reflected peak in the missing mass spectrum for events which fit $\pi^+ d \rightarrow (p)p[M.M.]$ was predicted.[28] We are not aware of any result from this method having been reported; it is mentioned here since it might be applicable in other experiments.]

We have made no study of our own on the muon contamination. We can extract an estimate from the following observations:

In his study of δ-rays, Gordon determined the muon contamination from the number of high-momentum δ-rays on beam tracks which subsequently interacted.[27] He quoted (15 ± 7)% muons; however, if we make a 5% correction for small-angle 1- and 2-prongs (which were presumably missed on Gordon's scan as they were on ours), we get (11 ± 7)%. (The pion fraction - the rest of the beam - then comes out as (75 ± 6)%, rather than the (71 ± 6)% given by Gordon. The errors quoted here are purely statistical.)

Brown estimated the muon contamination in his Bevatron experiment from a δ-ray count.[29] Using an assumed $1/P_{lab}$ dependence, he got a muon fraction ranging from (5.7 ± 2.6)% at 2.95 GeV/c to (4.1 ± 1.9)% at 4.08 GeV/c.

In the low-momentum part of our exposure, Danburg used the reduction of the observed cross section (and the absence of significant proton contamination) to estimate a muon contamination of 5% to 10%.[30] Davies estimated about 3% in the same exposure.[31]

The muons come from pions decaying along the beam line. Since the decay muons are more divergent than the parent pion beam, the muon fraction at the bubble chamber is sensitive to the beam geometry. The worst case would be expected to occur if all the muons are kept within the beam; that is, all the pions that decay are in effect replaced by muons. For our 56-meter beam line, at 4.2 GeV/c only 79% of the pions survive, giving a μ^+/π^+ ratio of 0.27. From Gordon's result, this ratio is 0.21 ± 0.10, which seems quite close to this limit; after the correction indicated above, it is 0.15 ± 0.09.

Taking all of the above facts into account, we average the "corrected" Gordon result with that of Brown and settle on a muon fraction $\alpha_\mu = (8 \pm 4)\%$.

We can now use these estimates of the contamination to predict the total cross section that should be observed. We use the known π^+d and pd cross sections as given in previous tables to get the results in Table 2.5. The observed total cross sections agree with those expected on the basis of the indicated contamination.

The path length for the pion component of the beam will be presented below (Table 2.7), after corrections have been made for scanning and measuring losses.

Any attempt to study the effect of proton contamination is complicated by the large number of final states involved. For example, for the two-prong one-vee events (about half the data), there are 18 "marks" (final-state hypotheses) with a pion beam and 14 marks with a proton beam. As a first approximation, we would expect hypotheses with 4 constraints at the production vertex to be relatively uncontaminated by proton events, as they are by pion events (see Section 2.8); also, 1-production-constraint and missing-mass final states might be as badly contaminated by the proton events as they are by other pion events.

We carried out an extensive program of remeasurements, which left only about 3% (598 out of 19072) of the apparently good events without a good (confidence level above 0.5%) fit. Evidently, most of the proton-induced events did end up with a successful pion-induced fit. We did prepare a version of the fitting program SIOUX for a proton beam, and used it on two samples of events at 4.2 GeV/c: those with no successful fits, and those with a 4-production-constraint fit. Some of the former fit to proton hypotheses, but there was no indication that even these events were primarily from a proton beam. Enough of the latter class of events fit some pd hypothesis to prevent us from concluding that all the highly-constrained final states should be free from the effects of proton contamination.

Although pn cross sections are not well known, the size of strange-particle production in pp interactions is a substantial fraction of that in π^+p. (The threshold is 2.3 GeV/c for pp, as compared to 0.9 GeV/c in π^+p, and around 8 GeV/c the strange-particle cross section is 1.8 mb for pp and 3.1 mb for π^+p.[32]) Thus, some contamination is to be expected. Under the circumstances, no further study was deemed appropriate.

The misassigned proton-induced events might fall preferentially into certain

P_{nom} (GeV/c)	Contamination		α_π	σ(expected) (mb)	σ(observed) (mb)	$\Delta\sigma$ (mb)
	α_μ	α_p	$(1-\alpha_\mu-\alpha_p)$	$\alpha_\pi\sigma_{\pi d}+\alpha_p\sigma_{pd}$	(Table 2.3)	$=(\sigma_{obs}-\sigma_{exp})$
2.7	(8 ± 4)%	(10 ± 5)%	(82 ± 6)%	58.8 ± 4.2	59.2 ± 3.2	0.4 ± 5.3
3.1	(8 ± 4)%	(10 ± 5)%	(82 ± 6)%	56.9 ± 4.1	61.4 ± 3.1	4.5 ± 5.1
3.7	(8 ± 4)%	(25 ± 10)%	(67 ± 11)%	58.2 ± 5.3	61.2 ± 3.2	3.0 ± 6.2
4.2	(8 ± 4)%	(25 ± 10)%	(67 ± 11)%	57.0 ± 5.3	56.3 ± 2.9	-0.7 ± 6.0

Contamination

Table 2.5

kinematic regions. This may, for example, be the result of strong resonance production, and may be a serious problem when subtle effects are being studied. Our Purdue collaborators found that a proton component of merely 3% in our film at 2.7 GeV/c would produce enough events of the reaction $pd \rightarrow (p)p\Delta^0$ to yield a bump in the missing-mass spectrum of $\pi^+ d \rightarrow (p)p(\text{neutrals})$ that might be taken to be evidence for the ϵ^0.[33]

We also note that preferential misassignment might result from purely kinematic considerations – that is, from the fact the the difference between two track-assignment hypotheses depends on the momenta involved. (For an example discussed in detail, see Ref. 8, page 11.) Such considerations are of course also relevant to misassignment within the pion-induced sample, but things should be even worse if the beam track may have two interpretations (since it has relatively high momentum and thus little difference in energy for the two hypotheses).

Generally speaking, misassignment tends to smear out a peak, so narrow resonance production in the $\pi^+ d$ reactions should be less contaminated than the phase-space background.

2.4 SCANNING

The film was scanned for events with at least one vee. (A vee is the characteristic two-track pattern formed by the visible (i.e., charged-mode) decay of a neutral strange particle.) The vee was required to point back to the primary vertex, and that vertex had to be within a specified fiducial volume. "Kinks" (possible decays of a charged strange particle, manifested by a momentum change in a charged track) were used in determining the event type; however, strange-particle topologies with a kink but no vee were not recorded. The topologies (event types) which were studied are shown in Fig. 2.2, along with the number of events in each topology in the final fitted sample. Both odd-prong events (those with a slow and therefore invisible spectator proton) and even-prongs were accepted; the dotted tracks in Fig. 2.2 are those which are missing in the odd-prongs. The units digit of the event type is the number of prongs (visible outgoing charged particles at the production vertex).

A flag was added to the topological event type [as a hundreds digit] to indicate the number of apparent stopping protons (i.e., dark positive tracks) but this information was not used in the fitting procedure. Additional strange-particle topologies and other rare events, such as Ξ candidates and

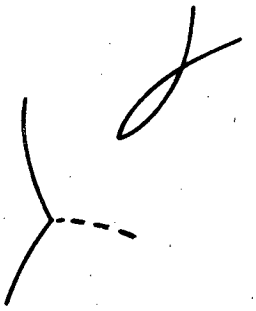

E.T. 31 (3502)
E.T. 32 (8519)

E.T. 41 (556)
E.T. 42 (1012)

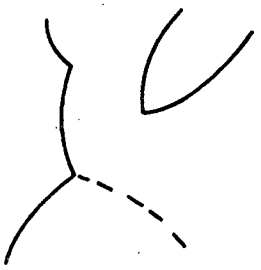

E.T. 61 (216)
E.T. 62 (889)

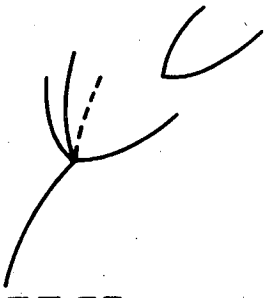

E.T. 33 (1366)
E.T. 34 (1699)

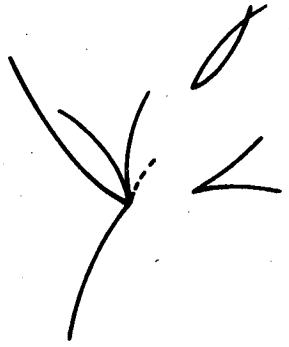

E.T. 43 (47)
E.T. 44 (75)

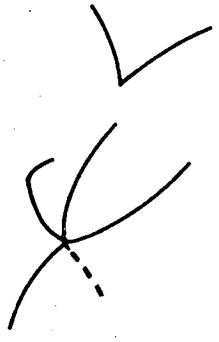

E.T. 63 (148)
E.T. 64 (187)

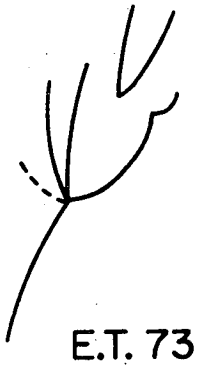

E.T. 73 (69)
E.T. 74 (77)

Event types

(With number of events)

(XBL729-4001)

Fig. 2.2

obvious leptonic decays, were recorded as "zoons" but not processed further. (For more details of the scanning method, see Ref. 18.)

Every second roll was rescanned, and the differences were resolved in a conflict scan. On the basis of events found in either case, it was determined that on each scan about 6% of the events are missed, 5% are assigned to the wrong event type, and the remaining 89% are correctly assigned.

These numbers do not reflect the full complexity of the situation, since the probability of missing or misassigning an event depends on the topology. For example, events with no vee but only a small-angle kink would certainly be missed more often than two-vee four-prong events. Since we required a vee, however, it is expected that not many of the desired events were completely missed. [For an example of a full treatment, taking into account the probability of missing or misassigning an event on each scan, see the report on the LBL π^-p experiment (Pi63).[34]]

Assignment of events to the wrong event type presumably was not a serious problem. The events were remeasured so thoroughly that essentially all of them were eventually assigned to a satisfactory event type. Some misassignments may have no effect on the physics of the fitted hypothesis – e.g., the omission of one of two vees, or not correctly noting the presence of a stopping proton. [The latter error was not included in the 5% misassignment rate.] Other errors would be expected to degrade the quality of the fit only slightly – e.g., a small-angle charged decay which is not noticed when measured (like an ignored small-angle scatter), or a missed very short spectator proton.

Thus, we have chosen simply to assign an inefficiency of 6% to each scan. Neglecting the fact that some events are inherently less visible than others, and assuming that the two scans were independent, we get an inefficiency of $(0.06)^2$, or less than 1/2%, for the half of the film that was double-scanned. This leads to an average scan efficiency for the entire experiment of (97 ± 3)%. (This error is just an estimate.)

In addition to making this 3% correction, we should bear in mind the possibility of scanning biases, especially those associated with certain kinematic regions. (Danburg, for example, considered the possibility of such a bias producing a spurious forward dip in his production angular distributions.[35] Davies studied the loss of vees with one slow decay product, and weighted his events to compensate.[36])

In further justification of this simple treatment of scanning inefficiency

and similar problems, we note that the determination of absolute cross sections is not of special interest in this experiment; the determinations in Section 2.9 are made quite imprecise by beam contamination and the misassignment of events. [Many of the reactions accessible to us have been studied by Hardy and Hess in the companion π^-p experiment (Pi63), where contamination was not a problem. At 5.1 GeV/c, Mettel has recently reported cross sections for many strange particle reactions in a π^+d exposure with a beam having only about 0.1% proton contamination.[37]]

Each of our scans will pick up a number of events which do not belong in the sample: many with apparent vees that are not strange-particle decays at all, and others with vees that do not point back to the primary vertex (because the neutral decayed in a three-body mode or was scattered.) Many such events were deleted upon examination; it is not known how many got through the fitting program. True "garbage" events would not be expected to produce distortions, especially not narrow ones, in mass spectra or angular distributions. (The similar but somewhat more touchy problem of proton-induced events was mentioned in the previous section.) Of the 23,225 events recorded on either scan, 3933 were deleted from the Master List, mostly because the vees were bad. (Other reasons for deleting events included a previous interaction along the same beam track, and location outside the fiducial volume.)

Events which had no good production fit were looked at before being measured for a second time. A special fitting program was used to study the suspicious vees. A fit was made to the vee alone; if it was found to be a Λ or K^o which did not point back to the production vertex, or if it was an e^+e^- pair, the event was deleted.

2.5 THE MEASURING AND REMEASURING PROCESS

All events found were measured on the Franckenstein measuring projector. About 3/4 of them [essentially all events found on the first scan, except those with charged decays] were also measured on the considerably faster Spiral Reader.

The Spiral Reader automatically records information on track ionization density which (as described in Section 2.8) is useful in resolving ambiguities between competing hypotheses. Therefore, only the Spiral Reader measurement was used if it gave a passing fit in the geometric reconstruction and kinematic

fitting program, SIOUX. A study of some events from this experiment which were measured on both machines showed that the results agree quite adequately.[38]

Events with no good fit after this first pass were remeasured on the Franckenstein. Events which still failed were examined by expert scanners and, if necessary, remeasured. Except for about 10% of the film [some rolls at 4.2 GeV/c], the sample was quite thoroughly processed. (541 of the 19292 non-deleted events were measured 4, 5, or 6 times.)

Table 2.6 is a tally of the final status of our events. [A technical note for the reader using our SIOUX output tapes: we have not presented a simple tally of "result class", the five-digit number assigned by the fitting program. This is because events in most failing classes were examined and, typically, put into another class; those that remain on the Master List mainly reflect the fact that after delays or repeated difficulty some events were not pushed through any further. Also, the two physically meaningful categories which contain most of the failing events ("bad beam track" and "unmeasurable") do not correspond to single result classes.]

The deleted events are those that in a sense should not have been recorded in the scan - they are not in the fiducial volume, they have apparent vees that are really neutron scatters or other artifacts, etc. (Of course, the inclusion of some events in the latter category can not be considered scanner errors.) Of the total events found in any scan, 17% were deleted.

The "bad beam track" events in the table differ from the beam-average value for the momentum by more than 3 standard deviations. This is a tighter cut than that imposed during the scanning, where only "obvious" non-beam incident tracks were excluded.

Events in the next two categories were dropped from the sample but, unlike other failures, were not processed much more. "Too many good fits" [result class 10003] is a problem which occurs when the SIOUX output buffer is not big enough to contain all the fit results. "Low confidence level only" [result classes 20018-9] means that the best fit had a confidence level less than 0.5%. SIOUX passed all fits with a confidence level above 10^{-5}. However, in bubble chamber experiments one often finds an excess of events at low confidence levels and discards them. To reduce the number of events thus lost without careful examination, we modified SIOUX to give a special result class to fits where either the vee barely passes and the production-vertex fits fail [result class 20018] or the overall fit barely passes [result class 20019]. [This was added after most of

Deleted	3933			
Active	19292			
	23225 events scanned			
				Fraction of active events
Bad beam track		220		1.1 %
Too many good fits		61		0.3 %
Low confidence level only		67		0.3 %
Called unmeasurable:				
Low confidence level fit	121			(0.6 %)
Good track reconstruction only	214			(1.1 %)
Other	119			(0.6 %)
	---→	454	Total	2.4 %
Pathological failures		77		0.4 %
	Total	879	failures	4.6 %
Good events:				
Ambiguity scanned		5461		28.3 %
Not examined		12952		67.1 %
	Total*	18413	good	95.4 %

[* 51 of these events were lost before the final tape was made.]

Tally of Final Status

Table 2.6

the fitting had been done, so we also fixed the result class of previously fitted events with confidence levels between 10^{-5} and 0.5%.] These events were then remeasured, but only once.

Events were called unmeasurable for various reasons; the term is something of a misnomer. An event was put in this category whenever it was decided that no further measurement was called for. The unmeasurable events include, for example, those with apparently successful vee fits that yield no production fit, and a few with successful fits all of which are inconsistent with the observed bubble densities. Of the events which had only a barely passing fit, 121 were called unmeasurable. The 214 events in the next unmeasurable category passed the spatial reconstruction part of the program [TVGP], but had no fits. The remaining 119 events include those which were unmeasurable in the conventional sense – a track or a vertex was obscured, a track had an evident scatter too close to the vertex to be measured, etc.

The pathological failures include 41 events which passed the spatial reconstruction only, 21 with the last requested measurement unrecorded, and a few other oddities.

We note that only ≈30% of the final good sample was examined on the scan table for removal of ambiguities. (This process is discussed in Section 2.8.) We did look at a few events which were not ambiguous and resolvable, and persuaded ourselves that it would be unnecessary as well as uneconomical to look at more events, although certainly some additional information could be obtained.

The indicated "good" events are those remaining before the fiducial cuts which are described in Section 2.7. (A few events were lost in the preparation of the final tape with the physics results for each event; that tape contains 18362 events. This additional 0.3% loss was inadvertently not corrected for.)

Corrected Path Length Values

The overall passing rate for non-deleted events is 95.4%. To a first approximation, for cross-section calculations we may assume that the failing events are real events which should be divided up among the available final states in the same proportions as the passing events. [This assumption is certainly false to some extent.] Thus, we decrease the path length (i.e., increase the "μb per observed event" factor) by 4.6% to compensate for the loss.

Table 2.7 presents the path length L^{obs} (from Table 2.2), modified to account for the scanning and measuring/fitting efficiencies ϵ_s and ϵ_m, and for the contamination of the beam. The pionic path length L_π is properly applied only

P_{nom} (GeV/c)	L_{obs} (ev/μb)	ϵ_{scan}	ϵ_{meas}	$L_{cor} = L_{obs}/\epsilon_s\epsilon_m$ (ev/μb)	$L_{p\pi} = L_{cor}(\alpha_\pi+\alpha_p)$ (ev/μb)	$L_\pi = L_{cor}\alpha_\pi$ (ev/μb)
2.7	4.99 ± 0.14	(97 ± 3)%	95.4%	5.39 ± 0.23	4.95 ± 0.32	4.42 ± 0.37
3.1	6.76 ± 0.15	"	"	7.30 ± 0.28	6.72 ± 0.39	5.99 ± 0.49
3.7	4.73 ± 0.11	"	"	5.11 ± 0.20	4.70 ± 0.28	3.42 ± 0.58
4.2	5.83 ± 0.13	"	"	6.30 ± 0.24	5.80 ± 0.34	4.22 ± 0.71
Totals:						
P≈3	11.75 ± 0.21			12.69 ± 0.36	11.67 ± 0.50	10.41 ± 0.61
P≈4	10.56 ± 0.17			11.41 ± 0.31	10.50 ± 0.44	7.64 ± 0.92
All P	22.31 ± 0.27			24.10 ± 0.48	22.17 ± 0.67	18.05 ± 1.10

Effective π^+ Path Length

Table 2.7

to final state samples with contamination from the proton beam absent or removed. One may alternatively assume that the proton-induced events pass and are divided up like the real ones, and use the path length $L_{p\pi}$, where only the (8 ± 4)% muon contamination has been removed. We give both values in Table 2.7 since one cannot say which is better for a given final state without examining its contamination in detail. In our rough cross section calculations (Section 2.9), we simply use the pionic path length.

2.6 DETAILS OF THE FITTING

For the geometric reconstruction of tracks in space from the measured points, and for the kinematic fitting to various final-state hypotheses, we used the standard Group A program SIOUX.[39,40] Here we mention only a few points peculiar to this experiment.

We tried essentially all possible constrained and missing mass π^+d hypotheses for all events. A list of all the final states tried, together with the number of events assigned to each, is presented below (Table 2.8).

SIOUX first attempted to fit each vee alone, to the decays $\Lambda \rightarrow p\pi^-$ and $K^o \rightarrow \pi^+\pi^-$. A hypothesis for the entire final state was attempted only if the corresponding vee test fit was successful; this allowed a considerable saving of computer time.

Decaying charged particles were tried as $\Sigma^\pm$ and $K^\pm$, but no attempt was made to fit the $K^\pm$ decay. (Reasons for this omission included the large fraction (about 15%) of 3-body decays, and the relative ease with which a short scattered $\pi^\pm$ can fake a decaying $K^\pm$.) Since $\Sigma^\pm$ and $K^\pm$ have respectively short and long mean decay distances, nondecaying tracks were not tried as Σ's, and the final-state samples from events with kinks are biased against fast $K^\pm$.

Final states with an unbroken deuteron were not fitted. We did examine some events for such hypotheses, both by using a special version of SIOUX and by examining some odd-pronged events for clustering in m(pn) at the deuteron mass. We found only a handful of candidates and no events with a definite final-state deuteron.

The fitting program requires a "scale factor" for the table used to convert particle momentum to residual range. This factor, and the index of refraction of the deuterium in the chamber, were determined from a measurement of the muon length in the $\pi^+ \rightarrow \mu^+ \rightarrow e^+$ decay chain.[41] Our result for the length, 1.01 ± 0.01

cm, agrees with the value of 1.00 ± 0.01 cm found independently by Gordon.[42]

The beam-averaging technique used to improve the measurement of the beam-track momentum has already been described (Sections 2.1 and 2.5).

The previous section explains the use of two different cutoffs [0.5% and 10^{-5}] on the kinematic confidence level. On Spiral-Reader measured events, a hypothesis was rejected if the confidence level for the bubble densities was less than 10^{-5}.[43]

The shape of the magnetic field in the chamber was taken from direct measurements. The magnitude was determined by trying to make the observed Λ and K^0 masses (as calculated from fits to the vees) agree with the accepted values.[44]

The treatment of the spectator nucleon by the fitting program is discussed in Section 2.10.

2.7 FIDUCIAL CUTS AND WEIGHTS

The output tapes from the fitting program were passed through CREE, a version of the program ARROW.[45] CREE was used to select the best fit and to put the information into a form convenient for our data-display programs.

Each event was assigned a weight and a fiducial code in CREE. As noted earlier, for an event to be accepted in the scan, only the production vertex was required to be in a fiducial volume. Here both the primary vertex and the vees were so constrained. Also, since vees and kinks very close to the production vertex tend to be missed or mishandled, a minimum separation (6 mm) was imposed. Each surviving event is weighted to compensate for similar events which were lost because of these cutoffs.

For example, the probability that a visible vee decay does not occur either before the 6 mm cutoff or beyond the boundary of the fiducial volume is

$$P = \exp(-\tau_c/\tau_o) - \exp(\tau_f/\tau_o),$$

where τ_c and τ_f are the proper times required for a particle of the given momentum to reach the cutoff and the fiducial wall respectively, and τ_o is the mean life. The appropriate weight for a non-cut event is then $W = 1/P$.

Events with a charged decay were given a similar weight for the kink, but with the close cutoff factor only. The mean $\Sigma^{\pm}$ decay distance is small ($c\tau_o$ = 2.4 cm for Σ^+ and 4.5 cm for Σ^-), so a fiducial cutoff is of no significance. [For the K^0, $c\tau_o$ is small too, so our application of a fiducial cutoff at large distances in

the latter case was not necessary.]

Events where a Λ or a K^0 decays outside the chamber will remain in our sample if there is a second Λ or K^0 producing a vee. Thus, final states with an unseen Λ or K^0 were given a weight to compensate for such events.[46]

Basic to the weighting technique is the requirement that the cutoffs must not deplete any kinematic region beyond repair - that is, for each occupied kinematic region, there must be some events that are not cut out and can be weighted. For example, $c\tau_0 = 371$ cm for $K^{\pm}$, so if these particles are produced with high momentum most of them decay outside the bubble chamber, regardless of their direction. Therefore, this bias against high-momentum $K^{\pm}$ in the topologies with a charged decay cannot be compensated for by weighting.

Cuts were imposed on the direction of the incoming beam track. The aim was to eliminate events resulting from interactions of beam particles which had been deflected on the way to the chamber; these particles were presumably rather highly contaminated by protons. The cutoffs in beam azimuth and dip were chosen after an examination of the distribution of these quantities for each momentum setting; they removed only a few events.[47]

We did not use the weights and cuts in all of our analyses. It is, of course, not ordinarily practical to make scatter plots with weighted events. Generally we examined the projections of our scatter plots without applying the weights or making the corresponding cuts. [This could be done since the cut events were given a non-zero fiducial code but otherwise processed like good events.] In Chapter 3, however, we did use the weights in the maximum-likelihood fits and in histograms of the data; in Chapter 4 we did confirm that the weights did not affect the relevant mass spectra. [We did make, but have not included in this thesis, event tallies like those given in Tables 2.8-2.9 but with cuts and weights.]

The fiducial cuts remove 15.6% of our 18362 events; the sum of the weights of the remaining 15496 events is 18096.2. The distribution of weights for all events is given in Fig. 2.3. The average weight depends on topology (it is 1.17 overall but 1.31 for the 2-vee events alone); the shape of this distribution depends only moderately on topology.

We have not examined in detail the effects of the cuts and weights; we note that we have not used any unconventional procedures. There probably were, however, other losses for which weights could have been used. For example, Davies introduced a factor to correct for lost Λ's with a large opening angle or one very short track.[48] Similarly, Klein used a weight which was dependent on

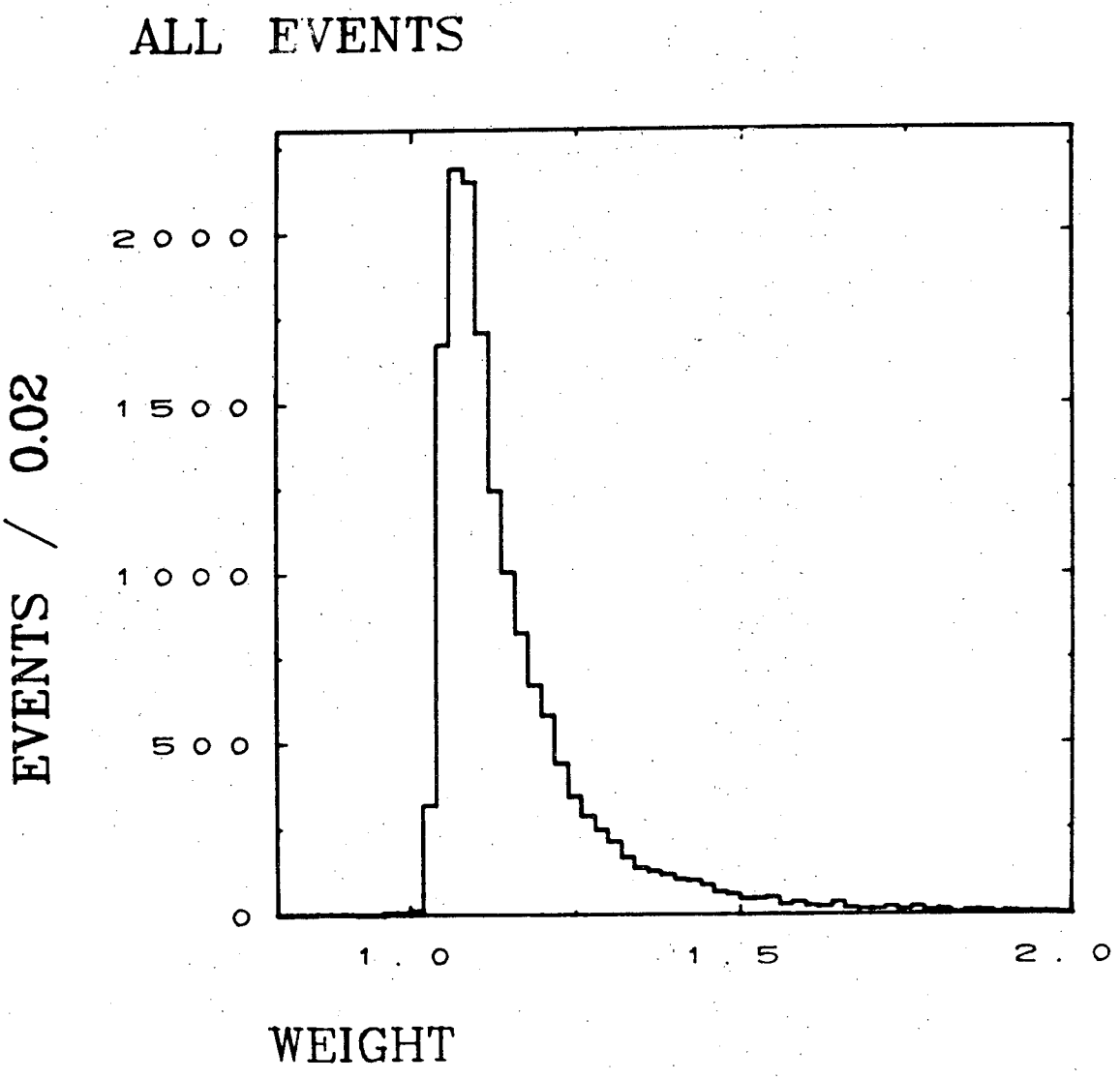

Fig. 2.3

both Λ momentum and opening angle. He also noted (but did not correct for) a loss of low-momentum K^0's. (A good and detailed discussion of general questions related to weighting is given in Klein's thesis.[49]) [We have not investigated such losses in our data; they might partially explain our problems with the 2V:1V ratio in ΛK^0 final states (see Section 2.9). They may also have something to do with the recently reported (but questionable) peculiarities in the branching ratio for $K^{*+} \rightarrow (K^0\pi^+)/(K^+\pi^0)$ in $\Lambda K\pi$ final states.[50]]

One other effect which is undoubtedly present in our data but has not been studied is the loss of the decay $\Sigma^+ \rightarrow p\pi^0$.[51] This could be a major effect in the topologies with charged decays.

2.8 ASSIGNMENT OF EVENTS TO FINAL STATES

2.81 INTRODUCTION

This section describes the method used to assign ambiguous events to the most likely final-state hypothesis. We have included details and discussion that might be valuable to an experimenter working on this or similar data. The reader who just wants to see what we did may find sections 2.82 and 2.87 sufficient.

First we summarize the procedure and present the badness function, a modification of the chisquare on which the assignment was based (Sections 2.82-2.83). In Sections 2.84-2.86 we motivate the form of the badness function, and then explain (in Section 2.87) how its parameters were extracted from various experimental distributions. Finally, before presenting the final-state tallies which result from this "disambiguation" scheme, we comment (in Section 2.88) on various indicators of how well it worked.

2.82 FORM AND USE OF THE BADNESS FUNCTION

For each reaction hypothesis accepted by the fitting program SIOUX, the badness B is calculated as follows:

$$B = (X^2_K - F_K) + \beta(X^2_B - F_B n_B) + N_{KV}F_{KV} + C_{MM} \quad .$$

Here X^2_K is the kinematic chisquare, and F_K is a parameter chosen to control the separation of hypotheses with different numbers of kinematic constraints. For events measured on the Spiral Reader, the ionization (bubble) chisquare X^2_B and the number of ionization constraints n_B enter, multiplied by the constants β and F_B. N_{KV} is the number of vees which are attributed to a K^o decay, and F_{KV} is a constant chosen to achieve separation of K^o and Λ vees. C_{MM} is a correction term to bias against marginally passing missing-mass hypotheses.

The parts of B are discussed in detail in the following sections. For convenient reference, we list here the values of the parameters used in making the final data tape. F_K depends on n_K, the number of kinematic constraints at the production vertex, and on the presence or absence of an invisible spectator proton. For n_K = 0, 1, and 2, F_K = 0, 1.5, and 6.5 respectively. For n_K = 4, F_K = 13.5 for odd-pronged events and 21.5 for even-prongs. We chose β = 1/2, F_B = 1, and F_{KV} = 10.

Basically, each event is assigned to the hypothesis with the smallest badness. However, we also incorporated a confidence level cutoff, and information from a partial ambiguity scan.

The minimum confidence level for a fit to be passed by SIOUX is roughly 0.00001. We chose to impose a confidence-level cutoff of 0.005. This was done because the confidence level distributions quite generally showed a great excess (i.e., far more than 0.5% of the events) below that level. (Our final confidence level distribution is shown in section 2.11.)

2.83 AMBIGUITY SCAN

Events which were measured on the Franckenstein only and which were considered ambiguous and potentially resolvable were examined on the scan table. Hypotheses whose fitted momenta and track-mass assignments were inconsistent with the observed bubble density were killed. A total of 28% of the (non-deleted) events in the entire experiment were examined in the ambiguity scan. (See Table 2.6.) Typically, several hypotheses were rejected per event.

For the purposes of the ambiguity scan, events were considered ambiguous if there was a hypothesis whose badness was within 10 of the smallest badness for that event. [The choice of 10 as a cutoff was rather arbitrary, and the badness was calculated using our first approximation to F_K.] Hypotheses were called 'resolvable' if the ratio of calculated bubble densities I_B {$I_B = I_{min}/[(v/c)^2\cos(\theta_{dip})]$} was greater than 1.5 for any track. After some of the scanning had been done, we decided that there would be very little disadvantage to looking only at events where some of the *best* hypotheses (i.e., those within 10 in badness of the best one) were resolvable, rather than at those where *any* of the passing hypotheses were resolvable. Each scanner made visual estimates of the bubble densities, so the standards used were not uniform. This may have caused some problems on events with short decaying tracks, where the error in the fitted momentum was not always taken into account in comparing the predicted and observed ionizations.

In addition to examining those tracks and hypotheses which caused the event to be classified as 'resolvable and ambiguous', the scanner was instructed to look at the other hypotheses and reject them if a reason was found. Sometimes events were found where none of the hypotheses were consistent with the observed properties; these were remeasured.

2.84 MOTIVATION FOR THE USE OF THE BADNESS FUNCTION

In this section we first consider the basic kinematic part of the badness:

$$B_K = \chi^2_K - F_K$$

This form was chosen empirically (i.e., out of the clear blue) for our preliminary disambiguation since it incorporates in a simple fashion two desired properties:

(1) Among hypotheses with the same number of constraints at the production vertex, the one with the smallest chisquare is selected as best.

(2) With the appropriate F_K, we favor hypotheses with more constraints. It is a well known and rather unsurprising fact that events with one or more missing neutrals rarely fake (i.e., fit successfully as) hypotheses with more constraints. Thus, we wanted to insert a bias in favor of highly constrained hypotheses.

A similar term for the bubble-density badness was added; the choice of parameters involved, and the other terms in the badness function, are motivated in later sections. Here we discuss briefly some of the distinctly different procedures that we did not use. It should be emphasized that we did not make a systematic study of these alternate procedures, so we have no reason to believe that ours is the best one. Nonetheless, for the reader who is considering using our scheme on his own data, the following comments may be useful.

To separate different constraint classes, we chose to work with the chisquare itself, using constant fudge factors F_K to provide the bias in favor of higher constraint class. Of course, both chisquare and constraint class are taken into account in the calculation of the confidence level. However, we felt that it is not adequate to choose between different constraint classes by selecting the hypothesis with the highest confidence level. The reason is simply that one has no *a priori* knowledge of the confidence level distribution for a wrong hypothesis. (By construction, of course, events correctly fitted to the correct hypothesis have a flat distribution in confidence level.) One might expect that any wrong hypothesis would have a confidence-level distribution that is strongly peaked at the low end; if this were the case it would be reasonable to disambiguate on the basis of confidence level alone. However, we have already noted that high-constraint events tend to fake low-constraint fits quite easily; it is not obvious that such fake low-constraint fits must have typically low confidence levels. We could have made an attempt to study these distributions, but we decided that working with the chisquare directly would be just as good.

We note, however, that the ratio of confidence levels has been used for the selection procedure by other workers; the dividing line between different constraint classes may be a ratio of confidence levels chosen after an examination of the experimental data, rather than simply unity. (See, e.g., Siegel's thesis.[52] For an example of cutting at a ratio of chisqares, see Ref. 4. Campbell used an iterative procedure, based on assignment by confidence level after multiplying χ^2 by a constant until the average value of χ^2 was correct.[53])

An alternate procedure which we considered briefly was to not assign each event to a single final state at all. Such a procedure would involve estimating the probability that each of several hypotheses is correct, and using the event in all such final states with a weight proportional to that probability. (Klein, for example, has used this scheme, assigning some events to two final states with weight 1/2.[54]) It seems that such a scheme might be appropriate at high energies, where most events are ambiguous and not resolvable. The procedure of assigning each event to the best hypothesis is a traditional one, obviously appropriate when only a small fraction of the events are ambiguous. However, a multiple-assignment scheme would certainly involve practical difficulties (e.g., the rewriting of programs) and perhaps also theoretical ones (e.g., in the assessment of statistical weights). Therefore, we only considered this method briefly before abandoning it.

A modification of the idea of not assigning each event to a single final state could be useful for determining cross sections. This problem requires only that we know the *number* of events that should be assigned to each final state. In some cases it is relatively easy to estimate the extent of the contamination of a sample from experimental distributions. For example, one could attempt to measure the contamination of a one-production-constraint fit (e.g., missing K^0) due to missing-mass events (missing $K^0\pi^0$) by looking at the distribution of missing mass. This method was used in our low-momentum exposure.[6] We have not, however, applied it to our data.

The badness-function scheme we have used was designed to apply to all final states with a minimum of parameters to be determined. Such an approach is the most practical one in a survey experiment of this kind, where there are a large number of final-state 'marks' (about 120 in our case). For a detailed study of any single final state, a more painstaking procedure may be called for. One could start with all events with a passing fit to that state and remove events ambiguous with other final states on the basis of experimental distributions

(missing mass, etc.). (In Appendix A, we look for D and E meson production in all events passing $\pi^+ d \rightarrow pp K^0 K^0 \pi^0$.) Perhaps one could get good separation of a single final state with badness-function parameters different from those chosen for the whole experiment.

Our approach could be modified by the use of more parameters in the badness. As described below, we evaluated F_K separately for even- and odd-pronged events. (We chose the same numerical value in most cases, however.) One might want to try allowing these parameters to depend on (for example) the beam momentum, or on properties of the final state other than just the number of constraints.

The only term in B which depends on the physical properties of the individual event under consideration (as opposed to the quality of the fit) is C_{MM}, which depends on the missing mass. One might look for other such properties which could be incorporated into the badness function. For example, Davies added a constant to B for any hypothesis which had no possible low-momentum ($P \leq 250$ MeV/c) spectator; this was intended to reduce the excess of high-momentum spectators.[55]

It should be noted that (except for the indirect effect of such correction terms) we separate hypotheses within the same constraint class solely by chisquare. However, there is no reason to expect the cross-contamination within a constraint class to be uniform. (For example, some one-constraint hypotheses lose more events to other one-constraint hypotheses than are replaced by contamination.) This expectation of nonuniformity was supported by a study of fake events generated by the program PHONY[56] at the beam momenta of our low-momentum exposure.[57] It was hoped that some simple explanation could be found - for example, that (other things being equal) there was a bias in favor of a proton rather than a π^+ for a given track. The study of fake events confirmed that there was considerable asymmetric cross-contamination, but no simple pattern was found. At the higher momenta of this exposure, we would expect things to be worse. Appendix B is an examination of the extent of our cross-contamination problem. (A nice example of how such contamination is detected and taken into account can be found in Ref. 8, p. 12.)

2.85 USE OF TRACK IONIZATION INFORMATION

As previously noted, track ionization (bubble density) information for events measured on the Franckensteins was used in the ambiguity scan. For events measured on the Spiral Reader, this information was incorporated automatically.

For details of the definition and calcuation of the bubble chisquare X^2_B, see Ref. 58. Basically, each track in each view contributes one degree of freedom and a term in the chisquare which corresponds to the difference between the calculated and measured pulse height. If there is gross disagreement for any one track, that track-mass hypothesis is not accepted in any fit. For other hypotheses, X^2_B is saved by SIOUX for later use.

Note that with $F_B = 1$, the bubble part of the badness function can be written as $B_B = (X^2_B - \langle X^2_B \rangle)/2$. This seemed like a reasonable way to treat hypotheses with differing numbers of constraints; the 'excess chisquare' is used. In most cases, of course, all hypotheses for a given event have the same number of measured tracks, and thus the same number of constraints; the principal exception comes from the fact that we fit a charged decay for $\Sigma^\pm$ but not for $K^\pm$ hypotheses. The factor β was set less than 1 to give each ionization degree of freedom less weight than a kinematic degree of freedom. The choice of $F_B=1$ and $\beta=1/2$ was made on the basis of arguments of this nature and no experimental study was made. (We did, however, do an ambiguity scan of some Spiral-Reader-measured events and confirmed that the bubble density routines were working reasonably well.)

2.86 CORRECTION TERM FOR MISSING-MASS HYPOTHESES

The quality of a missing-mass hypothesis tried by SIOUX is not indicated by a chisquare, since no constrained fit is involved. (For this discussion, one can consider that the fit to each vee gives the total kinematic chisquare and the number of constraints, and that it results in a measured Λ or K^o track which is used in the missing-mass calculation.) From the measured momenta and the hypothesized masses at the production vertex, SIOUX calculates a missing final-state four-vector $(\underline{p},E)$; the missing mass is given by $m^2=E^2-p^2$. We wish to create a chisquare-like function which reflects the two ways this missing-mass calculation may fail:

(1) The missing mass may be below the threshold for the hypothesis in question; that is, $m^2 < m_o^2$, where m_o is the smallest possible sum of rest masses for the missing particles.

(2) The missing energy may be negative. This means that energy conservation requires an incident, rather than an outgoing, unseen particle.

We use the test function $z = E-E_o$, where E_o is the minimum missing energy consistent with the observed momentum imbalance. ($E_o = +\sqrt{[p^2+m_o^2]}$) The smooth function z has the property of being negative if the missing mass calculation is bad for either of the reasons just given, and positive otherwise. (This is evident if we write $z = E-|E|[1-(m^2-m_o^2)/E^2]^{1/2}$.) We can form a chisquare-like measure of how bad the calculation is, namely

$$C_{MM} = [(z-0)/dz]^2 \quad \text{if } z < 0,$$

$$C_{MM} = 0 \quad \text{if } z > 0.$$

SIOUX fails a missing-mass hypothesis if C_{MM} is greater than some fixed (and rather large) number. For the surviving hypotheses, we simply add C_{MM} to the badness.

2.87 EVALUATION OF PARAMETERS FOR SEPARATION

In this section we present the physically significant distributions from which the biases in chisquare were extracted. The separation of Λ from K^o vees is the simplest and cleanest; it is discussed in considerable detail in order to illustrate the method. The next 3 subsections are concerned with the separation of different constraint classes (0C-1C, 1C-2C, and 2C-4C respectively).

Separation of Λ and K^o Decays

To disambiguate the vees, we looked at the decay distributions of the samples of Λ and K^o, as defined by various choices of the parameter F_{KV}.

In its rest frame, the parent particle decays isotropically; in particular, the cosine of the angle between the line of flight of the parent and either decay product should be flat (unless events are lost or misassigned). (This is obviously true for the spinless K^o, and holds for the Λ if it has no polarization along the line of flight.[59] This assumption is presumably valid for the experiment as a whole.)

If we simply assign each ambiguous vee to the hypothesis with the smallest chisquare, there is a noticeable excess of K^o decays with a backward-going π^-. This is shown by the unconnected histogram in Fig. 2.4(a), which gives the c.m. decay cosine relative to the line of flight (as found in the fit to the vee alone). This anisotropy comes from the fact that, among the ambiguous vees, there are more Λ's faking K^o's than K^o's faking Λ's.

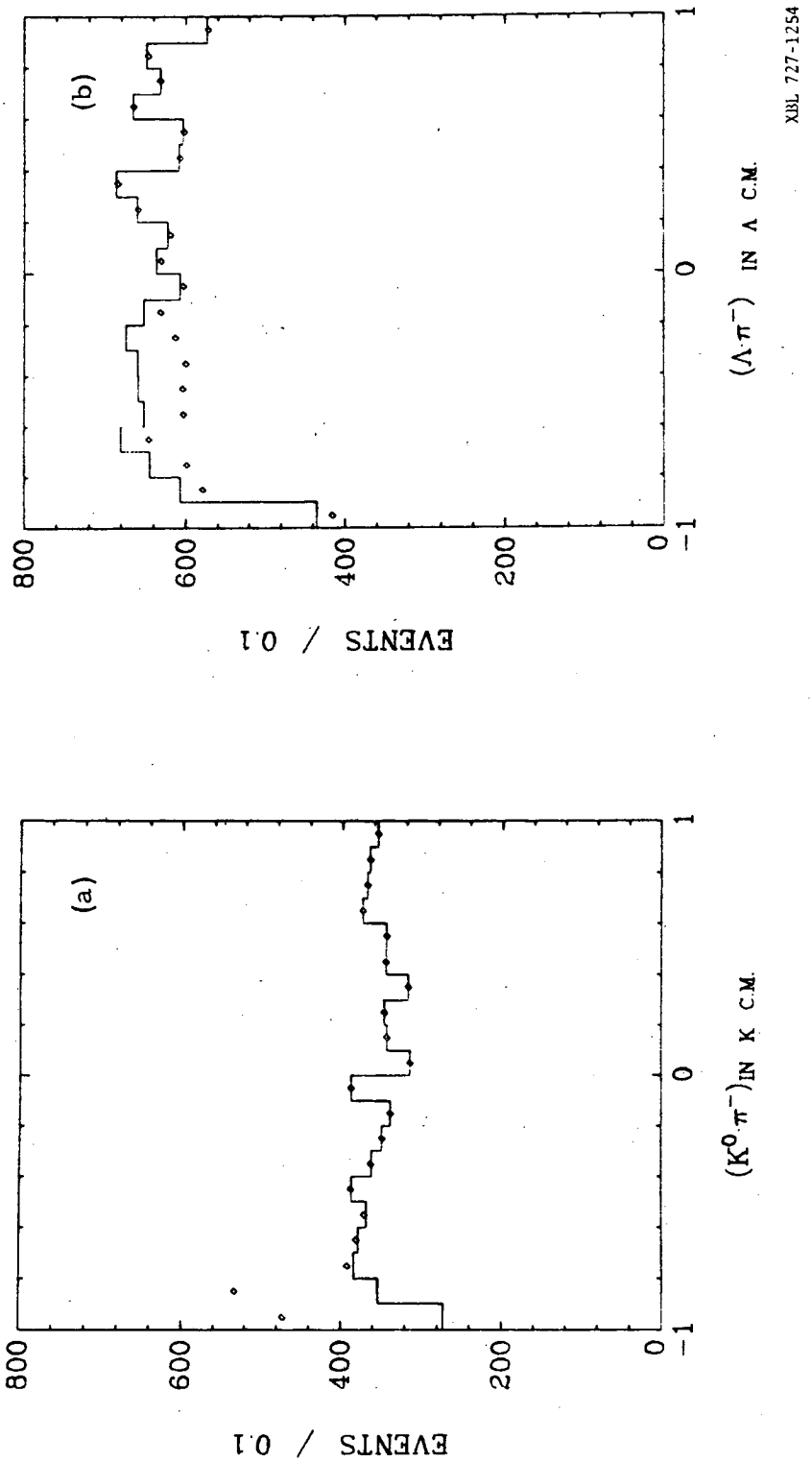
(b)
(a)
EVENTS / 0.1
800
600
400
200
0
-1
0
1
$(\Lambda\pi^-)$ IN Λ C.M.
$(K^0\pi^-)_{IN\ K\ C.M.}$
XBL 727-1254

Fig. 2.4

The physical reason for this is clear. The Λ decay has a much smaller q-value than the K^0 decay; specifically, the maximum transverse momentum is 100 MeV/c for the Λ and 206 MeV/c for the K^0. That is, the kinematically allowed region for the Λ falls entirely within that for the K^0. Thus, many Λ's can fake K^0's, with the K^0 having small transverse momentum, but only a fraction of the real K^0's are kinematically allowable as Λ's.

When the parent velocity is large (i.e., larger than that of the decay products), there is a maximum opening angle in the lab for the vee. However, the excess K^0 events are associated not simply with small opening angles but with only the π^--backward hemisphere. This forward-backward asymmetry can be understood as coming from the vees with momentum between roughly 120 and 750 MeV/c. In this region, either a Λ or a K^0 with the decay π^- going backward in the c.m. frame may have any lab opening angle up to 180°. This is also true for a K^0 with the π^- going forward, but a Λ with a forward π^- is restricted to a maximum opening angle less than 90° (because the proton is slow in the c.m.). Thus, the two cases with forward-going π^- look quite different, and the contamination comes from the hemisphere with backward-going π^-.

Therefore, we introduced a bias against K^0 fits, calling a vee a K^0 only if $\chi^2_K + F_{KV} < \chi^2_\Lambda$. (That is, we added various positive constants F_{KV} to the effective chisquare, or badness, of the K^0 fit to see if the decay distributions became flatter.) The resulting decay cosine distributions with $F_{KV} = 10$ are given in Figure 2.4. For comparison, the distributions with $F_{KV} = 0$ are shown by the unconnected dots. This bias gives essentially flat distributions in both cases; not only is the prominent excess in the K^0 distribution removed, but the broad depletion in the Λ distribution is filled in. This isotropy is consistent with, but does not prove, essentially perfect separation of K^0's and Λ's. (The narrow depletions remaining at decay cosines of ±1 in both cases are presumably associated with losses of decays with very small or very large opening angles which are not recognized as vees by the scanners.)

Another way of looking at our bias is that an ambiguous vee can not be called a K^0 unless $\chi^2_\Lambda > 10$; that is, unless it has a confidence level for the 3-constraint fit to a Λ of less than 0.019. Thus, it is not surprising that the net result of this scheme is not very different from calling any ambiguous vee a Λ Only 11.8% of the vees are passed by SIOUX with both Λ and K^0 fits; 80.4% of those have a lower chisquare as a Λ, and 97.5% are called Λ's when $F_{KV} = 10$. We examined some of the 58 ambiguous vees which were called K^0, and it does appear

that our method is slightly better than the common one of simply calling any ambiguous vee a Λ. [In the assignment of events we did not disambiguate the vee separately, but just added all the biases to the total badness function B. For Figure 2.4, we used the sum of the kinematic and ionization chisquares from the vee-only (pretest) fit.]

Separation of Zero- and One-Production Constraint Hypotheses

Note that throughout this report we classify a hypothesis as 0-C, 1-C, 2-C, or 4-C according to the nominal number of production constraints. (The total number of constraints is usually greater than this number by 3 times the number of vees. Some events were "constraint reduced" by the fitting program, usually because a track was not well measured. This is common only on events with charged decays - often the decaying track was too short to have a measured momentum.) [It would probably be good to study the disambiguation of these events in some detail before using them. Constraint-reduced events without a charged decay might well not be used, if statistics permit.]

The sample used for the 0-C vs. 1-C separation consisted of all events fitting these marks but with no better 2-C or 4-C fit. ["Better" was defined using a preliminary version of the badness function.] We looked at the distribution of the missing mass from the 0-C hypothesis corresponding to the best 1-C fit (that is, the missing mass calculated using the same mass assignments for the measured tracks). The true 1-C events should peak at the mass of the single missing neutral particle, while the true 0-C events should have a missing mass spectrum starting at the mass of the two (or more) missing neutrals. (Given our resolution, this threshold is not clearly separated from the single-missing-particle mass.)

We examined the missing mass distribution separately for the cases where the missing neutral was π^0, K^0, n, Λ, and Σ^0, and separately for even- and odd-prongs. We plotted this distribution for the events that would be called 1-C for various values of B_{01}, the bias in chisquare in favor of the 1-C hypothesis. (That is, an event is called 1-C if $\chi^2_{1C} - B_{01} < \chi^2_{0C}$. In terms of the F_{NK} listed in section 2.82, $B_{01} \equiv F_K(n_K=1) - F_K(n_K=0)$.) It was found that $B_{01}=1.5$ gave reasonable results.

An example of the distributions examined is given in Figure 2.5. The lower histogram shows the square of the missing mass for the 1195 events which are assigned to a 1-C hypothesis with an unseen K^0 when $B_{01} = 1.5$. There is a

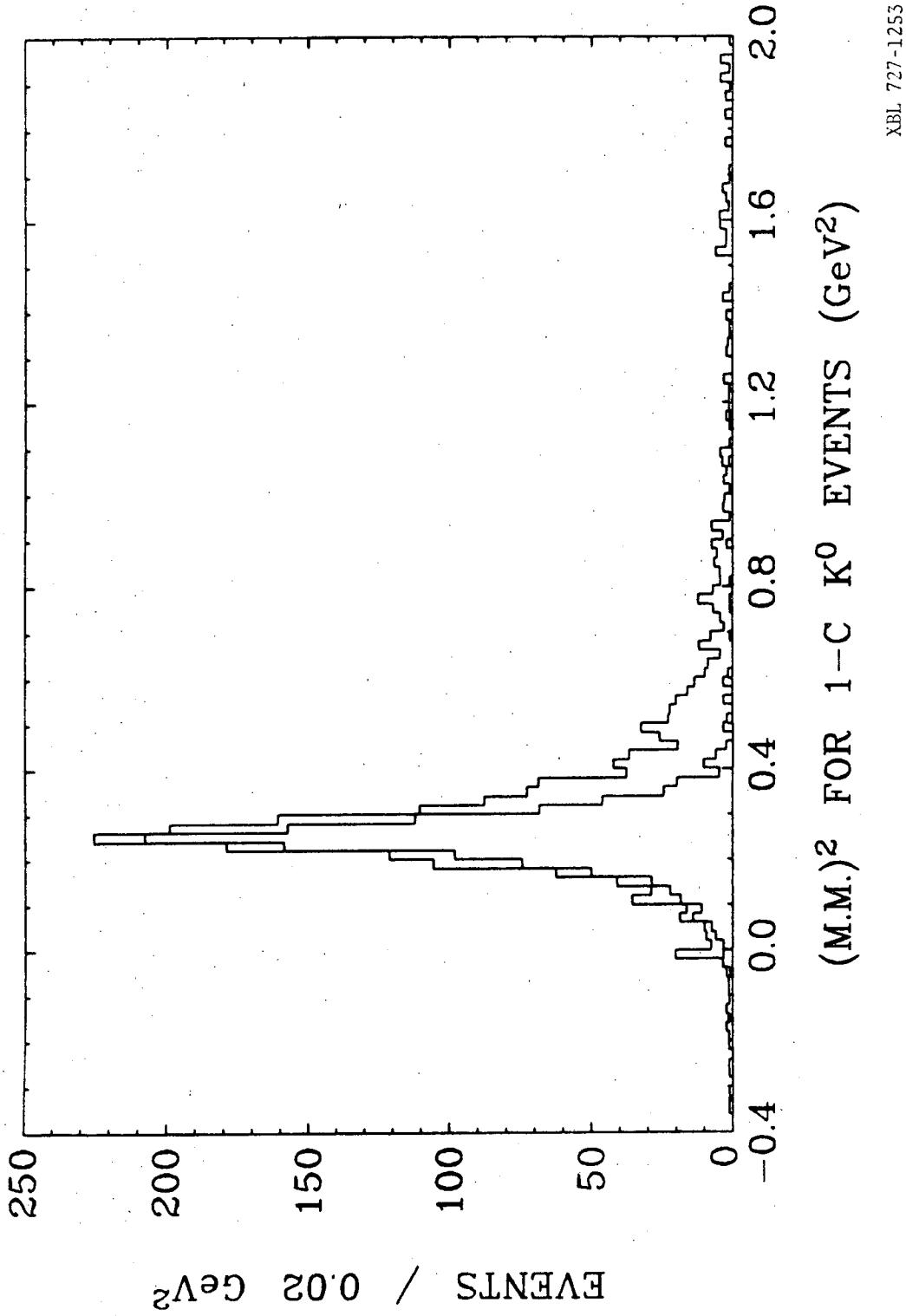
EVENTS / 0.02 GeV²
250
200
150
100
50
0
−0.4
0.0
0.4
0.8
1.2
1.6
2.0
(M.M.)² FOR 1−C K⁰ EVENTS (GeV²)
XBL 727-1253

Fig. 2.5

reasonably symmetric peak around $m^2(K^o)$. The upper histogram (2100 events) is the spectrum that would result if all the ambiguous events were called 1-C; there is a prominent tail at high m.m.^{2} due to events with more than just a K^o missing.

Separation of One-C and Two-C Hypotheses

The sample used in this section and the next one consisted of all 3048 events with a successful fit to the 2-C hypothesis

$$\pi^+ d \longrightarrow p K^+ \Sigma^o, \quad \Sigma^o \longrightarrow \Lambda \gamma.$$

We studied the 1C-2C separation and the 2C-4C separation in these events; we did not separately examine the 1C-4C separation of the events without a Σ^o fit. [Although we report only on ΛK final states in Chapters 3 and 4, we should have at least checked that separation on the $K\bar{K}$ final states, using the parameters determined here.]

We looked at the distribution of M(Λ+m.m.), the effective mass of the Λ (which is seen to decay) and the missing four-momentum at the primary vertex. The latter is obtained from the corresponding missing mass hypothesis. That is, to separate

	$\pi^+ d \longrightarrow p K^+ \Sigma^o, \ \Sigma^o \longrightarrow \Lambda \gamma$	(2-C)
from	$\pi^+ d \longrightarrow p K^+ \Lambda \pi^o$	(1-C)
we looked at	$\pi^+ d \longrightarrow p K^+ \Lambda$ (m.m.)	(0-C)

Figure 2.6 shows those events with both 1C and 2-C fits which were not assigned to a 4-C hypothesis. We have plotted $M^2(\Lambda$+m.m.) against the difference in chisquare between the 1-C and 2-C hypotheses. [For Spiral-Reader-measured events, the quantity used is $\chi^2_K+0.5(\chi^2_B-n_B)$.] For true 2-C events, $M^2(\Lambda$+m.m.) should fall in a narrow peak centered at $m^2(\Sigma^o)$. For true 1-C events, there should be a distribution going down to $[m(\Lambda)+m(\pi^o)]^2$. Neither the odd-prongs nor the even-prongs show a clear separation. There is, however, a definite tendency for events toward the right side of these plots to have smaller $M^2(\Lambda$+m.m.). After examination of these plots, we decided to use a bias in favor of 2-C fits of $B_{12} = 5$. (That is, the events to the right of the vertical lines are called 2-C.)

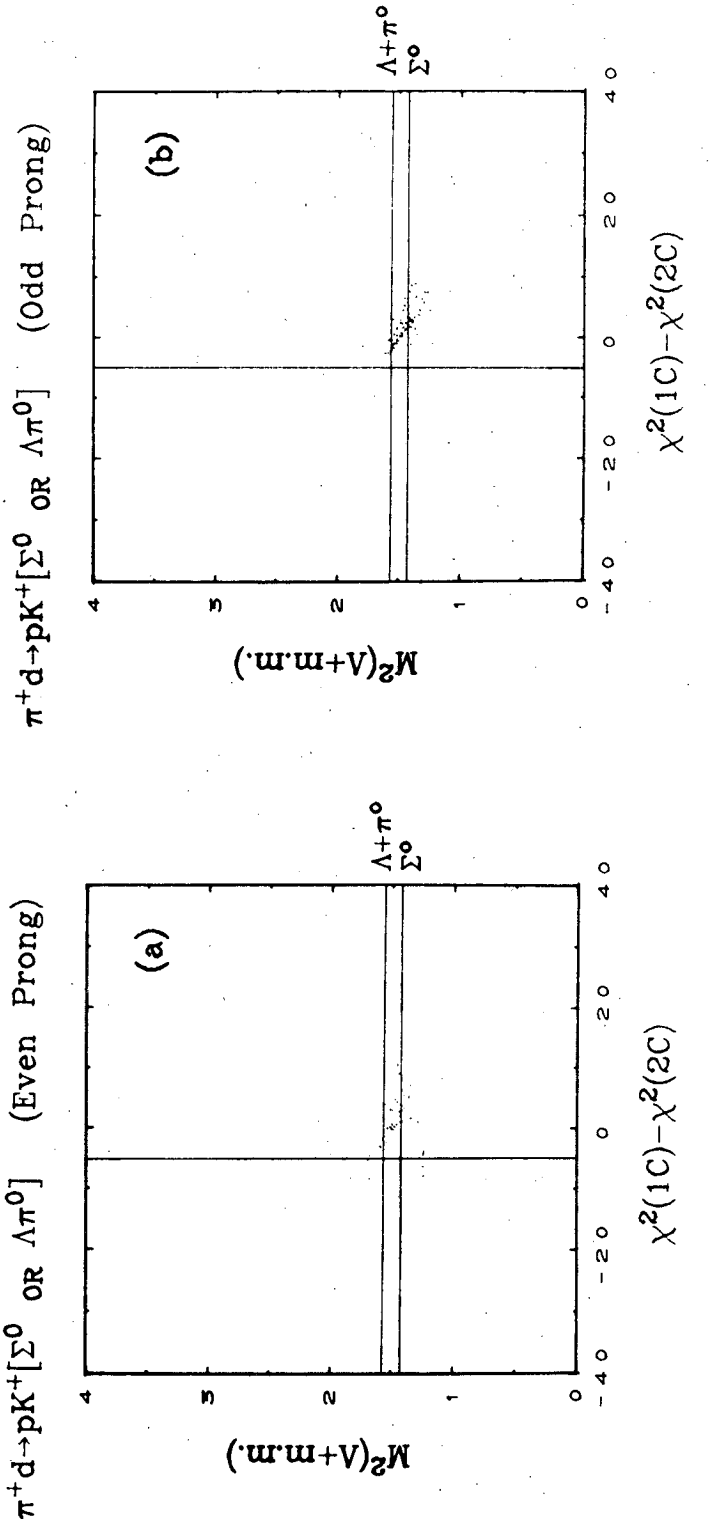
(a)
(b)
$\pi^+d\to pK^+[\Sigma^0$ OR $\Lambda\pi^0]$ (Even Prong)
$\pi^+d\to pK^+[\Sigma^0$ OR $\Lambda\pi^0]$ (Odd Prong)
$M^2(\Lambda+m.m.)$
$\chi^2(1C)-\chi^2(2C)$
Σ^0
$\Lambda+\pi^0$
XBL 729-1804

Fig. 2.6

Separation of Two-C and Four-C Hypotheses

We examined the 1141 events with a fit to either or both of the reactions

$$\pi^+ d \longrightarrow p K^+ \Lambda \qquad (4\text{-C})$$

$$\pi^+ d \longrightarrow p K^+ \Sigma^0, \quad \Sigma^0 \longrightarrow \Lambda \gamma \qquad (2\text{-C})$$

For true 2-C events, the Σ^0 decays isotropically in its rest frame (since the decay is electromagnetic). Following Hardy,[60] we make use of the fact that when a γ is added to a true 4-C event to fake (with the Λ) a Σ^0, the γ tends to lie in the production plane defined by the beam and the apparent Σ^0. The relatively large error in the beam momentum means that the momentum balance is less tightly determined in this plane than out of it, so the fake γ momentum (which is really the momentum unbalance) tends to be in this plane. In fact, as Butler has noted (and explained quite clearly), the γ tends very strongly to be parallel to the beam or to one of the other measured tracks.[61]

We therefore attempted to separate these hypotheses by taking ambiguous events from the 2-C hypothesis until we got a flat distribution in the cosine between the Σ^0 decay and the normal. Figure 2.7 shows the dependence of this cosine distribution on the chisquare difference, for even- and odd-pronged events separately. (The normal is defined as $\hat{n} \propto \hat{\pi}^+ \times \hat{\Sigma}^0$; the cosine is evaluated in the Σ^0 rest frame; the four-vectors from the Σ^0 fit are used.) Events with only the 2-C fit were added at the left side of each plot, plotted with a chisquare difference chosen randomly between -40 and -35. [The few events plotted with a chisquare difference between +35 and +40 are those which were treated as unambiguously 4-C but which had a 2-C fit with a confidence level below the 0.5% cutoff.]

By inspection of these plots and their projections, we determined a chisquare bias in favor of the 4-C fit of $B_{24} = 15$ for even-prongs and $B_{24} = 7$ for odd-prongs. The resulting angular distributions are given in Figure 2.8. (The lower histograms in the 2-C case are events with no 4-C fit.) We see that the 2-C distributions are flat and there is essentially no flat background under the 4-C peak.

For even-pronged events, this bias corresponds to calling almost all ambiguous events 4-C; this reflects the well known fact that it is very difficult to fake a 4-C fit. Although the $pK^+\Lambda$ final state with an invisible spectator proton is nominally 4-C, it is a degraded fit, because of the poor "measurement" of the proton, and it is more easily faked.[62]

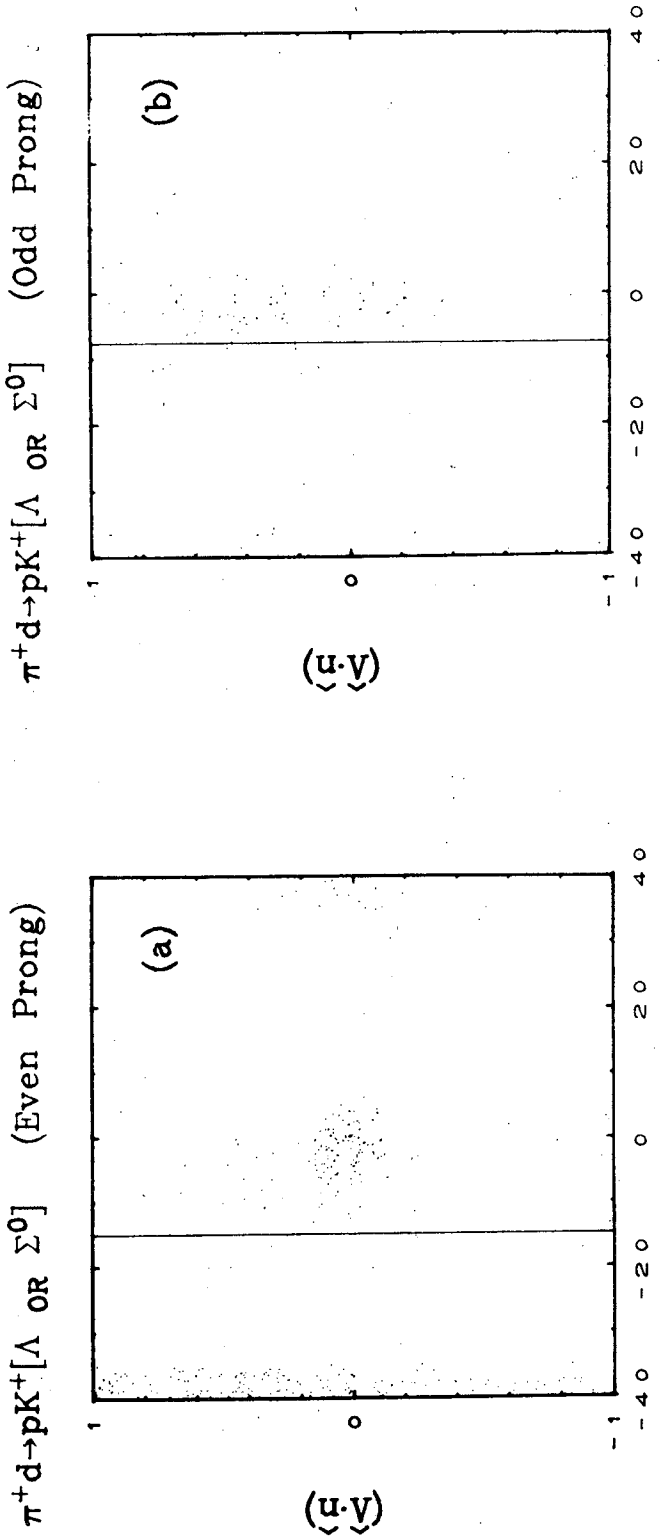

XBL 729-1805

Fig. 2.7

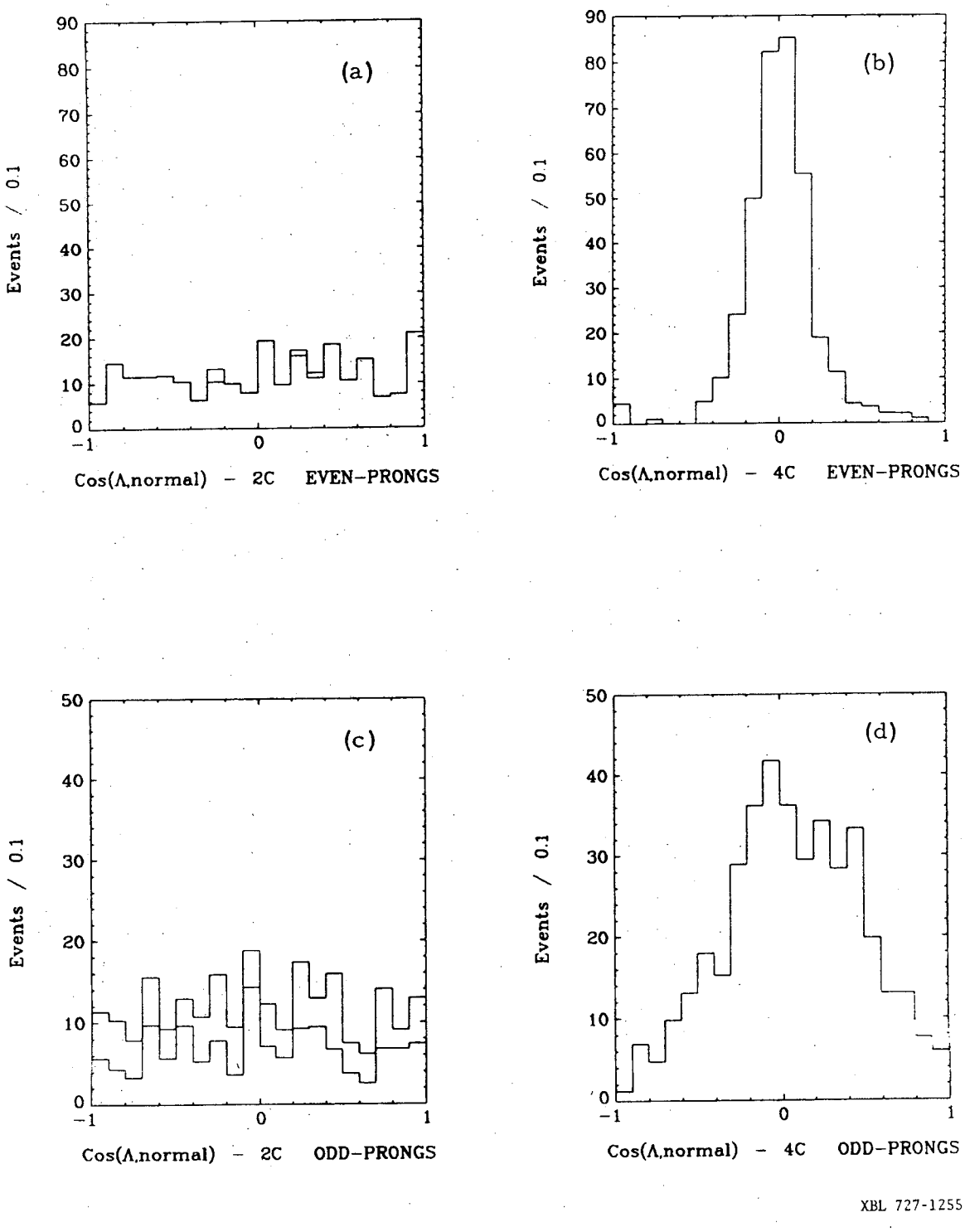
(a)
Events / 0.1
Cos(Λ,normal) – 2C EVEN-PRONGS
(b)
Events / 0.1
Cos(Λ,normal) – 4C EVEN-PRONGS
(c)
Events / 0.1
Cos(Λ,normal) – 2C ODD-PRONGS
(d)
Events / 0.1
Cos(Λ,normal) – 4C ODD-PRONGS
XBL 727-1255

Fig. 2.8

2.88 COMMENTS ON THE ADEQUACY OF THE DISAMBIGUATION

Although the just-described Σ^0 decay distribution looks good, two other indicators of 2-C vs. 4-C separation which we examined show that the separation is not clean.

First, we note that any other Σ^0 decay cosine should also be flat. Davies pointed out a possible source for some anisotropy he observed in the angle between the Σ^0 decay and the Σ^0 line of flight.[63] When a Σ^0 decays with the γ going backward with respect to the line of flight, the γ may have very little momentum in the lab frame. Such a Σ^0 with a "soft" γ of course cannot be distinguished from a Λ (with no γ at all). Our bias in favor of the Λ fit should lead to a depletion of the Σ^0 events with a backward γ (i.e., with $(\hat{\Lambda}\cdot\hat{\Sigma}^0)\approx+1$). Figure 2.9(a,c) shows such a depletion for both even- and odd-prongs. (The angle plotted is between the Λ in the Σ^0 rest frame and the Σ^0 in the lab.) The depletion also appears in the unambiguous events (lower histogram) and there is no corresponding surplus in the ambiguous events which we call Λ (Fig. 2.9(b,d)); therefore something is going on besides the loss of 2-C to 4-C events just explained. It is clear, nonetheless, that there is a definite (albeit small) anisotropy in this angle.

One should also be able to distinguish Λ and Σ^0 events on the basis of the corresponding missing mass hypothesis. As we did for the separation of 1-C and 2-C events, we can look at the dependence of the effective mass of the Λ plus the missing momentum on the difference in chisquare. This is done in Figure 2.10. One would expect to see symmetric peaks centered at $M^2(\Sigma^0)$ and $M^2(\Lambda)$ for 2-C and 4-C events respectively. There is no clear separation, but the correlation between $M^2(\Lambda+\text{m.m.})$ and the chisquare difference is apparent. From these plots alone, one would choose the same bias for both even- and odd-prongs, and it would be quite small ($\lesssim 5$). The biases we have chosen (vertical lines) appear to force too many events to be 4-C. This suggests that a separation on an event-by-event basis may not be possible. We decided that further analysis of this problem would not be worthwhile.

Although our final values for the bias parameters were the result of considerable effort, they were not picked in a completely systematic way and may not be the best possible choices for our data. Certainly any reader who is considering the use of such a badness function should not take these values as any more than first approximations. We note also that the data used in Chapter 3 of this thesis (and in most of our early surveys) was selected on the basis of

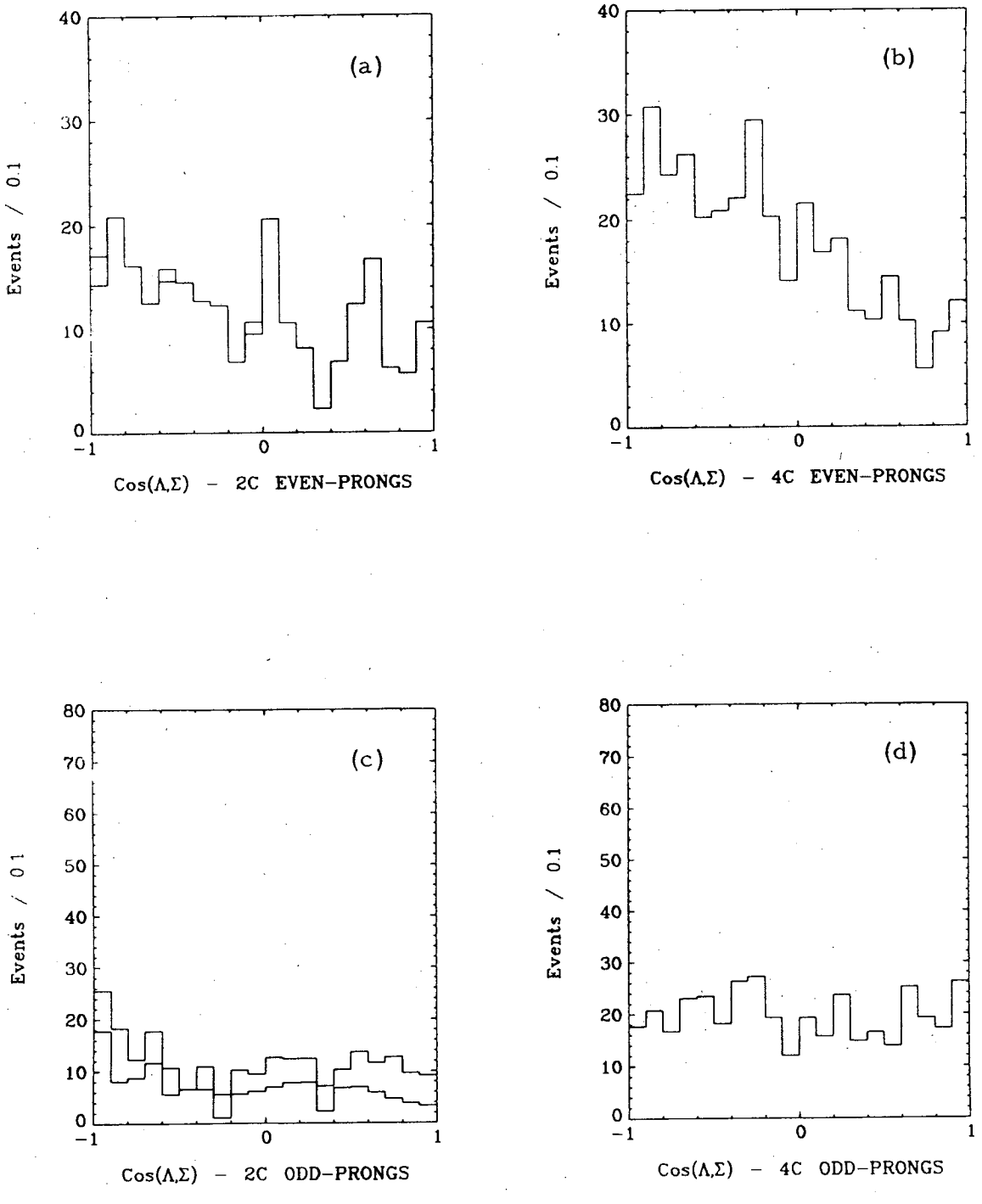
(a)
Events / 0.1
Cos(Λ,Σ) – 2C EVEN-PRONGS
(b)
Events / 0.1
Cos(Λ,Σ) – 4C EVEN-PRONGS
(c)
Events / 0.1
Cos(Λ,Σ) – 2C ODD-PRONGS
(d)
Events / 0.1
Cos(Λ,Σ) – 4C ODD-PRONGS
XBL 727-1256

Fig. 2.9

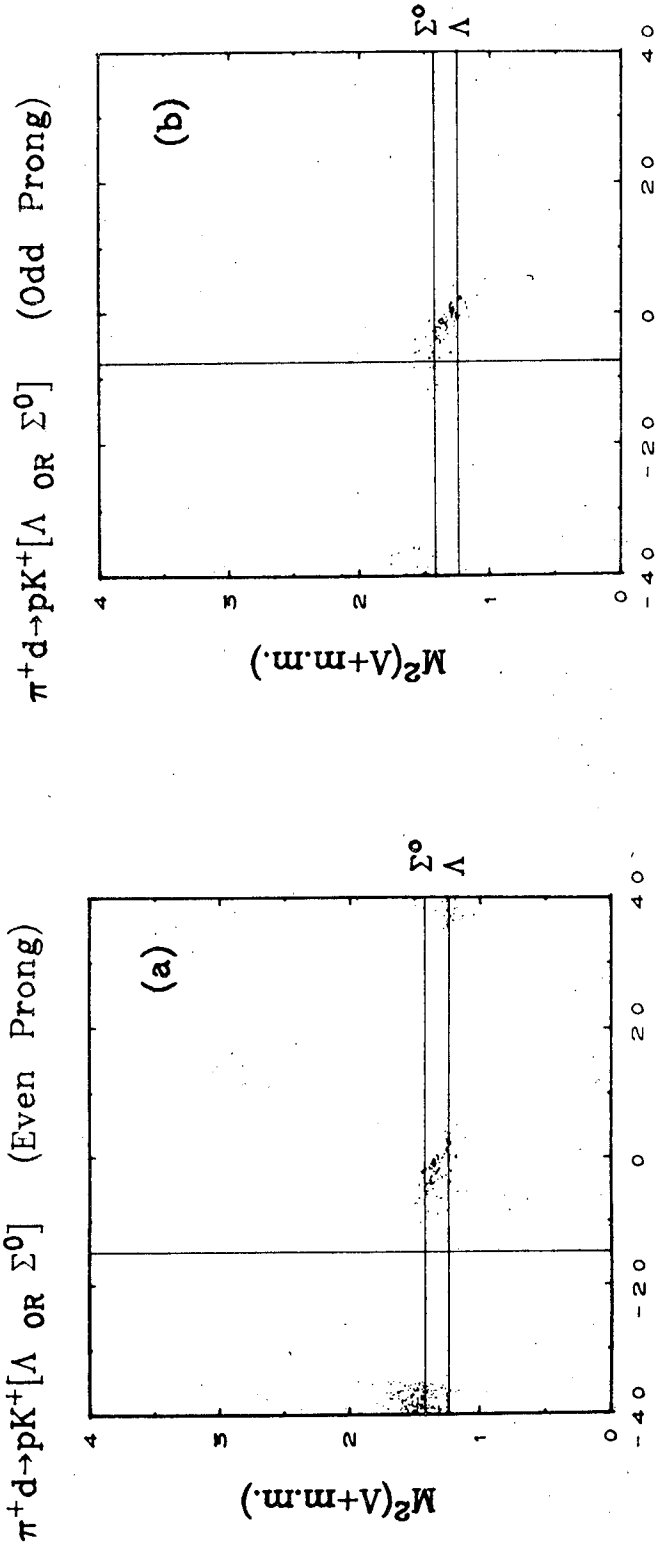

XBL 729-1806

Fig. 2.10

our preliminary disambiguation scheme, which used $F_K=5n_K$ throughout.

The final-state tallies resulting from our disambiguation are presented in Section 2.9. Some spectator momentum and confidence level distributions are given in Sections 2.10 and 2.11. In these subsequent sections, we will note several apparent anomalies, each of which probably results in some degree from misassignment of events. Specifically:

(1) The relative proportions of 2-vee and 1-vee events, for final states which can be detected in both topologies, are generally not those expected from the Λ and K^o branching ratios.

(2) There is an excess of high-momentum (p>300 MeV/c) spectators, which is generally greater for less-constrained hypotheses.

(3) The ratio of even-prongs to odd-prongs appears to depend too strongly on final state.

(4) The confidence level distributions are not flat.

In this section we have discussed only those distributions which allow us to work with the assignment of a number of final states together. When any single final state is being studied, there may be other indications of the extent of contamination, such as reflections of resonance production in the contaminating states.[64] In light of the problems we have noted, it is clear that the possible effects of reflections from misassigned events should be carefully considered before any conclusions are drawn about subtle effects that may appear in our data. (In Chapters 3 and 4, we comment on misassignment problems that might affect the results reported there.)

2.9 FINAL-STATE TALLIES AND CROSS SECTIONS

Results

Table 2.8 consists of a list of the final states, with the secondary decays indicated, and the number of events assigned to each. No cuts have been made. In Table 2.9 this tally is given separately for even-prongs and odd-prongs, and by beam momentum.

Table 2.10 gives the average cross section for each final state, and the visibility factor which has been included to take into account the secondary decay(s) observed. In Table 2.11 this cross section is given separately at P $\approx$3 and $\approx$4 GeV/c; the final state hypotheses have been arranged according to the number of kinematic constraints at the production vertex.

EVENT TYPE 34		
Mark	Final State	
11	$\Lambda nK^+\pi^+\pi^+\pi^-$	Λ-pπ^-
12	$\Lambda K^+\pi^+\pi^+\pi^-$ MM[n]	Λ-pπ^-
13	$K^+K^0\pi^+\pi^+\pi^-$ MM[nn]	K_s-$\pi^+\pi^-$
14	$K^0K^-\pi^+\pi^+\pi^+$ MM[nn]	K_s-$\pi^+\pi^-$
15	$K^0\pi^+\pi^+\pi^+\pi^-$ MM[Δn]	K_s-$\pi^+\pi^-$
16	$\Lambda\pi^+\pi^+\pi^+\pi^-$ MM[nK]	Λ-pπ^-
41	$\Lambda pK^+\pi^+\pi^-$	Λ-pπ^-
42	$\Lambda pK^+\pi^+\pi^0\pi^-$	Λ-pπ^-
43	$\Lambda pK^+\pi^+\pi^-$ MM[n]	Λ-pπ^-
44	$\Sigma^0 pK^+\pi^+\pi^-$	Σ^0-$\Lambda\gamma$, Λ-pπ^-
45	$pnK^+K^0\pi^+\pi^-$	K_s-$\pi^+\pi^-$
46	$pK^+K^0\pi^+\pi^-$ MM[nn]	K_s-$\pi^+\pi^-$
47	$pnK^0K^-\pi^+\pi^+$	K_s-$\pi^+\pi^-$
48	$pK^0K^-\pi^+\pi^+$ MM[nn]	K_s-$\pi^+\pi^-$
49	$\Lambda pK^0\pi^+\pi^+\pi^-$	K_s-$\pi^+\pi^-$
50	$\Sigma^0 pK^0\pi^+\pi^+\pi^-$	K_s-$\pi^+\pi^-$
51	$pK^0\pi^+\pi^+\pi^-$ MM[Δn]	K_s-$\pi^+\pi^-$
52	$\Lambda pK^0\pi^+\pi^+\pi^-$	Λ-pπ^-
53	$\Lambda pn^+\pi^+\pi^-$ MM[K]	Λ-pπ^-
71	$ppK^+K^0_{s}$	K_s-$\pi^+\pi^-$
72	$ppK^+K^0_{s}\pi^0_{\gamma}$	K_s-$\pi^+\pi^-$
73	$ppK^+K^0_{s}$ MM[nn]	K_s-$\pi^+\pi^-$
74	$ppK^0K^-\pi^+$	K_s-$\pi^+\pi^-$
75	$ppK^0K^-\pi^+\pi^0$	K_s-$\pi^+\pi^-$
76	$ppK^0K^-\pi^+$ MM[nn]	K_s-$\pi^+\pi^-$
77	$ppK^0K^0\pi^+\pi^-$	K_s-$\pi^+\pi^-$
78	$ppK^0K^0\pi^+\pi^-$ MM[Kn]	K_s-$\pi^+\pi^-$
Total		

Events
154
98
7
2
5
10
836
374
196
255
81
29
49
12
67
30
27
177
86
154
80
7
199
69
18
51
14
3065

EVENT TYPE 44		
Mark	Final State	
11-12	$\Lambda nK^0\pi^+\pi^+\pi^+\pi^-$	Λ-pπ^-, K_s-$\pi^+\pi^-$
13-14	$\Lambda K^0\pi^+\pi^+\pi^+\pi^-$ MM[n]	Λ-pπ^-, K_s-$\pi^+\pi^-$
15	$K^0K^0\pi^+\pi^+\pi^+\pi^-$ MM[nn]	K_s-$\pi^+\pi^-$, K_s-$\pi^+\pi^-$
41-42	$\Lambda pK^0\pi^+\pi^-$	Λ-pπ^-, K_s-$\pi^+\pi^-$
43-44	$\Lambda pK^0\pi^+\pi^+\pi^-$	Λ-pπ^-, K_s-$\pi^+\pi^-$
45-46	$\Lambda pK^0\pi^+\pi^+\pi^0\pi^-$	Λ-pπ^-, K_s-$\pi^+\pi^-$
47-48	$\Lambda pK^0\pi^+\pi^+\pi^-$ MM[n]	Λ-pπ^-, K_s-$\pi^+\pi^-$
49	$pnK^0K^0\pi^+\pi^+\pi^-$	K_s-$\pi^+\pi^-$, K_s-$\pi^+\pi^-$
50	$pK^0K^0\pi^+\pi^+\pi^-$ MM[nn]	K_s-$\pi^+\pi^-$, K_s-$\pi^+\pi^-$
71	$ppK^0K^0\pi^+\pi^-$	K_s-$\pi^+\pi^-$, K_s-$\pi^+\pi^-$
72	$ppK^0K^0\pi^+\pi^-\pi^0$	K_s-$\pi^+\pi^-$, K_s-$\pi^+\pi^-$
73	$ppK^0K^0\pi^+\pi^-$ MM[nn]	K_s-$\pi^+\pi^-$, K_s-$\pi^+\pi^-$
Total		

Events
6
3
0
53
18
18
2
2
17
2
1
122

XBL 729-1813

EVENT TYPE 32		
Mark	Final State	
11	$\Lambda nK^+\pi^+$	Λ-pπ^-
12	$\Lambda K^+\pi^+$ MM[n]	Λ-pπ^-
13	$K^+K^0\pi^+\pi^-$ MM[nn]	K_s-$\pi^+\pi^-$
14	$K^0\pi^+\pi^+\pi^-$ MM[Δn]	K_s-$\pi^+\pi^-$
15	$\Lambda\pi^+\pi^+\pi^-$ MM[nK]	Λ-pπ^-
41	ΛpK^+	Σ^0-$\Lambda\gamma$, Λ-pπ^-
42	$\Sigma^0 pK^+$	Λ-pπ^-
43	$\Lambda pK^+\pi^0$	1043
44	ΛpK^+ MM[n]	1613
45	pnK^+K^0	491
46	pK^+K^0 MM[nn]	507
47	$\Lambda pK^0\pi^+$	355
48	$\Sigma^0 pK^0\pi^+$	226
49	$pK^0\pi^+$ MM[Δn]	648
50	$\Lambda pK^0\pi^+$	808
51	Λpn^+ MM[K]	1060
71	ppK^0K^0	355
72	ppK^0 MM[Kn]	280
Total		12021

EVENT TYPE 42		
Mark	Final State	
11-12	$\Lambda nK^0\pi^+\pi^+$	Λ-pπ^-, K_s-$\pi^+\pi^-$
13-14	$\Lambda K^0\pi^+\pi^+$ MM[n]	Λ-pπ^-, K_s-$\pi^+\pi^-$
15	$K^0K^0\pi^+\pi^+$ MM[nn]	K_s-$\pi^+\pi^-$, K_s-$\pi^+\pi^-$
41-42	$\Lambda pK^0\pi^+$	Λ-pπ^-, K_s-$\pi^+\pi^-$
43-44	$\Sigma^0 pK^0\pi^+$	Σ^0-$\Lambda\gamma$, Λ-pπ^-, K_s-$\pi^+\pi^-$
45-46	$\Lambda pK^0\pi^+\pi^0$	Λ-pπ^-, K_s-$\pi^+\pi^-$
47-48	$\Lambda pK^0\pi^+$ MM[n]	Λ-pπ^-, K_s-$\pi^+\pi^-$
49	$pnK^0K^0\pi^+$	K_s-$\pi^+\pi^-$, K_s-$\pi^+\pi^-$
50	$pK^0K^0\pi^+$ MM[nn]	K_s-$\pi^+\pi^-$, K_s-$\pi^+\pi^-$
71	$ppK^0K^0\pi^-$	K_s-$\pi^+\pi^-$, K_s-$\pi^+\pi^-$
72	$ppK^0K^0\pi^-\pi^0$	K_s-$\pi^+\pi^-$, K_s-$\pi^+\pi^-$
73	$ppK^0K^0\pi^-$ MM[nn]	K_s-$\pi^+\pi^-$, K_s-$\pi^+\pi^-$
Total		1568

Events
175
139
7
283
139
284
238
121
29
121
40
12
1568

No fiducial cuts or weights have been applied.

Final States and Number of Events Assigned to Each

Table 2.8 (Page 1)

EVENT TYPE 64		
Mark	Final State	Events
11	$\Sigma^+ nK^0 \pi^+ \pi^-$	1
12	$\Sigma^+ nK^0 \pi^+ \pi^+ \pi^-$	4
13	$\Sigma^+ K^0 \pi^+ \pi^-$ MM[nn]	2
14	$\Sigma^+ K^0 \pi^+ \pi^+ \pi^-$ MM[nn]	2
15	$\Lambda n K^+ \pi^+ \pi^+ \pi^-$	13
16	$\Lambda K^+ \pi^+ \pi^+ \pi^-$ MM[n]	7
17	$K^+ \bar{K}^0 \pi^+ \pi^+ \pi^-$ MM[nn]	3
41	$\Sigma^+ pK^0 \pi^+ \pi^-$	45
42	$\Sigma^+ pK^0 \pi^+ \pi^-$	43
43	$\Sigma^+ pK^0 \pi^+ \pi^0 \pi^-$	11
44	$\Sigma^+ pK^0 \pi^+ \pi^0 \pi^-$	14
45	$\Sigma^+ pK^0 \pi^+ \pi^-$ MM[nn]	2
46	$\Sigma^+ pK^0 \pi^+ \pi^-$ MM[nn]	2
47	$\Lambda p K^+ \pi^+ \pi^-$	86
48	$\Lambda p K^+ \pi^+ \pi^0 \pi^-$	33
49	$\Lambda p K^+ \pi^+ \pi^-$ MM[n]	18
50	$\Sigma^0 p K^+ \pi^+ \pi^-$	18
51	$p n K^+ \bar{K}^0 \pi^+ \pi^-$ MM[nn]	20
52	$p K^+ \bar{K}^0 \pi^+ \pi^-$ MM[nn]	6
71	$p p K^+ \bar{K}^0 \pi^-$	15
72	$p p K^+ \bar{K}^0 \pi^0 \pi^-$	6
73	$p p K^+ \bar{K}^0 \pi^-$ MM[nn]	4
Total		335

EVENT TYPE 74		
Mark	Final State	Events
11	$\Sigma^- nK^0 \pi^+ \pi^+ \pi^-$	10
12	$\Sigma^- K^0 \pi^+ \pi^+ \pi^-$ MM[nn]	1
13	$K^0 K^- \pi^+ \pi^+ \pi^+ \pi^-$ MM[nn]	1
41	$\Sigma^- pK^0 \pi^+ \pi^-$	73
42	$\Sigma^- pK^0 \pi^+ \pi^+ \pi^0 \pi^-$	19
43	$\Sigma^- pK^0 \pi^+ \pi^+$ MM[nn]	4
44	$p n K^0 K^- \pi^+ \pi^+ \pi^-$	13
45	$p K^0 K^- \pi^+ \pi^+$ MM[nn]	5
71	$p p K^0 K^- \pi^+ \pi^-$	14
72	$p p K^0 K^- \pi^+ \pi^0 \pi^-$	3
73	$p p K^0 K^- \pi^+ \pi^-$ MM[nn]	3
Total		146

EVENT TYPE 88		
Mark	Final State	Events
11	$\Sigma^+ nK^0 \pi^+$	87
12	$\Sigma^+ nK^0 \pi^+ \pi^-$	139
13	$\Sigma^+ K^0 \pi^+$ MM[nn]	42
14	$\Sigma^+ K^0 \pi^+ \pi^-$ MM[nn]	48
15	$\Lambda n K^+ \pi^+$	91
16	$\Lambda K^+ \pi^+$ MM[n]	111
17	$K^+ \bar{K}^0 \pi^+$ MM[nn]	66
41	$\Sigma^+ pK^0$	32
42	$\Sigma^+ pK^0 \pi^-$	32
43	$\Sigma^+ pK^0 \pi^0$	26
44	$\Sigma^+ pK^0 \pi^0 \pi^-$	39
45	$\Sigma^+ pK^0$ MM[nn]	13
46	$\Sigma^+ pK^0$ MM[n]	15
47	$\Lambda p K^+$	17
48	$\Lambda p K^+ \pi^0$	69
49	$\Lambda p K^+$ MM[n]	80
50	$\Sigma^0 p K^+$	14
51	$p n K^+ \bar{K}^0$	132
52	$p K^+ \bar{K}^0$ MM[nn]	52
Total		1105

EVENT TYPE 64		
Mark	Final State	Events
11	$\Sigma^+ pn^0, K_s \pi^+ \pi^-$	1
12	$\Sigma^+ n\pi^+, K_s \pi^+ \pi^-$	4
13	$\Sigma^+ pn^0, K_s \pi^+ \pi^-$	2
14	$\Sigma^+ n\pi^+, K_s \pi^+ \pi^-$	2
15	$\Lambda p \pi^-$	13
16	$\Lambda p \pi^-$	7
17	$K_s \pi^+ \pi^+ \pi^-$	3
41	$\Sigma^+ pn^0, K_s \pi^+ \pi^-$	45
42	$\Sigma^+ n\pi^+, K_s \pi^+ \pi^-$	43
43	$\Sigma^+ pn^0, K_s \pi^+ \pi^-$	11
44	$\Sigma^+ n\pi^+, K_s \pi^+ \pi^-$	14
45	$\Sigma^+ pn^0, K_s \pi^+ \pi^-$	2
46	$\Sigma^+ n\pi^+, K_s \pi^+ \pi^-$	2
47	$\Lambda p \pi^-$	86
48	$\Lambda p \pi^-$	33
49	$\Lambda p \pi^-$	18
50	$\Sigma^0 \Lambda \gamma, \Lambda p \pi^-$	18
51	$K_s \pi^+ \pi^-$	20
52	$K_s \pi^+ \pi^-$	6
71	$K_s \pi^+ \pi^-$	15
72	$K_s \pi^+ \pi^-$	6
73	$K_s \pi^+ \pi^-$	4
Total		335

EVENT TYPE 74		
Mark	Final State	Events
11	$\Sigma^- n\pi^-, K_s \pi^+ \pi^-$	10
12	$\Sigma^- n\pi^-, K_s \pi^+ \pi^-$	1
13	$K_s \pi^+ \pi^-$	1
41	$\Sigma^- n\pi^-, K_s \pi^+ \pi^-$	73
42	$\Sigma^- n\pi^-, K_s \pi^+ \pi^-$	19
43	$\Sigma^- n\pi^-, K_s \pi^+ \pi^-$	4
44	$K_s \pi^+ \pi^-$	13
45	$K_s \pi^+ \pi^-$	5
71	$K_s \pi^+ \pi^-$	14
72	$K_s \pi^+ \pi^-$	3
73	$K_s \pi^+ \pi^-$	3
Total		146

XBL 729-1814

No fiducial cuts or weights have been applied.

Final States and Number of Events Assigned to Each

Table 2.8 (Page 2)

E.T. 32 Mark	EVEN	ALL P ODD	ODD/ALL	P=3	ALL P=4	ALL P
11	803	0	0	503	300	803
12	1728	0	0	852	876	1728
13	294	0	0	78	216	294
14	188	0	0	98	90	188
15	452	0	0	250	202	452
41	393	414	0.51	583	244	807
42	192	191	0.50	275	108	383
43	504	539	0.52	650	393	1043
44	956	657	0.41	811	802	1613
45	359	132	0.27	281	210	491
46	349	158	0.31	172	335	507
47	251	104	0.29	214	141	355
48	142	84	0.37	128	98	226
49	455	193	0.30	305	343	648
50	417	391	0.48	502	306	808
51	700	360	0.34	621	439	1060
71	183	172	0.48	186	169	355
72	153	107	0.41	106	154	260
Total	8519	3502	0.29	6595	5426	12021

E.T. 42 Mark	EVEN	ALL P ODD	ODD/ALL	P=3	ALL P=4	ALL P
11-12	175	0	0	93	82	175
13-14	139	0	0	49	90	139
15	7	0	0	1	6	7
41-42	148	135	0.48	208	75	283
43-44	89	70	0.50	91	48	139
45-46	126	138	0.52	127	137	264
47-48	148	90	0.38	82	156	238
49	96	25	0.21	46	75	121
50	26	3	0.10	6	23	29
71	50	71	0.59	72	49	121
72	22	18	0.45	20	20	40
73	6	6	0.50	1	11	12
Total	1012	556	0.35	796	772	1568

E.T. 34 Mark	EVEN	ALL P ODD	ODD/ALL	P=3	ALL P=4	ALL P
11	154	0	0	49	105	154
12	98	0	0	19	79	98
13	7	0	0	0	7	7
14	2	0	0	0	2	2
15	5	0	0	1	4	5
16	10	0	0	0	10	10
41	368	468	0.56	500	336	836
42	183	191	0.51	109	265	374
43	127	69	0.35	51	145	196
44	111	144	0.58	128	127	255
45	57	24	0.30	16	65	81
46	20	9	0.31	1	28	29
47	45	4	0.08	12	37	49
48	8	4	0.33	1	11	12
49	36	31	0.46	26	41	67
50	21	9	0.30	10	20	30
51	18	9	0.33	5	22	27
52	90	87	0.49	45	132	177
53	59	27	0.31	20	66	86
71	63	91	0.59	55	89	154
72	38	22	0.37	13	47	60
73	3	4	0.57	0	7	7
74	91	108	0.54	84	115	199
76	38	31	0.45	6	63	69
76	10	6	0.38	3	13	16
77	30	21	0.41	4	47	51
78	7	7	0.50	3	11	14
Total	1699	1368	0.45	1161	1904	3065

E.T. 44 Mark	EVEN	ALL P ODD	ODD/ALL	P=3	ALL P=4	ALL P
11-12	6	0	0	4	2	6
13-14	3	0	0	0	3	3
15	0	0	-	0	0	0
41-42	27	26	0.49	14	39	53
45-46	11	7	0.39	1	17	18
47-48	11	7	0.39	1	17	18
49	2	0	0	0	2	2
50	2	0	0	0	2	2
71	10	7	0.41	1	16	17
72	2	0	0	0	2	2
73	1	0	0	0	1	1
Total	75	47	0.39	21	101	122

No fiducial cuts or weights have been applied.

See Table 2.8 for identification of final states by mark number.

There are separate tallies for even- and odd-pronged events, and for beam momenta ≈3 GeV/c (2.7 and 3.1) and ≈4 GeV/c (3.7 and 4.2).

Event Tally by Spectator Visibility and Beam Momentum

Table 2.9 (Page 1)

XBL 729-1815

E.T. 67 Mark	EVEN	ALL P ODD	ODD/ALL	P=3	ALL P=4	ALL P
11	87	0	0	64	23	87
12	139	0	0	104	35	139
13	42	0	0	22	20	42
14	48	0	0	20	28	48
15	91	0	0	55	36	91
16	111	0	0	56	55	111
17	66	0	0	34	32	66
41	14	18	0.56	27	5	32
42	16	16	0.50	27	5	32
43	16	10	0.38	14	12	26
44	22	17	0.44	24	15	39
45	7	6	0.46	7	6	13
46	6	9	0.60	7	8	15
47	10	7	0.41	15	2	17
48	33	36	0.52	44	25	69
49	50	30	0.38	42	38	80
50	6	8	0.57	12	2	14
51	90	42	0.32	76	56	132
52	35	17	0.33	25	27	52
Total	889	216	0.20	675	430	1105

E.T. 64 Mark	EVEN	ALL P ODD	ODD/ALL	P=3	ALL P=4	ALL P
11	1	0	0	0	1	1
12	4	0	0	0	4	4
13	2	0	0	0	2	2
14	2	0	0	1	1	2
15	13	0	0	4	9	13
16	7	0	0	2	5	7
17	3	0	0	0	3	3
41	26	19	0.42	20	25	45
42	14	29	0.67	23	20	43
43	8	3	0.27	4	7	11
44	10	4	0.29	4	10	14
45	2	0	0	0	2	2
46	2	0	0	2	0	2
47	25	41	0.62	44	22	66
48	17	16	0.48	10	23	33
49	12	6	0.33	7	11	18
50	9	9	0.50	12	6	18
51	11	9	0.45	2	18	20
52	4	2	0.33	1	5	6
71	6	9	0.60	7	8	15
72	5	1	0.17	1	5	6
73	4	0	0	1	3	4
Total	187	148	0.44	145	190	335

E.T. 74 Mark	EVEN	ALL P ODD	ODD/ALL	P=3	ALL P=4	ALL P
11	10	0	0	4	6	10
12	1	0	0	0	1	1
13	1	0	0	0	1	1
41	29	44	0.60	36	35	73
42	13	6	0.32	6	13	19
43	3	1	0.25	1	3	4
44	8	5	0.38	2	11	13
45	2	3	0.60	1	4	5
71	6	8	0.57	2	12	14
72	2	1	0.33	0	3	3
73	2	1	0.33	2	1	3
Total	77	69	0.47	56	90	146

XBL 729-1816

No fiducial cuts or weights have been applied.

See Table 2.8 for identification of final states by mark number.

There are separate tallies for even- and odd-pronged events, and for beam momenta ≈3 GeV/c (2.7 and 3.1) and ≈4 GeV/c (3.7 and 4.2).

Event Tally by Spectator Visibility and Beam Momentum

Table 2.9 (Page 2)

EVENT	TYPE 32		AVERAGE
Mark	Final State	Vis.	σ (μb)
11	$\Lambda pK^+\pi^+$	(590)	73.7 ± 5.8
12	$\Lambda K^+\pi^+\pi^-$ M.M.[n]	(590)	156.3 ± 11.6
13	$K^+K^0\pi^+\pi^-$ M.M.[nn]	(317)	51.1 ± 4.6
14	$K^0\pi^+\pi^+\pi^-$ M.M.[Λn]	(344)	29.5 ± 2.8
15	$\Lambda\pi^+\pi^+$ M.M.[nK]	(640)	37.8 ± 3.0
41	ΛpK^+	(590)	75.6 ± 5.9
42	Σ^0pK^+	(590)	34.8 ± 3.0
43	$\Lambda pK^+\pi^0$	(590)	95.8 ± 7.4
44	ΛpK^+ M.M.[π]	(590)	145.0 ± 10.8
45	pnK^+K^0	(317)	86.0 ± 7.1
46	pK^+K^0 M.M.[nn]	(317)	86.6 ± 7.2
47	$\Lambda pK^0\pi^+$	(124)	145.7 ± 12.4
48	$\Sigma^0pK^0\pi^+$	(124)	97.0 ± 9.1
49	$pK^0\pi^+$ M.M.[Λn]	(344)	104.8 ± 7.7
50	$\Lambda pK^0\pi^+$	(420)	100.3 ± 7.2
51	Λpn^+ M.M.[K]	(640)	88.4 ± 6.1
71	ppK^0K^0	(226)	86.2 ± 7.0
72	ppK^0 M.M.[Kπ]	(344)	43.1 ± 3.7

EVENT	TYPE 42		AVERAGE
Mark	Final State	Vis.	σ (μb)
11-12	$\Lambda nK^0\pi^+\pi^+$	(220)	44.1 ± 4.3
13-14	$\Lambda K^0\pi^+\pi^+$ M.M.[n]	(220)	33.7 ± 3.6
15	$K^0K^0\pi^+\pi^+$ M.M.[nn]	(118)	3.8 ± 1.4
41-42	$\Lambda pK^0\pi^+$	(220)	68.2 ± 6.0
43-44	$\Sigma^0pK^0\pi^+$	(220)	34.5 ± 3.7
45-46	$\Lambda pK^0\pi^+\pi^0$	(220)	70.3 ± 6.1
47-48	$\Lambda pK^0\pi^+$ M.M.[π]	(220)	55.0 ± 5.1
49	$pnK^0K^0\pi^+$	(118)	55.9 ± 6.2
50	$pK^0K^0\pi^+$ M.M.[nn]	(118)	14.9 ± 2.8
71	ppK^0K^0	(118)	59.0 ± 6.4
72	$ppK^0K^0\pi^0$	(118)	16.6 ± 3.0
73	ppK^0K^0 M.M.[ππ]	(118)	4.5 ± 1.5

EVENT	TYPE 34		AVERAGE
Mark	Final State	Vis.	σ (μb)
11	$\Lambda nK^+\pi^+\pi^-$	(590)	14.9 ± 1.6
12	$\Lambda K^+\pi^+\pi^-$ M.M.[n]	(590)	9.0 ± 1.1
13	$K^+K^0\pi^+\pi^-$ M.M.[nn]	(317)	1.26 ± .48
14	$K^0K^-\pi^+\pi^+\pi^+$ M.M.[nn]	(317)	.40 ± .27
15	$K^0\pi^+\pi^+\pi^-$ M.M.[Λn]	(344)	.91 ± .39
16	$\Lambda\pi^+\pi^+\pi^-$ M.M.[nK]	(640)	.75 ± .26
41	$\Lambda pK^+\pi^+\pi^-$	(590)	76.8 ± 6.0
42	$\Lambda pK^+\pi^+\pi^0\pi^-$	(590)	34.3 ± 3.0
43	$\Lambda pK^+\pi^+\pi^-$ M.M.[π]	(590)	18.4 ± 1.8
44	$\Sigma^0pK^+\pi^+\pi^-$	(590)	22.8 ± 2.2
45	$pnK^+K^0\pi^+\pi^-$	(317)	13.7 ± 1.8
46	$pK^+K^0\pi^+\pi^-$ M.M.[nn]	(317)	5.3 ± 1.0
47	$p\Lambda K^0K^-\pi^+\pi^+$	(317)	8.9 ± 1.4
48	$p\Lambda K^0K^-\pi^+\pi^+$ M.M.[nn]	(317)	2.01 ± .61
49	$\Lambda pK^0\pi^+\pi^+\pi^-$	(124)	30.1 ± 4.2
50	$\Sigma^0pK^0\pi^+\pi^+\pi^-$	(124)	14.8 ± 2.7
51	$pK^0\pi^+\pi^+\pi^-$ M.M.[Λn]	(344)	4.15 ± .86
52	$\Lambda pK^0\pi^+\pi^+\pi^-$	(420)	23.7 ± 2.3
53	$\Lambda pn^+\pi^-$ M.M.[K]	(640)	7.30 ± .92
71	$ppK^+K^0\pi^-$	(317)	28.4 ± 3.1
72	$ppK^+K^0\pi^0\pi^-$	(317)	11.3 ± 1.8
73	$ppK^+K^0\pi^-$ M.M.[ππ]	(317)	1.42 ± .51
74	$ppK^0K^-\pi^+$	(317)	35.9 ± 3.5
75	$ppK^0K^-\pi^+\pi^0$	(317)	12.5 ± 1.7
76	$ppK^0K^-\pi^+$ M.M.[ππ]	(317)	3.00 ± .75
77	$ppK^0K^0\pi^+\pi^-$	(226)	12.5 ± 1.9
78	$ppK^0\pi^+\pi^-$ M.M.[Kπ]	(344)	2.49 ± .85

EVENT	TYPE 44		AVERAGE
Mark	Final State	Vis.	σ (μb)
11-12	$\Lambda nK^0\pi^+\pi^+\pi^-$	(220)	1.26 ± .57
13-14	$\Lambda K^0\pi^+\pi^+\pi^-$ M.M.[n]	(220)	.70 ± .42
15	$K^0K^0\pi^+\pi^+\pi^-$ M.M.[nn]	(118)	0.
41-42	$\Lambda pK^0\pi^+\pi^-$	(220)	14.0 ± 2.1
43-44	$\Lambda pK^0\pi^+\pi^0\pi^-$	(220)	4.8 ± 1.1
45-46	$\Lambda pK^0\pi^+\pi^+\pi^-$ M.M.[π]	(220)	4.9 ± 1.1
47-48	$pn\Lambda K^0\pi^+\pi^+\pi^-$	(118)	.67 ± .56
49	$p\Lambda K^0K^0\pi^+\pi^-$	(118)	.70 ± .58
50	$p\Lambda K^0K^0\pi^+\pi^-$ M.M.[nn]	(118)	10.4 ± 2.3
71	$ppK^0K^0\pi^+\pi^-$	(118)	.70 ± .57
72	$ppK^0K^0\pi^+\pi^-\pi^0$	(118)	.69 ± .57
73	$ppK^0K^0\pi^-$ M.M.[nn]	(118)	

XBL 729-1817

SEE TEXT.

These estimates for the average cross section in the region of 3 to 4 GeV/c were obtained from the event tallies with cuts, using the indicated visibility factors.

Final-State Cross-Section Estimates with Statistical Uncertainties

Table 2.10 (Page 1)

EVENT TYPE 62			AVERAGE
Mark	Final State	Vis.	σ (μb)
11	$\Sigma^+ nK^0\pi^+\pi^-$	(.178)	36.3 ± 4.1
12	$\Sigma^+ nK^0\pi^+\pi^-$	(.166)	50.4 ± 5.2
13	$\Sigma^+ K^0\pi^+\pi^-$ M.M.[nn]	(.178)	17.2 ± 2.6
14	$\Sigma^+ K^0\pi^+\pi^-$ M.M.[nn]	(.166)	17.8 ± 2.7
15	$\Lambda pK^+\pi^+\pi^-$	(Not used)	5.12 ± .62
16	$\Lambda K^+\pi^+\pi^-$ M.M.[n]	(Not used)	5.71 ± .66
17	$K^+K^0\pi^+\pi^-$ M.M.[nn]	(Not used)	3.74 ± .51
41	$\Sigma^+ pK^0$	(.178)	9.0 ± 1.8
42	$\Sigma^+ pK^0$	(.166)	10.7 ± 2.0
43	$\Sigma^+ pK^0\pi^0$	(.178)	11.0 ± 2.0
44	$\Sigma^+ pK^0\pi^0$	(.166)	13.0 ± 2.2
45	$\Sigma^+ pK^0$ M.M.[nn]	(.178)	4.6 ± 1.2
46	$\Sigma^+ pK^0$ M.M.[nn]	(.166)	5.6 ± 1.4
47	ΛpK^+	(Not used)	.77 ± .21
48	$\Lambda pK^+\pi^0$	(Not used)	3.71 ± .51
49	ΛpK^+ M.M.[n]	(Not used)	4.47 ± .57
50	$\Sigma^0 pK^+$	(Not used)	.67 ± .20
51	$pnK^+\bar{K}^0$	(Not used)	6.72 ± .74
52	$pK^+\bar{K}^0$ M.M.[nn]	(Not used)	3.01 ± .45

EVENT TYPE 64			AVERAGE
Mark	Final State	Vis.	σ (μb)
11	$\Sigma^+ nK^0\pi^+\pi^-$	(.178)	0.
12	$\Sigma^+ nK^0\pi^+\pi^-$	(.166)	1.95 ± .82
13	$\Sigma^+ K^0\pi^+\pi^-$ M.M.[nn]	(.178)	.98 ± .56
14	$\Sigma^+ K^0\pi^+\pi^-$ M.M.[nn]	(.166)	.47 ± .40
15	$\Lambda nK^+\pi^+\pi^-$	(Not used)	.74 ± .21
16	$\Lambda K^+\pi^+\pi^-$ M.M.[n]	(Not used)	.36 ± .14
17	$K^+\bar{K}^0\pi^+\pi^-$ M.M.[nn]	(Not used)	.20 ± .11
41	$\Sigma^+ pK^0\pi^+\pi^-$	(.178)	18.2 ± 2.8
42	$\Sigma^+ pK^0\pi^+\pi^-$	(.166)	16.8 ± 2.6
43	$\Sigma^+ pK^0\pi^+\pi^0\pi^-$	(.178)	4.0 ± 1.1
44	$\Sigma^+ pK^0\pi^+\pi^0\pi^-$	(.166)	6.0 ± 1.5
45	$\Sigma^+ pK^0\pi^+\pi^-$ M.M.[nn]	(.178)	0.
46	$\Sigma^+ pK^0\pi^+\pi^-$ M.M.[nn]	(.166)	0.
47	$\Lambda pK^+\pi^+\pi^-$	(Not used)	3.28 ± .47
48	$\Lambda pK^+\pi^+\pi^0\pi^-$	(Not used)	1.93 ± .35
49	$\Lambda pK^+\pi^+\pi^-$ M.M.[n]	(Not used)	1.05 ± .25
50	$\Sigma^0 pK^+\pi^+\pi^-$	(Not used)	1.04 ± .25
51	$pnK^+\bar{K}^0\pi^+\pi^-$	(Not used)	1.24 ± .27
52	$pK^+\bar{K}^0\pi^+\pi^-$ M.M.[nn]	(Not used)	.41 ± .15
71	$ppK^+\bar{K}^0\pi^-$	(Not used)	.84 ± .22
72	$ppK^+\bar{K}^0\pi^0\pi^-$	(Not used)	.39 ± .15
73	$ppK^+\bar{K}^0\pi^-$ M.M.[nn]	(Not used)	.25 ± .12

EVENT TYPE 74			AVERAGE
Mark	Final State	Vis.	σ (μb)
11	$\Sigma^- nK^0\pi^+\pi^+$	(.344)	1.71 ± .53
12	$\Sigma^- K^0\pi^+\pi^+$ M.M.[nn]	(.344)	.29 ± .22
13	$K^0\Sigma^-\pi^+\pi^+$ M.M.[nn]	(Not used)	.06 ± .06
41	$\Sigma^- pK^0\pi^+$	(.344)	12.7 ± 1.6
42	$\Sigma^- pK^0\pi^+\pi^0$	(.344)	3.86 ± .82
43	$\Sigma^- pK^0\pi^+$ M.M.[nn]	(.344)	.88 ± .33
44	$pnK^0\Sigma^-\pi^+$	(Not used)	.76 ± .21
45	$pK^0\Sigma^-\pi^+\pi^+$ M.M.[nn]	(Not used)	.36 ± .14
71	$ppK^0\Sigma^-\pi^+$	(Not used)	.68 ± .20
72	$ppK^0\Sigma^-\pi^+\pi^0$	(Not used)	.16 ± .09
73	$ppK^0\Sigma^-\pi^+$ M.M.[nn]	(Not used)	.21 ± .11

XBL 729-1818

SEE TEXT.

These estimates for the average cross section in the region of 3 to 4 GeV/c were obtained from the event tallies with cuts, using the indicated visibility factors.

Final-State Cross-Section Estimates with Statistical Uncertainties

Table 2.10 (Page 2)

4C–2C Hypotheses

ET.MK	Final State	Vis.	σ (μb) P~3 GeV/c	P~4 GeV/c
32.41	ΛpK^+	(.590)	88.1 ± 7.1	58.6 ± 8.1
32.42	$\Sigma^0 pK^+$	(.590)	42.0 ± 3.9	24.9 ± 3.9
34.41	$\Lambda pK^+\pi^+\pi^-$	(.590)	76.1 ± 6.3	77.7 ± 10.5
34.44	$\Sigma^0 pK^+\pi^+\pi^-$	(.590)	18.5 ± 2.1	28.6 ± 4.4
34.71	$ppK^+\bar{K}^0\pi^-$	(.317)	18.7 ± 2.7	43.9 ± 6.9
34.74	$ppK^0K^-\pi^+$	(.317)	25.5 ± 3.3	50.2 ± 7.7
42.41–42	$\Lambda pK^0\pi^+$	(.220)	83.7 ± 7.9	49.4 ± 8.1
42.43–44	$\Sigma^0 pK^0\pi^+$	(.220)	37.5 ± 4.6	30.5 ± 5.6
42.71	$ppK^0\bar{K}^0$	(.118)	59.1 ± 7.8	58.8 ± 10.7
44.41–42	$\Lambda pK^0\pi^+\pi^+\pi^-$	(.220)	6.8 ± 1.8	23.9 ± 4.7
44.71	$ppK^0\bar{K}^0\pi^+\pi^-$	(.118)	1.3 ± 1.0	22.8 ± 5.7
62.41	$\Sigma^+ pK^0$	(.178)	12.5 ± 2.7	4.2 ± 1.8
62.42	$\Sigma^+ pK^0$	(.166)	15.5 ± 3.2	4.1 ± 1.9
62.47	ΛpK^+	(Not used)	1.11 ± .33	.30 ± .20
62.50	$\Sigma^0 pK^+$	(Not used)	.94 ± .30	.31 ± .20
64.41	$\Sigma^+ pK^0\pi^+\pi^-$	(.178)	13.4 ± 2.8	24.7 ± 5.2
64.42	$\Sigma^+ pK^0\pi^+\pi^-$	(.166)	16.4 ± 3.2	17.3 ± 4.3
64.47	$\Lambda pK^+\pi^+\pi^-$	(Not used)	3.94 ± .66	2.38 ± .63
64.50	$\Sigma^0 pK^+\pi^+\pi^-$	(Not used)	1.19 ± .34	.85 ± .35
64.71	$ppK^+\bar{K}^0\pi^-$	(Not used)	.57 ± .24	1.22 ± .42
74.41	$\Sigma^- pK^0\pi^+\pi^+$	(.344)	12.0 ± 2.0	13.6 ± 2.8
74.71	$ppK^0K^-\pi^+$	(Not used)	.22 ± .15	1.31 ± .44

SEE TEXT.

The indicated uncertainties are statistical only.

XBL 729-1819

Cross-Section Estimates by Production Constraint Class and Beam Momentum

Table 2.11 (Page 1)

1C Hypotheses

ET.MK	Final State	Vis.	σ (μb) P~3 GeV/c	P~4 GeV/c
32.11	$\Lambda n K^+\pi^+$	(.590)	79.5 ± 6.5	65.8 ± 9.1
32.43	$\Lambda p K^+\pi^0$	(.590)	99.4 ± 7.9	90.8 ± 12.2
32.45	$pn K^+\bar{K}^0$	(.317)	79.7 ± 7.3	94.7 ± 13.4
32.47	$\Lambda p K^0\pi^+$	(.124)	145.4 ± 14.0	146.3 ± 21.7
32.48	$\Sigma^0 p K^0\pi^+$	(.124)	90.6 ± 10.1	105.8 ± 16.7
32.50	$\Lambda p K^0\pi^+$	(.420)	105.9 ± 8.0	92.6 ± 12.4
32.71	$pp K^0\bar{K}^0$	(.226)	76.2 ± 7.3	99.9 ± 14.2
34.11	$\Lambda n K^+\pi^+\pi^+\pi^-$	(.590)	7.7 ± 1.2	24.6 ± 3.9
34.42	$\Lambda p K^+\pi^+\pi^0\pi^-$	(.590)	15.2 ± 1.9	60.3 ± 8.4
34.45	$pn K^+\bar{K}^0\pi^+\pi^-$	(.317)	3.6 ± 1.1	27.6 ± 4.8
34.47	$pn K^0 K^-\pi^+\pi^+$	(.317)	4.0 ± 1.1	15.6 ± 3.2
34.49	$\Lambda p K^0\pi^+\pi^+\pi^-$	(.124)	19.2 ± 4.0	45.0 ± 8.8
34.50	$\Sigma^0 p K^0\pi^+\pi^+\pi^-$	(.124)	7.8 ± 2.5	24.4 ± 5.9
34.52	$\Lambda p K^0\pi^+\pi^+\pi^-$	(.420)	10.5 ± 1.7	41.6 ± 6.2
34.72	$pp K^+\bar{K}^0\pi^0\pi^-$	(.317)	4.4 ± 1.2	20.8 ± 3.9
34.75	$pp K^0 K^-\pi^+\pi^0$	(.317)	1.82 ± .75	26.9 ± 4.7
34.77	$pp K^0\bar{K}^0\pi^+\pi^-$	(.226)	1.01 ± .66	28.2 ± 5.3
42.11-12	$\Lambda n K^0\pi^+\pi^+$	(.220)	39.3 ± 4.8	50.7 ± 8.2
42.45-46	$\Lambda p K^0\pi^+\pi^0$	(.220)	54.4 ± 5.9	91.9 ± 13.3
42.49	$pn K^0\bar{K}^0\pi^+$	(.118)	33.7 ± 5.6	86.1 ± 14.3
42.72	$pp K^0\bar{K}^0\pi^0$	(.118)	13.5 ± 3.4	20.8 ± 5.4
44.11-12	$\Lambda n K^0\pi^+\pi^+\pi^+\pi^-$	(.220)	1.64 ± .85	.74 ± .67
44.45-46	$\Lambda p K^0\pi^+\pi^+\pi^0\pi^-$	(.220)	.66 ± .54	10.4 ± 2.8
44.49	$pn K^0\bar{K}^0\pi^+\pi^+\pi^-$	(.118)	0.	1.6 ± 1.3
44.72	$pp K^0\bar{K}^0\pi^+\pi^-\pi^0$	(.118)	0.	1.6 ± 1.4
62.11	$\Sigma^+ n K^0\pi^+$	(.178)	43.9 ± 5.6	25.9 ± 5.4
62.12	$\Sigma^+ n K^0\pi^+$	(.166)	63.3 ± 7.2	32.8 ± 6.5
62.15	$\Lambda n K^+\pi^+$	(Not used)	5.27 ± .78	4.93 ± 1.00
62.43	$\Sigma^+ p K^0\pi^0$	(.178)	9.3 ± 2.3	13.2 ± 3.5
62.44	$\Sigma^+ p K^0\pi^0$	(.166)	12.0 ± 2.7	14.3 ± 3.8
62.48	$\Lambda p K^+\pi^0$	(Not used)	3.98 ± .86	3.35 ± .78
62.51	$pn K^+\bar{K}^0$	(Not used)	6.50 ± .88	7.0 ± 1.3
64.11	$\Sigma^+ n K^0\pi^+\pi^+\pi^-$	(.178)	0.	0.
64.12	$\Sigma^+ n K^0\pi^+\pi^+\pi^-$	(.166)	0.	4.6 ± 2.0
64.15	$\Lambda n K^+\pi^+\pi^+\pi^-$	(Not used)	.33 ± .18	1.31 ± .44
64.43	$\Sigma^+ p K^0\pi^+\pi^0\pi^-$	(.178)	2.4 ± 1.1	6.3 ± 2.3
64.44	$\Sigma^+ p K^0\pi^+\pi^0\pi^-$	(.166)	2.4 ± 1.2	10.9 ± 3.2
64.48	$\Lambda p K^+\pi^+\pi^0\pi^-$	(Not used)	.95 ± .31	3.27 ± .76
64.51	$pn K^+\bar{K}^0\pi^+\pi^-$	(Not used)	.22 ± .14	2.64 ± .67
64.72	$pp K^+\bar{K}^0\pi^0\pi^-$	(Not used)	.11 ± .10	.76 ± .33
74.11	$\Sigma^- n K^0\pi^+\pi^+\pi^+$	(.344)	1.16 ± .57	2.5 ± 1.0
74.42	$\Sigma^- p K^0\pi^+\pi^+\pi^0$	(.344)	2.11 ± .78	6.3 ± 1.7
74.44	$pn K^0 K^-\pi^+\pi^+$	(Not used)	.23 ± .15	1.49 ± .48
74.72	$pp K^0 K^-\pi^+\pi^0$	(Not used)	0.	.38 ± .23

SEE TEXT.

The indicated uncertainties are statistical only.

XBL 729-1820

Cross-Section Estimates by Production Constraint Class and Beam Momentum

Table 2.11 (Page 2)

0C Hypotheses

FT.MK	Final State	Vis.	σ (μb) P~3 GeV/c	P~4 GeV/c
32.12	$\Lambda K^+\pi^+$ M.M.[n]	(.590)	124.9 ± 9.6	199.1 ± 25.7
32.13	$K^+\bar{K}^0\pi^+$ M.M.[nn]	(.317)	19.9 ± 2.8	93.6 ± 13.2
32.14	$K^0\pi^+\pi^+$ M.M.[Λn]	(.344)	25.2 ± 3.0	35.4 ± 5.6
32.16	$\Lambda\pi^+\pi^+$ M.M.[nK]	(.640)	33.8 ± 3.0	43.2 ± 6.0
32.44	ΛpK^+ M.M.[π]	(.590)	117.9 ± 9.2	182.0 ± 23.6
32.46	$pK^+\bar{K}^0$ M.M.[nπ]	(.317)	44.6 ± 4.8	143.7 ± 19.5
32.49	$pK^0\pi^+$ M.M.[$\Lambda\pi$]	(.344)	82.4 ± 6.9	135.4 ± 17.8
32.51	$\Lambda p\pi^+$ M.M.[K]	(.640)	84.9 ± 6.2	93.1 ± 12.0
32.72	ppK^0 M.M.[Kπ]	(.344)	30.1 ± 3.4	60.8 ± 8.7
34.12	$\Lambda K^+\pi^+\pi^+\pi^-$ M.M.[n]	(.590)	3.06 ± .74	17.1 ± 2.9
34.13	$K^+\bar{K}^0\pi^+\pi^+\pi^-$ M.M.[nn]	(.317)	0.	3.0 ± 1.2
34.14	$K^0K^-\pi^+\pi^+\pi^+$ M.M.[nn]	(.317)	0.	.94 ± .63
34.15	$K^0\pi^+\pi^+\pi^+\pi^-$ M.M.[Λn]	(.344)	.32 ± .30	1.70 ± .83
34.16	$\Lambda\pi^+\pi^+\pi^+\pi^-$ M.M.[nK]	(.640)	0.	1.77 ± .64
34.43	$\Lambda pK^+\pi^+\pi^-$ M.M.[π]	(.590)	7.7 ± 1.2	33.1 ± 4.9
34.46	$pK^+\bar{K}^0\pi^+\pi^-$ M.M.[nπ]	(.317)	.33 ± .32	12.0 ± 2.7
34.48	$pK^0K^-\pi^+\pi^+$ M.M.[nπ]	(.317)	.33 ± .32	4.3 ± 1.4
34.61	$pK^0\pi^+\pi^+\pi^-$ M.M.[$\Lambda\pi$]	(.344)	1.14 ± .57	8.3 ± 2.0
34.63	$\Lambda p\pi^+\pi^+\pi^-$ M.M.[K]	(.640)	2.71 ± .66	13.6 ± 2.3
34.73	$ppK^+K^0\pi^-$ M.M.[$\pi\pi$]	(.317)	0.	3.4 ± 1.2
34.76	$ppK^0K^-\pi^+$ M.M.[$\pi\pi$]	(.317)	1.03 ± .56	5.7 ± 1.7
34.78	$ppK^0\pi^+\pi^-$ M.M.[Kπ]	(.344)	.63 ± .42	5.0 ± 1.5
42.13-14	$\Lambda K^0\pi^+\pi^+$ M.M.[n]	(.220)	15.1 ± 2.7	59.0 ± 9.3
42.15	$K^0\bar{K}^0\pi^+\pi^+$ M.M.[nn]	(.118)	1.2 ± 1.0	7.2 ± 3.0
42.47-48	$\Lambda pK^0\pi^+$ M.M.[π]	(.220)	31.7 ± 4.2	86.7 ± 12.7
42.50	$pK^0\bar{K}^0\pi^+$ M.M.[nπ]	(.118)	4.6 ± 2.0	28.9 ± 6.6
42.73	$ppK^0\bar{K}^0$ M.M.[$\pi\pi$]	(.118)	0.	10.6 ± 3.7
44.13-14	$\Lambda K^0\pi^+\pi^+\pi^+\pi^-$ M.M.[n]	(.220)	0.	1.7 ± 1.0
44.15	$K^0\bar{K}^0\pi^+\pi^+\pi^+\pi^-$ M.M.[nn]	(.118)	0.	0.
44.47-48	$\Lambda pK^0\pi^+\pi^+\pi^-$ M.M.[π]	(.220)	.58 ± .51	10.7 ± 2.8
44.50	$pK^0\bar{K}^0\pi^+\pi^+\pi^-$ M.M.[nπ]	(.118)	0.	1.7 ± 1.4
44.73	$ppK^0\bar{K}^0\pi^+\pi^-$ M.M.[$\pi\pi$]	(.118)	0.	1.6 ± 1.4
62.13	$\Sigma^+K^0\pi^+$ M.M.[nπ]	(.178)	14.2 ± 2.9	21.3 ± 4.7
62.14	$\Sigma^+K^0\pi^+$ M.M.[nπ]	(.166)	10.1 ± 2.5	28.4 ± 5.9
62.16	$\Lambda K^+\pi^+$ M.M.[n]	(Not used)	4.85 ± .74	6.9 ± 1.3
62.17	$K^+\bar{K}^0\pi^+$ M.M.[nn]	(Not used)	2.91 ± .56	4.89 ± .99
62.45	Σ^+pK^0 M.M.[$\pi\pi$]	(.178)	3.3 ± 1.3	6.4 ± 2.3
62.46	Σ^+pK^0 M.M.[$\pi\pi$]	(.166)	2.5 ± 1.2	9.8 ± 3.0
62.49	ΛpK^+ M.M.[π]	(Not used)	3.77 ± .64	5.4 ± 1.1
62.52	$pK^+\bar{K}^0$ M.M.[nπ]	(Not used)	2.34 ± .49	3.92 ± .86
64.13	$\Sigma^+K^0\pi^+\pi^+\pi^-$ M.M.[nπ]	(.178)	0.	2.3 ± 1.3
64.14	$\Sigma^+K^0\pi^+\pi^+\pi^-$ M.M.[nπ]	(.166)	0.	1.10 ± .94
64.16	$\Lambda K^+\pi^+\pi^+\pi^-$ M.M.[n]	(Not used)	.12 ± .11	.70 ± .31
64.17	$K^+\bar{K}^0\pi^+\pi^+\pi^-$ M.M.[nn]	(Not used)	0.	.48 ± .26
64.45	$\Sigma^+pK^0\pi^+\pi^-$ M.M.[$\pi\pi$]	(.178)	0.	0.
64.46	$\Sigma^+pK^0\pi^+\pi^-$ M.M.[$\pi\pi$]	(.166)	0.	0.
64.49	$\Lambda pK^+\pi^+\pi^-$ M.M.[π]	(Not used)	.65 ± .25	1.59 ± .49
64.52	$pK^+\bar{K}^0\pi^+\pi^-$ M.M.[nπ]	(Not used)	.12 ± .11	.81 ± .34
64.73	$ppK^+\bar{K}^0\pi^-$ M.M.[$\pi\pi$]	(Not used)	.11 ± .10	.44 ± .25
74.12	$\Sigma^-K^0\pi^+\pi^+\pi^+$ M.M.[nπ]	(.344)	0.	.68 ± .52
74.13	$K^0K^-\pi^+\pi^+\pi^+$ M.M.[nn]	(Not used)	0.	.14 ± .14
74.43	$\Sigma^-pK^0\pi^+\pi^+$ M.M.[$\pi\pi$]	(.344)	0.	1.60 ± .80
74.45	$pK^0K^-\pi^+\pi^+$ M.M.[nπ]	(Not used)	.18 ± .13	.60 ± .29
74.73	$ppK^0K^-\pi^+$ M.M.[$\pi\pi$]	(Not used)	.25 ± .15	.15 ± .14

SEE TEXT.

XBL 729-1821

The indicated uncertainties are statistical only.

Cross-Section Estimates by Production Constraint Class and Beam Momentum

Table 2.11 (Page 3)

Some explanation of the notation used may be necessary. The final states are grouped in Tables 2.8-2.10 by event type (ET). [See Fig. 2.2.] 'ET 32' denotes both odd-prongs [which are properly called ET 31] and even-prongs [ET 32]. The states are in order of mark number (MK); the only significance of this number is that the numbering starts with 11 [41,71] for hypotheses with 0 [1,2] protons. Missing mass hypotheses are denoted by "M.M.[x]", where the mass of x is the minimum missing mass required. Two-vee hypotheses with a Λ and a K^o have 2 marks, corresponding to the two different vee assignments. In ET 44, mark numbers 43 and 44 were reserved (for the final states corresponding to ET 42, MK 43 and 44 with $\pi^+\pi^-$ added) but were not used because they involved too many tracks for our version of the the fitting program.

The cross sections have been calculated from

$$\sigma = N/(VL).$$

Here N is the number of events, L is the pionic path length (from the last column of Table 2.7), and V is a visibility factor. We have applied the usual cut on fiducial volume and the corresponding weights, but not the cut on spectator momentum. Note especially that the indicated error comes from the statistical error in N (approximated by the square root of the sum of the weights) and from the error in L. No attempt has been made to estimate the error resulting from our disambiguation scheme and fold it in. The small Glauber-screening correction (for the shielding of one nucleon by the other) has not been made.[65]

The visibility factor gives the probability that the secondary decays associated with a specific mark do in fact occur when that final state is produced. The branching ratio for the visible decay of the Λ is roughly 2/3, and for the K^o (via K_s) it is 1/3.[66] The appropriate factor is also included when a Λ or K^o is present (in a track other than a missing mass) but does not decay visibly. We assumed that all Σ's decay. and put in the branching ratio (51.7%) for $\Sigma^+ \rightarrow (p\pi^o)/(n\pi^+)$. Because of the greater probability of scanning losses, the cross sections from the $p\pi^o$ mode are less reliable.

The average probability of a $K^\pm$ not decaying in the chamber was estimated to be (92 ± 3)%, from the tallies of marks with and without these decays. This factor was included if no decay was seen. However, no visibility factor was used for the marks where a $K^\pm$ decay is seen. As noted in Section 2.7, these marks are very biased and no weight for the $K^\pm$ decay was used. Thus, with this exception (for which the tables indicate that the visibility factor is not used), the cross section is for the production of the indicated final state, not of the final

state with the secondary decays.

Comments on the Cross Sections

We have not made any systematic comparison of our cross sections with other reported values. We have compared the results for some of our constrained hypotheses with the cross sections found by Pi63 for the charge symmetric reactions.[67] Our numbers are generally not grossly inconsistent. (The comparison is not shown.) A very crude guess of our systematic error is ±15% for 4C and 2C fits, and ±30% for 1C fits; the cross-sections for missing mass hypotheses should not be taken seriously at all.

As an internal check on the cross-section determinations, we can look at those final states which show up in more than one mark. For example, for a final state containing ΛK^o, the ratios of the number of events with various visible decays should be approximately

$$\Lambda K^o : K^o : \Lambda : \text{none} = 2 : 1 : 4 : 2.$$

(Since these factors have been taken into account, the cross sections in Tables 2.10-2.11 should be the same.) Table 2.12 gives the cross-section ratios for all of the final states with more than one mark.

These ratios show a relative deficiency of the highly constrained 2V events. Several different causes could be involved here, in addition to a systematic bias in the disambiguation scheme. We note, for example, that about 10% of the events which were scanned as 2V were finally called 1V because one of the vees was considered unmeasurable; since this reclassification should result in a passing fit, no remeasurements were done (as was the case for 1V events with a marginal vee). Also, we see that there is an excess of K^o's relative to Λ's (even though we have introduced a strong bias in favor of the Λ hypotheses). We have not investigated these features of the data further.

Reaction	Decays (x/y)	σ_x/σ_y
$\Lambda K^o \pi^+$	$K^o/\Lambda K^o$	2.11 ± 0.26
	$\Lambda/\Lambda K^o$	1.45 ± 0.16
	K^o/Λ	1.45 ± 0.16
$\Lambda K^o \pi^+ \pi^+ \pi^-$	$K^o/\Lambda K^o$	2.15 ± 0.43
	$\Lambda/\Lambda K^o$	1.69 ± 0.30
	K^o/Λ	1.27 ± 0.21
$\Sigma^o K^o \pi^+$	$K^o/\Sigma^o K^o$	2.81 ± 0.40
ppK^oK^o	K^o/K^oK^o	1.46 ± 0.20
$ppK^oK^o\pi^+\pi^-$	K^o/K^oK^o	1.20 ± 0.32

Cross-Section Ratios

Table 2.12

2.10 THE SPECTATOR

For a study of pion-nucleon interactions, the spectator model says that the deuteron can be considered as consisting of a target nucleon and a second nucleon which does not take part in the interaction with the pion beam. The model essentially allows us to ignore the noninteracting spectator (i.e., to make the "impulse approximation"). This model and its application to such a study have been presented in detail elsewhere; the reader who is unfamiliar with it is referred to an extensive review by Musgrave[68] and to the other theses which we have been citing. Here we restrict ourselves to a summary of noteworthy points. We discuss how an invisible spectator is treated in the fitting program and how a visible spectator is identified. The distributions of the fitted momentum of the spectator, and of the spectator direction with respect to the beam, are presented.

Odd-pronged events occur when a spectator proton has lab momentum $\lesssim 80$ MeV/c. Thus, we do have some information about the momentum of an unseen spectator, unlike an unseen neutral. In the fits, an invisible spectator was treated like a measured track with momentum $(p_x,p_y,p_z) = [(0,0,0) \pm (30,30,40)]$ MeV/c. When the momentum components are pulled away from zero in a highly constrained fit, the result is a reasonably good approximation to the distribution of p^2 obtained from the Hulthén wave function for the deuteron. The errors are chosen to make the peaks of the two distributions roughly the same. (The error is larger in the z direction because a short track is more likely to be unseen if it is pointing toward or away from the cameras.)

It should be noted that this method, which is widely used, does have some serious limitations. A final state with no unseen particles other than the spectator is still a 4-production constraint fit, but it is somewhat degraded - for example, there is more contamination from 2-C and 1-C fits (as noted in Section 2.8). In events with one or more other missing particles, there are distortions in the missing four-momentum, and correlations between the beam and the pseudo-measured spectator. [For a detailed discussion of various methods of treating the invisible spectator, see Ref. 69, Chapter 6.]

The program CREE[45] was used to prepare a final physics-data tape from the output of SIOUX. Among other things, CREE performed the Lorentz transformation to the c.m. frame for the pion-nucleon interaction. The effective target four-vector was the difference between the four-vectors of the deuteron (at rest in the lab) and the spectator. If there is only one nucleon in

the final state, it is called the spectator. If there are two nucleons (e.g., $\pi^+ d \rightarrow pnK^+K^0$), the one with the smaller lab momentum is called the spectator; since the non-spectator final-state particles typically have large momenta, this should lead to only a small incidence of misidentification of the spectator. Events with a neutron-containing missing-mass track and a proton with $p_{lab} > 200$ MeV/c, and final states (such as $\Lambda\pi^+\pi^+$ + M.M.) with no measured or calculated nucleon four-vector, were treated as if a neutron at rest were the spectator.

Turning to our results, first we look at the distributions of spectator momentum. Here we divide up the data according to the number of constraints and the identity of the spectator; even and odd prongs have been examined separately. The spectator momentum distributions (in the lab frame) are given in Figure 2.11.

We have not attempted to compare these shapes with the prediction of the Hulthén wave function for the deuteron. (The Hulthén distribution goes to zero at $p_{sp} = 0$ and peaks at about 45 MeV/c.[70]) We take note only of the division into even- vs. odd-prongs, and the fraction of events with $p_{sp} > 300$ MeV/c. This data is given in Table 2.13.

In the impulse approximation, the spectator momentum distribution (and therefore the odd/even ratio) does not depend on the final state (if we neglect the energy dependence of the cross sections). Of course, hypotheses with no final-state protons can appear only in the even prongs. Thus, the other final states can be lost to more marks in the even prongs. The last column of Table 2.13 gives the fraction of the 'good' ($p_{sp} < 300$ MeV/c) events which are odd-prongs (with the statistical error); this percentage does not vary much with constraint class. However, Table 2.9 shows that there is quite a bit of variation among the individual final states.

For the 3 classes which appear in both odd- and even-prongs, we have plotted the odd-prong spectator distribution separately (lower histograms in Fig. 2.11). We see that the 4-C distribution goes to zero at p = 0, with a peak around 40 MeV/c; the even- and odd-prongs join smoothly. As the number of constraints decreases, the odd-prong spectrum is shifted down toward zero and the total spectrum develops a dip around 60 MeV/c. Recall that the spectator momentum was set to zero by the fitting program and gets pulled away as required; the less-constrained hypotheses can conserve momentum without pulling the spectator much.

The Hulthén wave function predicts that about 2% of the spectators have

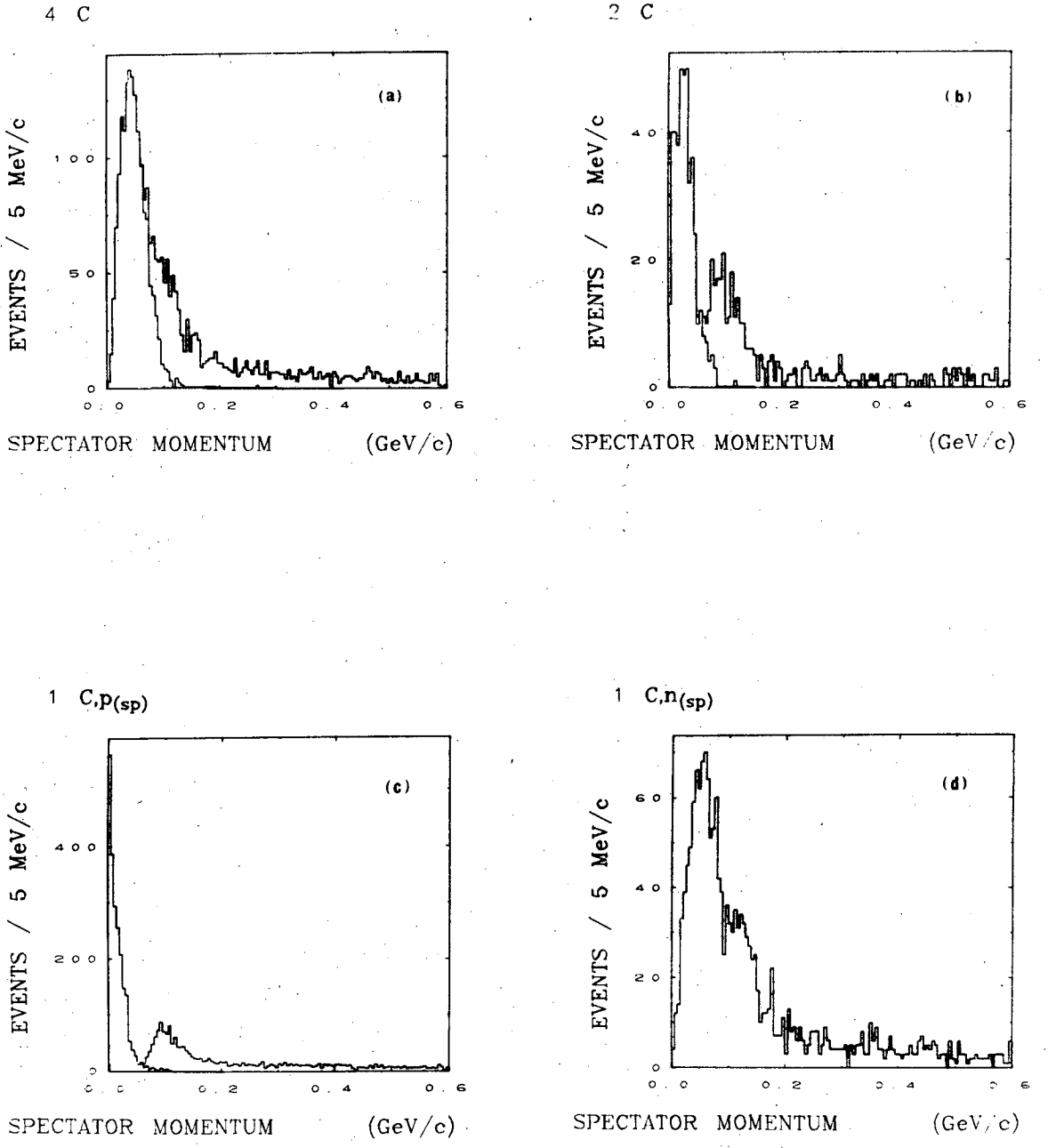
4 C
(a)
EVENTS / 5 MeV/c
SPECTATOR MOMENTUM (GeV/c)
2 C
(b)
EVENTS / 5 MeV/c
SPECTATOR MOMENTUM (GeV/c)
1 C,p(sp)
(c)
EVENTS / 5 MeV/c
SPECTATOR MOMENTUM (GeV/c)
1 C,n(sp)
(d)
EVENTS / 5 MeV/c
SPECTATOR MOMENTUM (GeV/c)
XBL 727-1315

Fig. 2.11

		p_{sp} > 300 MeV/c		Odd-prongs	
#C, N(sp)	Total	#	%	#	% (p_{sp}<300)
4C, p	2807	477	17.0 ± 0.8	1511	64.8 ± 2.1
2C, p	809	124	15.3 ± 1.5	422	61.6 ± 3.8
1C, p	4650	1194	25.7 ± 0.8	2180	63.1 ± 1.7
1C, n	1901	468	24.6 ± 1.3	0	0
0C, p	4279	1168	27.3 ± 0.9	1791	57.6 ± 1.7
0C, none	3916	0	0	0	0
Total	18362	3431	18.7 ± 0.3	5904	39.5 ± 0.6

Spectator Momentum by Constraint Class

Table 2.13

lab momentum above 300 MeV/c.[71] We see much greater percentages; this is a common occurence in deuterium experiments. The excess may be attributed to interactions with the deuteron as a single entity; to multiple scattering (also known as rescattering), where one of the final-state particles interacts with the spectator;[72] misassignment of events, etc. (See Ch. 2 of Benson's thesis, Ref. 69, for an extensive but somewhat speculative discussion of this problem.)

Table 2.13 shows that the excess is greater for the less constrained events. This is not surprising, since the contamination is worse there. Since the typical lab momentum of interacting particles is greater than that of the typical spectator, calling the wrong track the spectator leads to an excess at high momentum.[73] Double scattering and other real physics effects no doubt contribute to the excess. In a study of some 4-C events in our low-momentum $\pi^+ d$ exposure, Rader concluded that the high-momentum excess was not due to misassignment problems.[74] We suggest, however, that the *variation* of the degree of excess among various final states primarily reflects the contribution of misassignment of events.

The impulse approximation suggests that the spectator is left with the direction, as well as the momentum, which it had in the deuteron before the collision. Although the deuteron wave function has no preferred direction in the lab frame, the spectator angular distribution is not expected to be flat. The effect of the invariant Møller flux factor in the rate is to give a dependence on the angle between the spectator and the beam. (The forward-spectator events have a larger relative beam-target momentum and thus a larger flux factor; this gives a roughly linear dependence on $\cos\theta_{sp} = (\hat{N}_{sp} \cdot \hat{\pi}^+_{in})$. The effective c.m. energy of the beam-target system depends on the spectator direction, so any energy dependence in the cross section will affect the shape of this distribution.[75]

Our distributions of $\cos\theta_{sp}$ are given in Figs. 2.12-2.13. The highly constrained even-prong events (Fig. 2.12(a)) show roughly this linear behavior in $\cos\theta_{sp}$. The less constrained fits show a strong peaking in the forward direction which is presumably an artifact of the fitting program. The 4-C odd prongs are roughly flat, as expected. (Since the spectator momentum must be low, the range of the flux factor is smaller than in the even-prong case.) As the number of constraints is reduced we again see in the odd-prongs what are presumably biases introduced by the fitting program: strong peaking in the forward and backward directions and subsidiary peaking at $\cos\theta_{sp} \approx 0$.

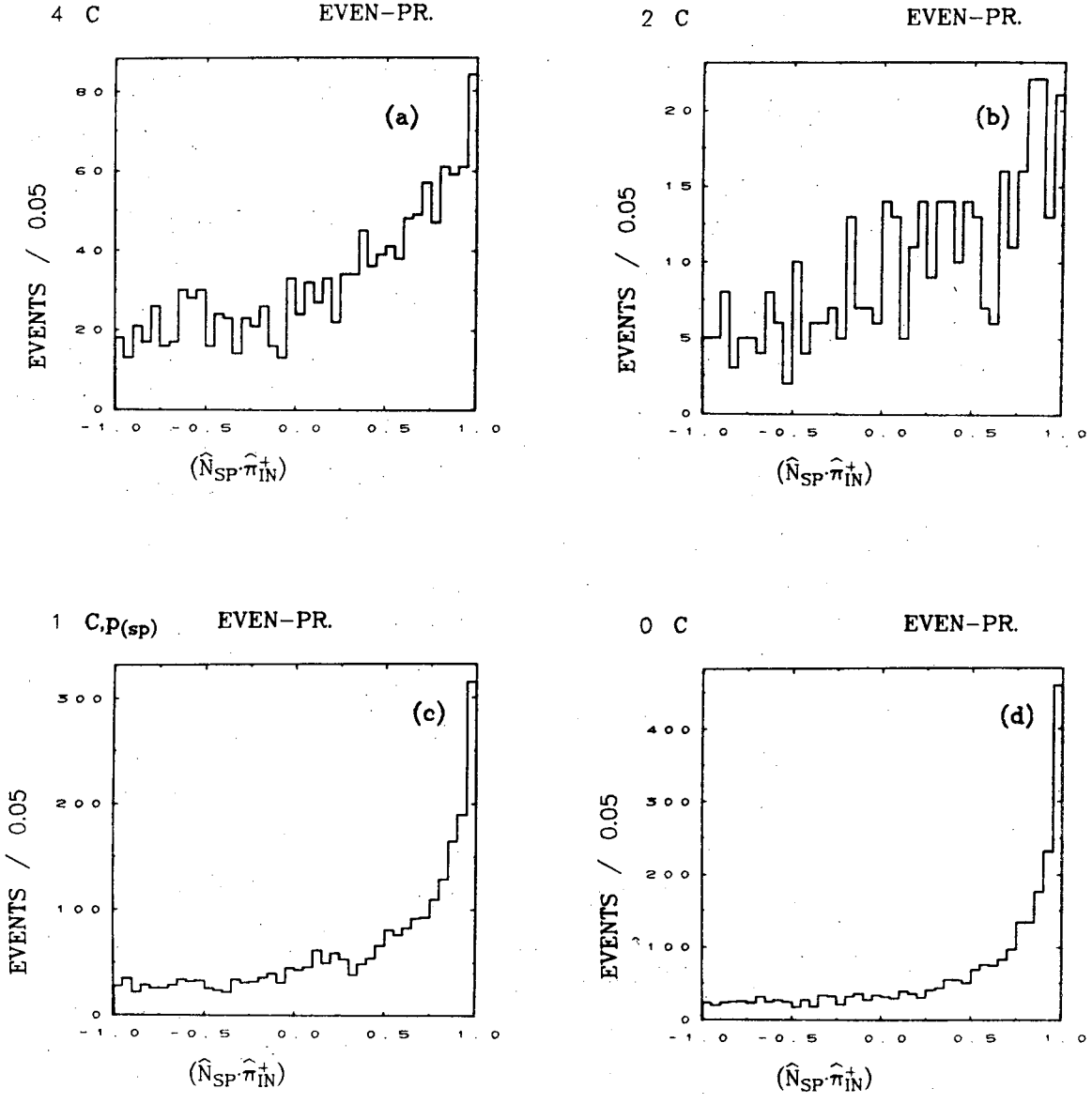

XBL 729-1807

Fig. 2.12

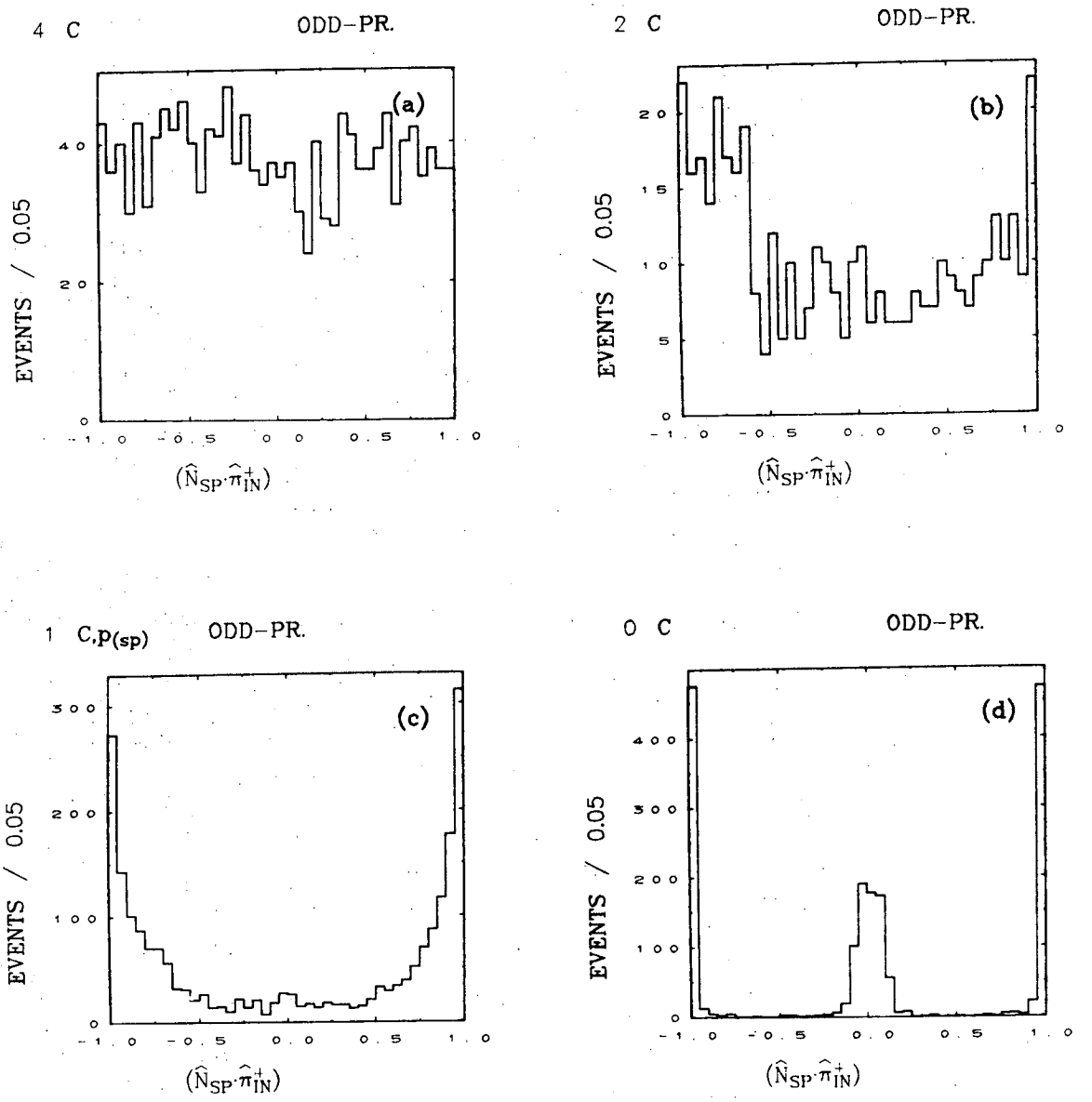

XBL 729-1808

Fig. 2.13

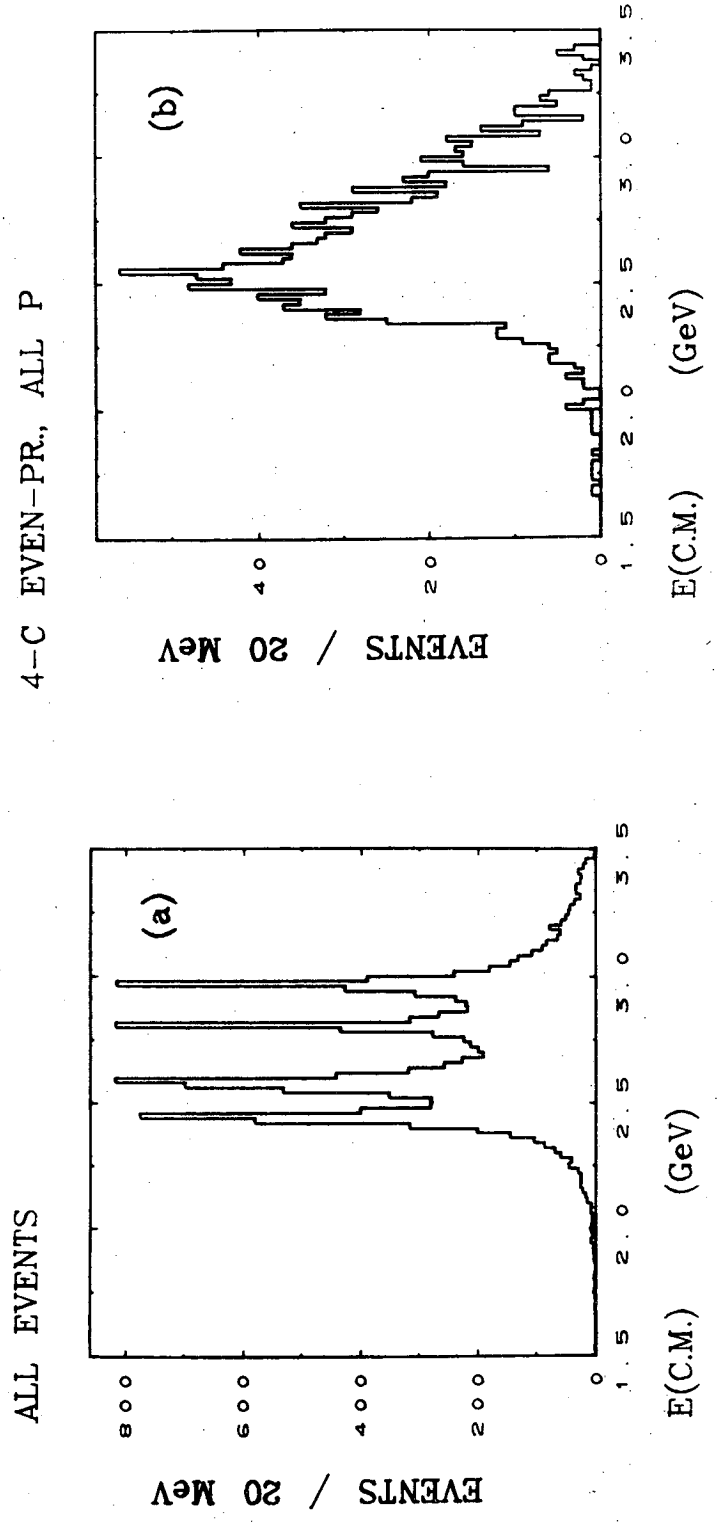

XBL 729-1809

Fig. 2.14

The Fermi motion of the nucleons in the deuteron results in a spread of effective πN c.m. energy for any single beam momentum. The width of that effective c.m. energy spectrum is about 250 MeV at 2 GeV/c[76] and about 400 MeV at 5.2 GeV/c.[77] Thus, our exposure at 2.7 to 4.2 GeV/c (which is 2.4 to 2.9 GeV in $E_{c.m.}$) covers all the intermediate momenta. The effective πN energy (from the fitted momenta) of all our events is given in Figure 2.14(a). For the 4-production-constraint events, this spectrum (Fig. 2.14(b)) does not show the sharp peaks, which come from the less constrained fits where the spectator momentum systematically comes out low, and from events where a nucleon at rest was taken to be the spectator.

We mention in passing some features of the spectator model which we have not taken into account; they are insignificant for the results presented in Chapters 3 and 4. In final states with two protons, there is suppression at small momentum transfer in the non-spin-flip amplitude due to the Pauli exclusion principle. This effect is usually small.[78] The fact that the target nucleon is slightly off the mass shell is generally ignored.[79]

If cross sections are to be calculated precisely, the relative excess of high-momentum spectators in each final state must be considered. (In Section 2.9 we did not remove these events; an alternative approach would be to cut them out and divide up the total number in proportion to the remaining events.) Also, precise cross-section determinations should take note of Glauber screening, the shielding from the beam of one nucleon by the other.

2.11 CONFIDENCE LEVEL DISTRIBUTIONS

The kinematic confidence level distribution for all events (except those outside the fiducial volume or with p_{sp}>300 MeV/c) is given in Figure 2.15(a). If all events have been correctly assigned, and the measurement errors correctly estimated, it should be flat. It is quite flat above 20%, with a strong peak below that point. (The usual cutoff at 0.5% has already been imposed.) There are no noteworthy differences in the shape of this distribution in the corresponding plots for odd- and even-prongs alone, for each constraint class separately, or without the fiducial and spectator cuts imposed.

Figure 2.15(b) presents the kinematic confidence levels of the best and second-best fits. The prominent features of this plot can be easily understood. The many events above the diagonal reflect the fact that we did not always

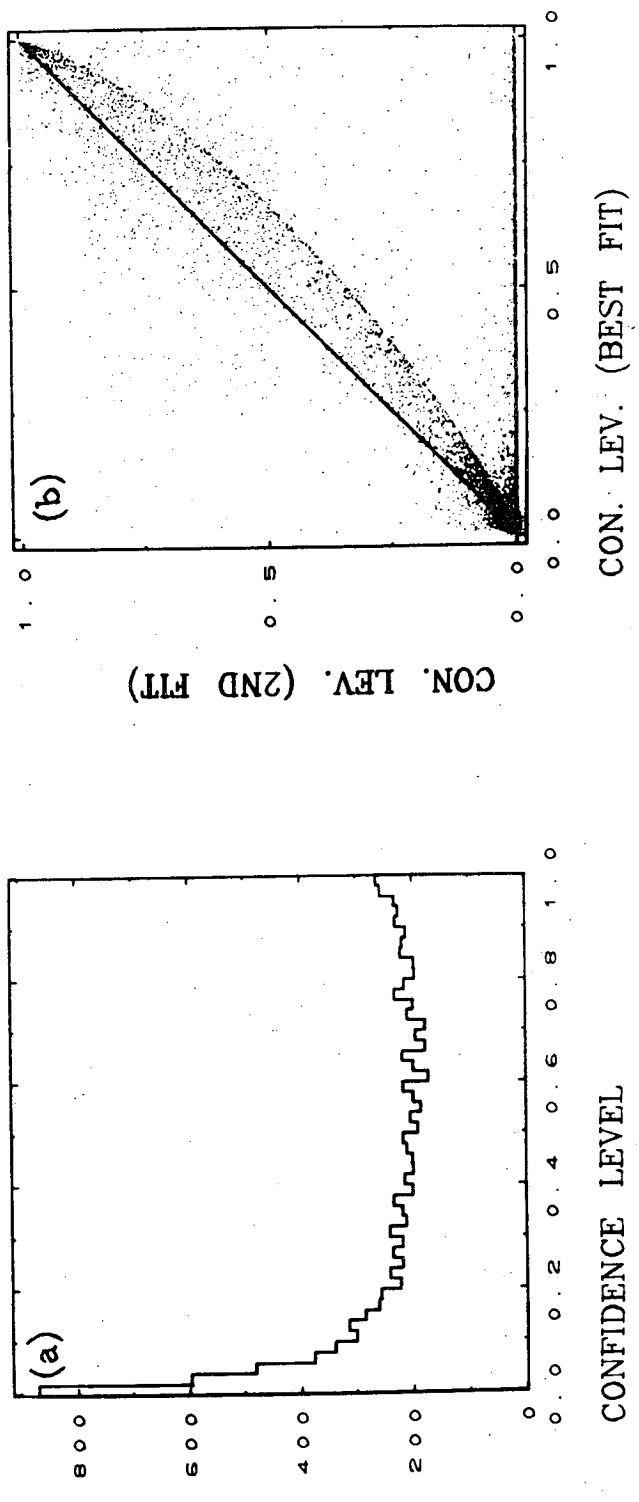
(a)
(b)
EVENTS / 0.02
CONFIDENCE LEVEL
CON. LEV. (2ND FIT)
CON. LEV. (BEST FIT)
XBL 729-1810

Fig. 2.15

assign an event to the hypothesis with the highest confidence level. The events forming the diagonal are mostly missing-mass events; the horizontal line comes from unambiguous events. The curved line comes from events where the best mark is a 1-C fit with a negligible chisquare contribution from the production vertex. (That is, the entire chisquare and all of the total constraints come from the vees.) The second best hypothesis is 0-C; that is, it has the same total chisquare and one fewer constraint (and therefore a lower confidence level).

2.12 SUMMARY

[Please refer to previous sections for the arguments, assumptions, and qualifications behind the results summarized here, for explanation of the figures and tables, and for other details.]

We have studied strange-particle production from 2.7 to 4.2 GeV/c in a $\pi^+ d$ exposure of the 72-inch bubble chamber at the Bevatron. The single-stage separated beam was designed to maximize the separation of π^+ from protons. A triggered "stepper" magnet spread out the beam in the chamber. The average beam momenta (Table 2.1) were used as a second measurement of each beam track.

The path length was calculated directly, from a special scan to determine the number and average length of beam tracks entering the chamber, leaving through the end or the sides, and interacting (Table 2.2). The non-pionic component of the beam affects calculations of cross sections, and may preferentially contaminate certain final states. The proton contamination was estimated to range from ≈10% to ≈25% from spectrometer curves (Fig. 2.1); those estimates are consistent with others in the same exposure or the same beam. The μ^+ contamination was estimated to be ≈10%. The observed total cross sections, calculated from the number of interactions found on the special scan, are consistent with those predicted by this contamination (Table 2.5).

We scanned for the strange-particle topologies shown in Fig. 2.2. Half the film was rescanned and conflict-scanned; our net scanning efficiency is (97 ± 3)%. (We neglect the dependence on topology.) Many apparent events with no real vee were deleted upon re-examination. The events were measured on both the Franckenstein and the Spiral Reader, and were fitted by the standard SIOUX program. Fiducial weights were calculated to take into account events lost because the secondary decay was too far from or too near the primary vertex (Fig. 2.3); the corresponding cuts were defined. Failing events were extensively remeasured. The final status of the ≈20000 events is given in Table 2.6.

Ambiguous events were assigned to the single final state with the lowest value of the badness function B, calculated from the kinematic and ionization χ^2 from the fit (χ^2_K, χ^2_B) and from the number of constraints n:

$$B = (\chi^2_K - F_K) + (\chi^2_B - n_B)/2 + 10*N_{KV} + C_{MM} \quad .$$

The parameters in B were chosen to give appropriate biases in favor of various hypotheses. For example, N_{KV} is the number of vees attributed to $K^0 \rightarrow \pi^+\pi^-$;

the term $10*N_{KV}$ counteracts the tendency of a Λ to fake a K^o. The factor 10 was chosen to make the net Λ and K^o decay distributions as isotropic as possible (Fig. 2.4).

C_{MM} is a correction term to bias against marginally acceptable missing mass hypotheses, and the term $(X^2_B - n_B)$ uses the bubble-density information obtained automatically by the Spiral Reader and compared with the predictions of the fit. Ambiguous events which were potentially resolvable on the basis of track ionization density were looked at in am ambiguity scan.

The bias term $F_K(n_K)$ separates different production constraint classes, and was chosen to make various physical distributions look good. Specifically,

From the distribution of missing mass (Fig. 2.5), we favored 1-C hypotheses (that is, those with one constraint at the production vertex - i.e., one missing neutral particle) over 0-C by a bias in X^2 of 1.5.

2-C (Σ^o) hypotheses are favored over 1-C ($\Lambda\pi^o$) by a bias of 5, chosen on the basis of the distribution of $M^2[\Lambda$ + (missing mass)] (Fig. 2.6).

2-C hypotheses and the corresponding 4-C (Λ) fits were separated on the basis of the decay angle of the (apparent) Σ^o with respect to the normal (Fig. 2.7, 2.8). We chose a bias in favor of the 4-C fit of 15 for even-pronged events, and 7.5 for odd prongs. The difference reflects the fact that the fits with an invisible spectator proton are degraded in quality. The anisotropy of another Σ^o decay angle (Fig. 2.8) and the distribution of $M^2[\Lambda$ + (missing mass)] (Fig. 2.10) shows that the separation was not perfect.

This scheme for the handling of ambiguous events was chosen to provide a sample of each of the many final states in a simple manner: with a relatively small number of parameters to be chosen, without looking at each final state individually, without assigning events to more than one final state, and without using the confidence level (the distribution of which is not known for an incorrect hypothesis). (The final confidence level distribution (Fig. 2.15) is flat above $\approx$20%.) No attempt was made to separate hypotheses with the same number of constraints except on the basis of X^2. (The complexity of that problem is discussed in Appendix B.)

In Tables 2.8 and 2.9, the final states are listed, with the number of events assigned to each. Cross section estimates (Tables 2.10, 2.11) were calculated using these tallies, the π^+ path length, and the visibility factor to take into account the secondary decays observed. These values are to be considered estimates; we have not examined the final states individually. In the final states

which appear with several secondary decays, we see a relative deficiency of two-vee events. (Table 2.12)

To the extent that one nucleon is only a spectator, π^+N interactions can be studied in this π^+d exposure. Odd-pronged events (those with an invisibly slow spectator proton) are handled by the fitting program as if the proton had a measured momentum of zero, with appropriate errors. The resulting distributions of lab spectator momentum (Fig. 2.11) are pulled away from the Hulthén distribution for the less constrained hypotheses. The angle between the fitted spectator and the beam (Fig. 2.12-2.13) departs from the isotropy of the deuteron because of the flux factor effect and correlations introduced by the fitting program. The Fermi momentum within the deuteron results in a spread of π^+N c.m. energies, covering the entire range spanned by the incident momenta. (Fig. 2.14)

APPENDIX A. POSSIBLE D AND E MESON PRODUCTION IN $\pi^+ d \rightarrow pp K_s K_s \pi^0$

One of the few specific purposes of this experiment was to study the D and E mesons in $KK\pi$ final states. The D and the E were found in the LBL $\pi^- p$ experiment (Pi63) at about the same time they were observed in $\bar{p}p$ interactions. Hess suggested a further study in a $\pi^+ d$ exposure around 2.6 GeV/c.[80] The advantage of a $\pi^+ d$ exposure is that it allows a search for D or E $\rightarrow K_s K_s \pi^0$ in the 1-C, 2-vee reaction $\pi^+ d \rightarrow (p) p K_s K_s \pi^0$. If I = 0, this decay mode establishes G = +.

Since 1966, when our experiment was run, the D and E have been studied extensively, especially in $\bar{p}p$ collisions. The quantum numbers $I^G = 0^+$ are now considered well established for both mesons. (See the Particle Data Group compilation for references on their properties and history.[81]) Nonetheless, we felt it would be appropriate to see if we had any data on D and E production.

We assigned only 40 events to the reaction

$$\pi^+ d \rightarrow p p K_s K_s \pi^0$$

As discussed in Section 2.8, the assignment of events is not very reliable for such a 1-production-constraint fit. Thus, we decided to use as a tentative sample all 90 events which had a passing fit to this hypothesis. The $KK\pi$ mass spectrum for these events is given in Figure A1. The shaded events are those for which this final state is called best. The D and E regions (defined as 1280 ± 30 MeV and 1420 ± 70 MeV respectively) are indicated. (The masses and widths are M_D = 1285 MeV, Γ_D = 31 MeV, M_E = 1424 MeV, and Γ_E = 71 MeV.) There is no sign of D or E production. For an upper limit, we note that there are 5 events in the D region, 4 of them having the final state $pp K^0 K^0 \pi^0$ best; there are 15 events in the E region, 11 having this fit called best.

We can estimate the number of D and E events expected by using the cross sections reported by Pi63.[82] These cross sections for D and E production in $K^\pm K^0 \pi^\mp$ are given in Table A1. The table also gives the $\pi^- p$ and $\pi^+ d$ path lengths; the momentum regions denoted as approximately 3 and 4 GeV/c are similar enough for our purposes. The expected number in $\pi^+ d$ is based on the assumption that the mesons have $I^G = 0^+$; if that is the case than the branching ratios are $K^0 K^\pm \pi^\mp / K^0 \bar{K}^0 \pi^0 = 4$ and $K^0 \bar{K}^0 \pi^0 / K_s K_s \pi^0 = 2$.[83] Noting that the probability of a visible decay (vee) is $K_v / K_s = 2/3$ and $K_v / K^0 = 1/3$, we conclude that $K_v K_v \pi^0 / K^0 K^\pm \pi^\mp = 1/18$. The product of this factor and the indicated path lengths and cross sections gives the expected number of events.

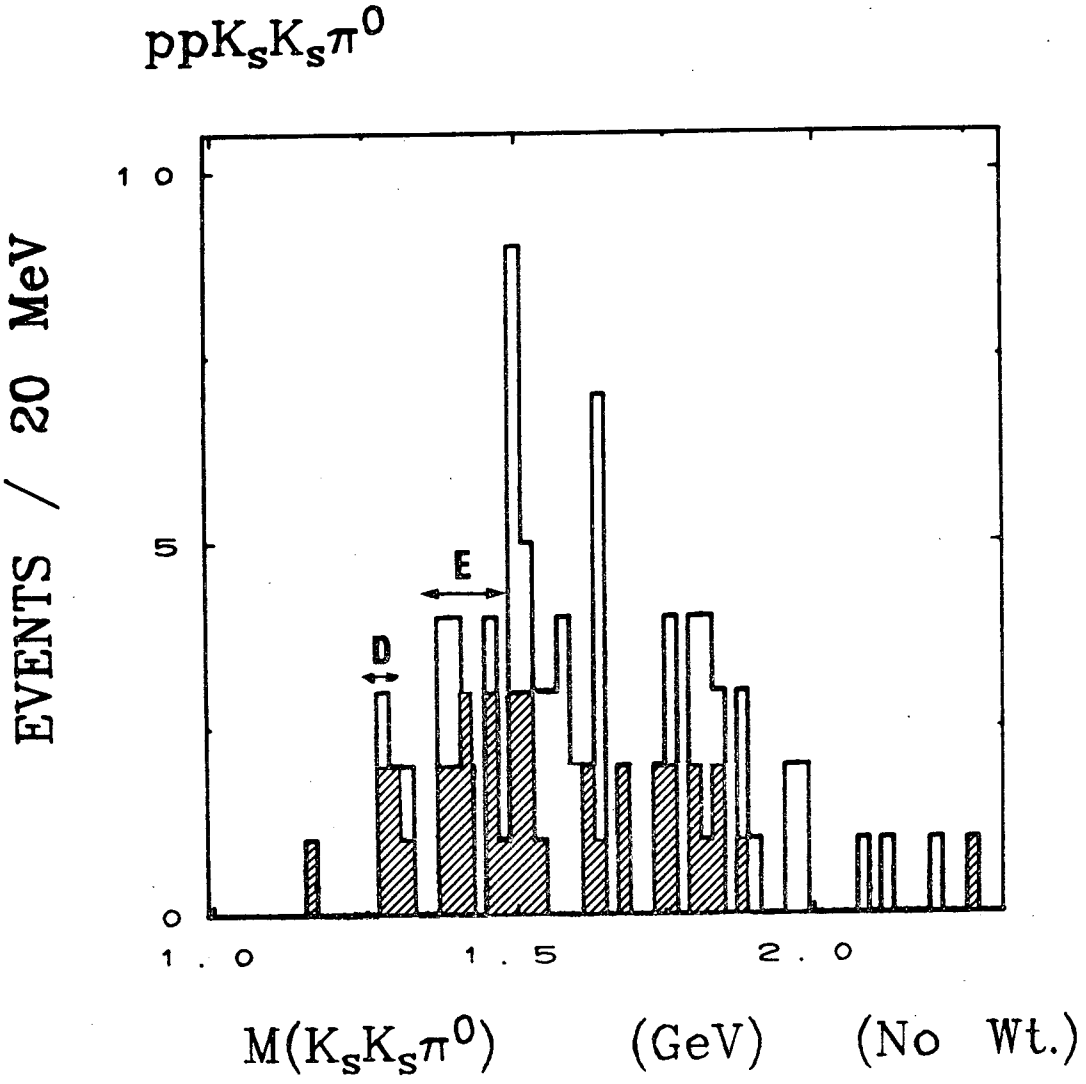

Fig. A1

P_{bm} (GeV/c)	$L(\pi^-p)$ (ev/μb)	$L(\pi^+d)$ (ev/μb)	σ(From π^-p) (μb) D	(μb) E	Expected in π^+d # D	# E
≈3	12.8	10.4 ± 0.6	7 ± 2	17 ± 5	Total (both P_{bm}):	
≈4	5.6	7.6 ± 0.9	10 ± 4	3 ± 2	8.3 ± 2.1	11.1 ± 3.1

D and E Meson Production

Table A1

When this calculation is applied using the $\pi^- p$ path lengths and branching ratios, we predict 49 ± 11 D events and 78 ± 22 E events; Pi63 reported 35 ± 8 D's and 50 ± 10 E's. We have not been able to understand this discrepancy, but it suggests that we should scale down our prediction to only 5.9 D's and 7.1 E's. (The discrepancy may have something to do with weights and cuts.) In any case it is now clear to us that the expected number of events is too small for a study of this decay mode of the D or E; the best that we could have hoped for was establishing the presence of the resonance. We conclude that the mass spectrum in Fig. A1 is not inconsistent with the expected amount of D and E production.

APPENDIX B. A STUDY OF THE CROSS-CONTAMINATION PROBLEM

One of the purposes of this appendix is to illustrate the complexity of the problem of assigning each event to the most probable final state. (Our method was discussed in Section 2.8.) Here we will not examine any physical quantities which reflect the contamination of specific states; rather we discuss the relationships among the final states and make some observations about the pattern of the cross-contamination from a tally of the best and second-best hypotheses.

We restrict ourselves to a discussion of events with one vee and one prong (E.T. 31) or two prongs (E.T. 32). This includes 12021 of the 18362 events in the final sample. Figure B1 is intended to clarify the relationship of the 18 marks (final state hypotheses). The figure is divided into two halves, for Λ and K^o vees. The z axis corresponds to the number of production constraints. At each constraint class level, the location in the x-y plane is determined by the identity of the charged tracks. Thus, hypotheses with pK^+ are depicted on top of each other. Lines have been drawn to indicate the simplest channels for cross-contamination. The wavy lines connect marks with the same vee and charged track assignments but with different missing particles - i.e., different production constraint classes. Among the marks which have the same vee and number of constraints, a solid line indicates a different mass assignment for one of the two prongs. Of course, an event may have any combination of best and second best marks, but it is not surprising that these pathways are the key ones. Even with this restriction to these two paths, it is clear that a typical final state can be expected to lose events to, or gain them from, quite a few different marks. It should be clear that if many events are ambiguous, preparing a clean sample would be a difficult task.

On a copy of this figure, we indicated the number of events in each mark and (from the tally of best vs. second-best mark) the number on each pathway. Several patterns became apparent. First we point out those that were a function of our disambiguation scheme as well as of the behavior of the events. Then we will discuss the ambiguities between different track-mass assignments, which we did not consider in Chapter 2.

First we note that only 1953 of the 12021 events (16%) are unambiguous. In this appendix, "unambiguous" means there was only one fit with a confidence level above 0.5%. [In terms of chisquare, this is a cutoff ranging from 20 for a

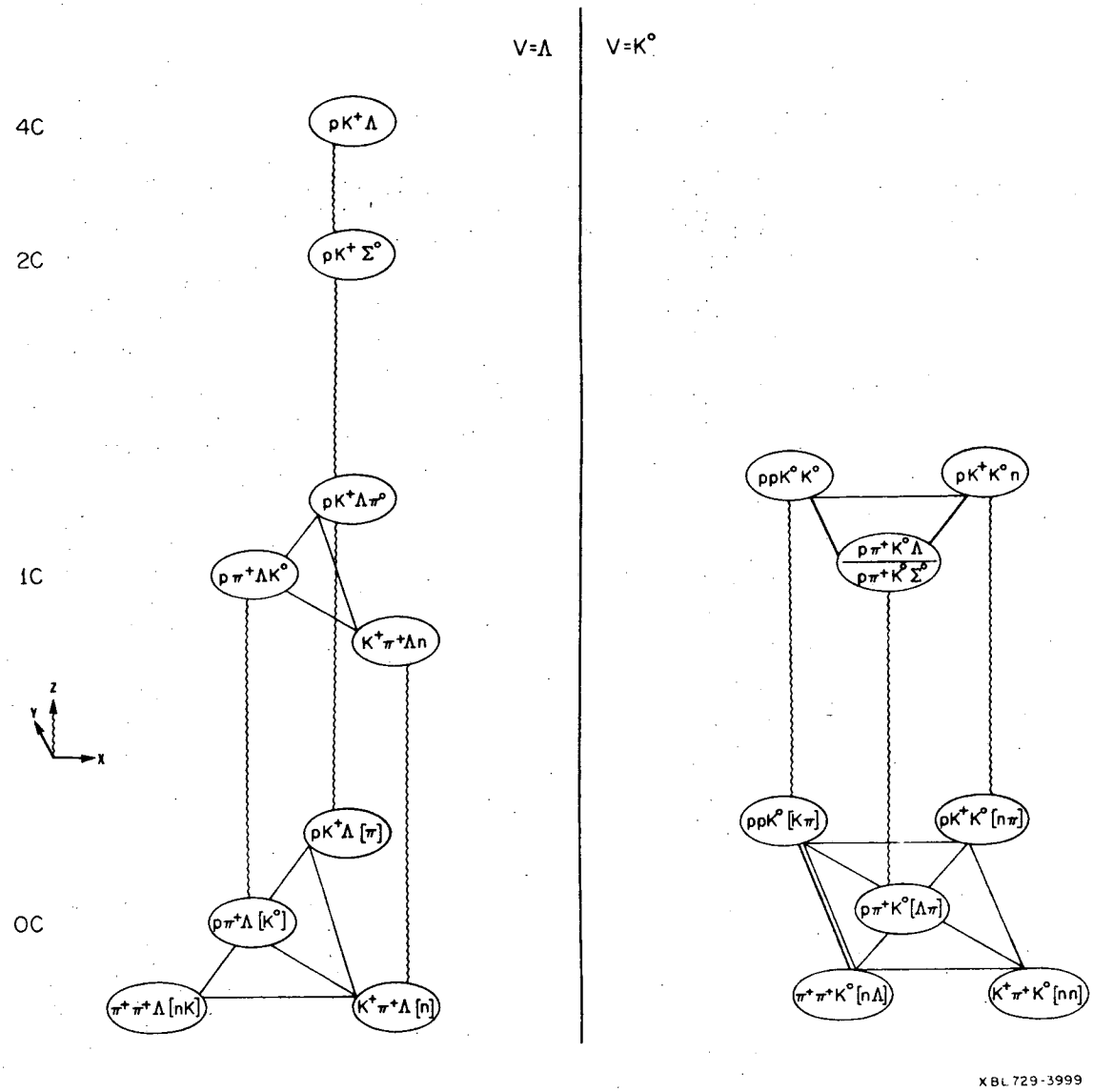
V=Λ
V=K°
4C
2C
1C
0C
pK+Λ
pK+Σ°
pK+Λπ°
pπ+ΛK°
K+π+Λn
pK+Λ[π]
pπ+Λ[K°]
π+π+Λ[nK]
K+π+Λ[n]
ppK°K°
pK+K°n
pπ+K°Λ
pπ+K°Σ°
ppK°[Kπ]
pK+K°[nπ]
pπ+K°[Λπ]
π+π+K°[nΛ]
K+π+K°[nn]
Z
Y
X
XBL 729-3999

Fig. B1

4-production-constraint fit to 13 for a 0-C fit (3-C overall). Since the biases we used in the badness were as large as 15, this is not an unreasonable way to define "ambiguous".]

Table B1 tallies the best and second best vees. Since we introduced a large bias in favor of the Λ hypotheses, it is not surprising that there is a negligible number of events where the best and second best marks have different vees.

Table B2 is a similar tally by constraint class. Note that there are few events where the second best fit has a higher constraint class (except in the 0C-1C case, where the bias was only 1.5.)

Table B3 is a tally of Δ_c, the constraint-class difference between the best two fits, and of Δ_t, the *minimum* number of track-assignment changes. (That is, pK^+ and $p\pi^+$ differ by $\Delta_t = 1$, but both tracks may be different.) We see that with our biases to separate constraint classes, the second best hypothesis is about as likely to be one track-assignment different as one constraint-class different. Sixty percent of the ambiguous events have a track-assignment ambiguity that has been handled only via a chisquare cut.

In the following examination of this track ambiguity, we will for simplicity restrict ourselves to the cases where $\Delta_c = 0$. For each possible track-assignment combination, the fraction of events where the second best mark is the same as the best one is given in Table B4. This "self-ambiguity" can occur without a track-assignment change, from purely kinematic peculiarities; this is the only explanation for the entries with pp or $\pi^+\pi^+$. Since there is only one such event we can infer that almost all of the other entries come from changing both tracks. That is, for example, in the self-ambiguous π^+K^+ events both tracks are switched between π^+ and K^+. We see that the fraction of self-ambiguous events is correlated with the mass difference [$m^2(\pi^+) = 0.02$, $m^2(K^+) = 0.24$, and $m^2(p) = 0.88$]. We conclude that, not surprisingly, a track is relatively likely to be ambiguous between π^+ and K^+ and quite unlikely to be ambiguous between π^+ and p.

This pattern is also reflected in the ambiguities between different marks. Figure B2 gives the number of events by track assignment for all 0C and 1C events. The numbers indicated on the lines are the ambiguous events with $\Delta_c = 0$; the arrow points to the chosen track assignment. Since the $\pi^+\pi^+$ and $K^+\pi^+$ marks appear in the even-prongs only, they are potentially ambiguous only with the even-pronged events in the other hypotheses; the even-prong tallies are in

	2nd Best Fit:				
Best Fit	Λ	K^o	Tot. Amb.	Unamb.	Total
Λ	7547	4	7551	1146	8697
K^o	72	2445	2517	807	3324
Total	7619	2449	10068	1953	12021

Vees in Best and Second-Best Fits

Table B1

	2nd Best:						
Best	0C	1C	2C	4C	Tot. Amb.	Unamb.	Total
0C	4325	816	3	1	5145	1605	6750
1C	2646	1150	15	0	3811	270	4081
2C	116	152	2	77	347	36	383
4C	83	21	660	1	765	42	807
Total	7170	2139	680	79	10068	1953	12021

Constraints of Best and Second-Best Fits

Table B2

	Δ_c				
Δ_t	0	1	2	3	Total
0	473	3329	130	81	4013
1	4950	1015	8	3	5976
2	1	2	0	0	3
Total	5424	4346	138	84	9992

Constraint and Track-Assignment Differences

Table B3

Tracks	Total	Self-ambig.	%
pp or $\pi^+\pi^+$	1255	1	0.1
π^+K^+	2825	387	13.7
K^+p	4844	77	1.6
π^+p	3097	8	0.3
Total	12021	473	3.9

Self-Ambiguous Events

Table B4

L $\leftrightarrow$ H	% L Total	% L Ambig.	#L+#H Total	#L+#H Ambig.	Amb. (%)
$\pi^+ \leftrightarrow K^+$	37%	27%	10216	3346	33%
$K^+ \leftrightarrow p$	72%	53%	9059	1062	12%
$\pi^+ \leftrightarrow p$	58%	70%	11310	287	3%

Track-Permutation Ambiguities

Table B5

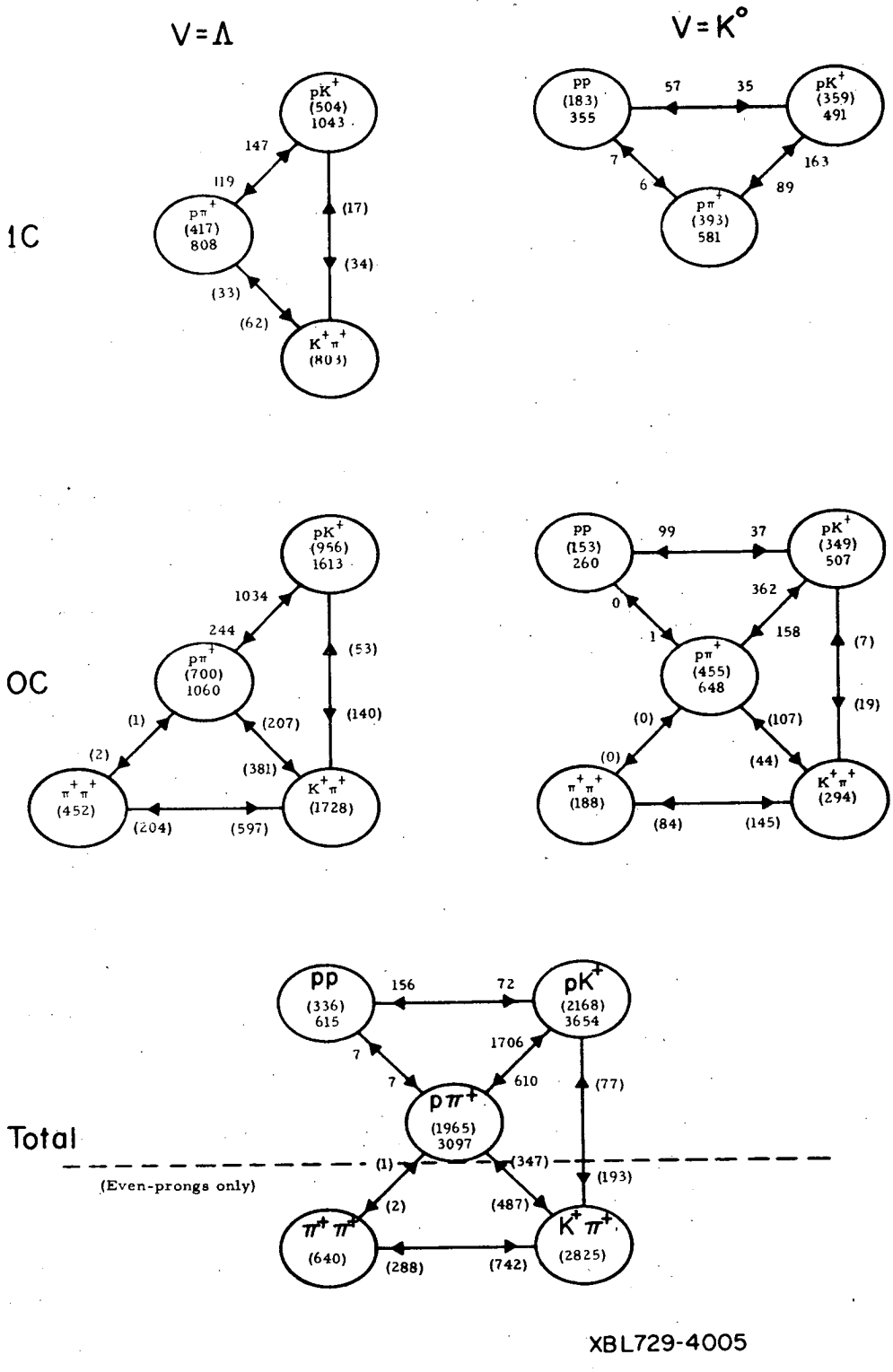
V=Λ
V=K°
1C
OC
Total
(Even-prongs only)
pK+ (504) 1043
pπ+ (417) 808
K+π+ (805)
147
119
(17)
(34)
(33)
(62)
pp (183) 355
pK+ (359) 491
pπ+ (393) 581
57
35
7
6
163
89
pK+ (956) 1613
pπ+ (700) 1060
π+π+ (452)
K+π+ (1728)
1034
244
(53)
(140)
(1)
(207)
(2)
(381)
(204)
(597)
pp (153) 260
pK+ (349) 507
pπ+ (455) 648
π+π+ (188)
K+π+ (294)
99
37
362
0
1
158
(7)
(19)
(0)
(107)
(0)
(44)
(84)
(145)
pp (336) 615
pK+ (2168) 3654
pπ+ (1965) 3097
π+π+ (640)
K+π+ (2825)
156
72
1706
7
7
610
(77)
(1)
(347)
(193)
(2)
(487)
(288)
(742)
XBL729-4005

Fig. B2

parentheses. In Table B5 we present the division of ambiguous events (those with $\Delta_c = 0$ and $\Delta_t = 1$) between the hypotheses containing the lighter (L) rather than the heavier (H) particle. The division is also given for the "total" sample (i.e., events for which a fit to both cases was attempted). The row marked "$\pi \leftrightarrow$ p", for example, is the total of "πp $\leftrightarrow$ pp" and "πK $\leftrightarrow$ pK even-prongs" .We see that for "$\pi \leftrightarrow$ K" only about 1/3 of the events are assigned to the hypothesis containing the lighter particle (the π), both for all events and the $\Delta_c = 0$ ambiguous ones. In the other two cases, the percentage assigned to the lighter particle is larger, and comparable for the total sample and the ambiguous events.

We have also computed the ratio of these ambiguous events to the indicated totals. Here again we see that the $\pi \leftrightarrow$ K ambiguity is most likely and that $\pi \leftrightarrow$ p is very unlikely.

If one wants to include in the disambiguation scheme some way of separating events with the same constraint class (other than by kinematic and ionization chisquares), it would be necessary to understand, or at least incorporate, whatever patterns of this nature appear in the data.

APPENDIX C.
AVAILABILITY OF DATA FROM THIS EXPERIMENT

We have no plans for further study of this data. There are a large number of final states which were examined quickly or not at all. To the degree possible, we would like to make copies of our material available to other experimenters. For the next year or so, we might be able to examine the data to answer specific questions; it would, for example, be very easy to run off some mass plots for a specified final state.

Here we list, in the order of our data processing, the main items (data and programs) that are being kept permanently. "Set" is the name of the information on the Chipstore library PI66LIB.

FILM: 563 rolls, known as Experiment 18.

MEASUREMENTS: Various POOH and PANAL library tapes.

MASTER LIST (Catalog of scanning, measuring, and status): Set PHMLIST.

KINEMATIC RECONSTRUCTION AND FITTING: Program SIOUX,[39,40] Set PHSIOUX.

SIOUX OUTPUT (Data Summary Tapes): Set PLHDST.

FIT-SELECTION AND TRANSFORMATION: Program CREE[45], Set PHCRI.

FINAL DATA TAPES (Arrow output): Set X181271. This can be the input for a data-display program such as KIOWA.

Please address inquiries to the Pi66 Experiment, Attention: Dr. Orin Dahl, Group A, LBL.

ACKNOWLEDGEMENTS

I am especially indebted to my fellow Pi66 graduate students, Jerry Danburg, Don Davies, and Bob Rader. It is a pleasure to thank the physicists on the experiment: Maris Abolins, Orin Dahl, Janos Kirz, and Don Miller. I have used the editorial "we" throughout this thesis, but often the plural refers to work done by, or with, my colleagues.

I wish to thank Ron Ross, Orin Dahl, and John Woodyard for serving on my thesis committee.

The scanning and measuring effort was under the able supervision of experiment coordinator Wally Hendricks and librarians Betty Armstrong, Maureen Nassiri, Meredeth Vogler, and David Blohm.

The progress of this experiment over many years has depended on the assistance of dozens of people: the Bevatron and bubble chamber crews, the Group A and Math and Computing programming staffs, computer operations personnel, and many graduate students and physicists. It is difficult to see how this thesis could ever have been finished without – to select just a few examples – the Math and Computing Group's Red Keyboard system (on which this is typed), or the cheerful service of Brian Noste and the other night-shift computer operators. The many individuals who have gone out of their way to help me know of my appreciation. I am grateful to Ed McMillan, Luis Alvarez, Frank Solmitz, and Art Rosenfeld for leadership, encouragement, and support.

It is a special pleasure (☺) to acknowledge the encouragement, support (moral and otherwise), and diversion provided by V.A., S.S.B., S.M., D.T., M.M., M.T.V., K.C., E.H., and particularly S.R.S.

In my first years of graduate study, support was provided by the National Science Foundation. This work was performed under the auspices of the Atomic Energy Commission.

REFERENCES

1. Purdue:

   (a) J. Gezelter *et al.*, A Search for the ϵ^0 Meson, Nuovo Cimento 53A, 213 (1968).

   (b) R. J. Miller *et al.*, Four-Charged-Particle Final States from the Interaction of 2.7-GeV/c π^+ on Deuterium, Phys. Rev. 178, 2061 (1969).

   (c) A. F. Garfinkel *et al.*, Reaction $\pi^+ n \rightarrow K^+K^-p$ at 2.7 GeV/c, Phys. Rev. 186, 1400 (1969).

   (d) J. H. Campbell *et al.*, Study of $D^0 \rightarrow \pi^\pm\delta^\mp$ and $\delta^\mp \rightarrow \pi^\mp\eta$ in the Reaction $\pi^\pm d \rightarrow p_s p D^0$ at 2.7 GeV/c, Phys. Rev. Letters 22, 1204 (1969).

   (e) D. H. Miller *et al.*, Confirmation of an Enhancement in the $\pi^-\pi^+$ System at M = 1.05 GeV, Phys. Letters 28B, 51 (1968).

   Illinois:

   (f) G. S. Abrams, B. Eisenstein, and H. Gordon, Omega Production in $\pi^+ d \rightarrow \pi^+\pi^-\pi^0 pp$ at 4.19 GeV/c, Phys. Rev. Letters 23, 673 (1969).

   (g) B. Eisenstein and H. Gordon, Features of the Reaction $\pi^+ d \rightarrow \pi^+ d\pi^+\pi^-$ at 4.2 GeV/c, Phys. Rev. D1, 841 (1970).

   (h) B. Eisenstein and H. Gordon, Backward f^0 Production in $\pi^+ d \rightarrow pp\pi^+\pi^-$ at 4.19 GeV/c, Univ. of Illinois Report COO-1195-194 (1970).

2. R. J. Miller (Ph. D. thesis), Purdue Univ. (1969). (Published version: Ref. 1b.)

3. John H. Campbell (Ph. D. thesis), Purdue Univ. (1969). (Published version: Ref. 1d.)

4. Howard A. Gordon (Ph. D. thesis), Univ. of Illinois Report COO-1195-179 (1970).

5. (a) Donald W. Davies *et al.*, Strange-Particle Production in $\pi^+ d$ Interactions from 1.1 to 2.4 GeV/c, Phys. Rev. D2, 506 (1970). (Based on Davies' thesis, Ref. 6.)

   (b) Donald W. Davies *et al.*, Σ^+ Polarization in $\pi^+ n \rightarrow K^0\Sigma^+$ from 1.1 to 2.4 GeV/c, (to be submitted to the Comments and Addenda section of Phys. Rev. D).

6. Donald W. Davies (Ph. D. thesis), LBL Report UCRL-19263 (1969). (Published version: Ref. 5a.)

7. (a) Jerome S. Danburg *et al.*, Evidence Against an I=5/2 Baryon Resonance of Mass 1640 MeV/c^2, Phys. Rev. Letters 23, 41 (1969).

   (b) $\pi^+ n \rightarrow \eta p$: A Regge Parametrization Over a Large Energy Range Using

Veneziano-Type Residue Functions, Phys. Letters 30B, 270 (1969).

(c) Jerome S. Danburg *et al.*, Production and Decay of η and ω Mesons in the Reaction $\pi^+ d \rightarrow (p)p\pi^+\pi^-\pi^0$ between 1.1 and 2.4 GeV/c, Phys. Rev. D2, 2564 (1970). (Based on Danburg's thesis, Ref. 8.)

(d) Robert K. Rader *et al.*, η' Production in $\pi^+ d$ Interactions from Threshold to 2.4 GeV/c, (based on Rader's thesis, Ref. 9; to be published in Phys. Rev. D).

(e) G. A. Smith and R. J. Manning, Search for a $2\pi^0$ Resonance Near 730 MeV in $\pi^+ d$ Interactions, Phys. Rev. 171, 1399 (1968).

(f) G. A. Smith and R. J. Manning, $\pi^0\pi^0$ Mass Spectrum and δ_0^0 Below 1 GeV, Phys. Rev. Letters 23, 335 (1969).

8. Jerome S. Danburg (Ph. D. thesis), LBL Report UCRL-19275 (1969). (Published version: Ref. 7c.)
9. Robert K. Rader (Ph. D. thesis), LBL Report UCRL-19431 (1969). (Version to be published: Ref. 7d.)
9A. Robert J. Manning (Ph. D. thesis), LBL Report UCRL-19339 (1969).
10. Richard I. Hess (Ph. D. thesis), LBL Report UCRL-16832 (1966). (Published version: Ref. 67.)
11. Ref. 3 (Campbell thesis), p. 4.
12. (a) W. Chinowsky, G. Smith, and J. Kirz, Bevatron Secondary Beam 1B, in Bevatron Experimenters' Handbook, Sec. C, 1965 [LBL report (unpublished)].
(b) Ref. 4 (Gordon thesis), p. 2.
13. Jerry Danburg, private communication.
14. Ref. 3 (Campbell thesis), p. 10.
15. Ref. 2 (Miller thesis), p. 12.
16. Ref. 4 (Gordon thesis), p. 13.
17. Janos Kirz, Cross Section Measurement in Bubble Chambers, LBL Group A Memo 640 (1968). For the application of this procedure to our low-momentum exposure, see Appendix A of Danburg's thesis, Ref. 8.
18. Maris Abolins *et al.*, Pi66 Scan Instructions, LBL Group A Memo 586 (1966). The scan volume extended from rake 0 to rake 15. (See p. 8.)
19. Ref. 8 (Danburg thesis), p. 129.
20. Ref. 8 (Danburg thesis), p. 130.
21. Ref. 3 (Campbell thesis), pp. 29-32.
22. Ref. 4 (Gordon thesis), p. 36.
23. Howard Gordon (Illinois), private communication.

24. W. F. Baker *et al.*, in 'Proceedings of the Sienna International Conference on Elementary Particles (1963),' p. 634.
25. D. V. Bugg *et al.*, Phys. Rev. 146, 980 (1966).
26. David G. Brown (Ph. D. thesis), LBL Report UCRL-18254 (1968).
27. Ref. 4 (Gordon thesis), p. 23.
28. Private communication: unpublished memo from Purdue.
29. Ref. 26 (Brown thesis), p. 5.
30. Ref. 8 (Danburg thesis), p. 137.
31. Ref. 6 (Davies thesis), p. 5.
32. J. D. Hansen *et al.*, Compilation of Cross Sections. I - Proton Induced Reactions, CERN Report CERN/HERA 70-2 (1970); E. Flaminio *et al.*, Compilation of Cross Sections. IV - π^+ Induced Reactions, CERN Report CERN/HERA 70-5 (1970).
33. J. Gezelter *et al.*, Nuovo Cimento 53A, 213 (1968).
34. O. I. Dahl *et al.*, Phys. Rev. 163, 1377 (1967), p. 1385.
35. Ref. 8 (Danburg thesis), p. 90.
36. Ref. 6 (Davies thesis), p. 7.
37. Denyse Mettel (Ph. D. thesis), Paris Report C.N.R.S.-A.O.4164 (1970), p. 48.
38. Bob Rader, LBL Group A Memo 677 (1968). See also Gerry Lynch, The Accuracy of the Spiral Reader, LBL Group A Memo 575 (1965).
39. F. T. Solmitz, A. D. Johnson, and T. B. Day, Three View Geometry Program [TVGP], LBL Group A Programming Note P-117 (1967).
40. O. I. Dahl *et al.*, SQUAW - Kinematic Fitting Program, LBL Group A Programming Note P-126 (1968).
41. Paul Hoch, LBL Group A Memo 616 (1967).
42. Ref. 4 (Gordon thesis), p. 16.
43. J. S. Danburg and G. R. Lynch, Group A Programming Note P-160 (1967).
44. For a detailed description of a determination of this kind, see Ref. 4 (Gordon thesis), p. 9.
45. Orin Dahl and Don Davies, LBL Group A Programming Note P-154 (1966).
46. The formula is given in Ref. 6 (Davies thesis), p. 9.
47. The values of these cutoffs and the fiducial volume boundaries can be found in the subroutine FIDWT in the program CREE.
48. Ref. 6 (Davies thesis), p. 7.
49. Stanley L. Klein (Ph. D. thesis), LBL Report UCRL-18306 (1968), App. A.
50. J. Lynch *et al.*, Phys. Letters 35B, 457 (1971).

51. See Ref. 6 (Davies thesis), p. 9.
52. Daniel M. Siegel (Ph. D. thesis), LBL Report UCRL-18041 (1967).
53. Ref. 3 (Campbell thesis), pp. 14 ff.
54. Ref. 49 (Klein thesis), p. 7.
55. Don Davies, private communication. See the subroutine SPBIAS of CREE.
56. E. Burns and D. Drijard, PHONY, LBL Trilling-Goldhaber Group Technical Note 143 (1968).
57. Don Davies, private communication.
58. J. S. Danburg and G. R. Lynch, LBL Group A Programming Note P-160 (1967).
59. Ref. 49 (Klein thesis), p. 9.
60. Lyndon M. Hardy (Ph. D. thesis), LBL Report UCRL-16788 (1966). (Published version: Ref. 67.)
61. W. Ralph Butler (Ph. D. thesis), LBL Report UCRL-19845 (1970).
62. See Section 2.10.
63. Ref. 6 (Davies thesis), p. 13.
64. For examples of how such reflections can be dealt with, see Ref. 8 (Danburg thesis), pp. 12 ff., and Ref. 4 (Gordon thesis), pp. 28-31.
65. Cf. Ref. 8 (Danburg thesis), pp. 33 ff.
66. The exact values used, respectively (0.640 ± 0.007) and (0.3435 ± 0.0025), were taken from the Particle Data Group Review of Particle Properties, LBL Report UCRL-8030 (now LBL-100).
67. Orin I. Dahl *et al.*, Phys. Rev. 163, 1377 (1967). See Table VII.
68. B. Musgrave, in 'Phenomenology in Particle Physics 1971,' (Cal. Tech.), p. 467.
69. G. C. Benson (Ph. D. thesis), University of Michigan Report COO-1112-4 (1966).
70. See, for example, Ref. 8 (Danburg thesis), pp. 18 ff.
71. Ref. 37 (Mettel thesis), p. 20.
72. See, e.g., Nathan W. Dean, Phys. Rev. Letters 27, 276 (1971).
73. As noted in Section 2.84, in our low-momentum $\pi^+ d$ exposure Davies attempted to improve the disambiguation by introducing a bias (a constant term in the badness) against hypotheses in which there was no candidate for a spectator nucleon with p<250 MeV/c. We did not apply such a bias in our data.
74. R. Rader *et al.*, to be published in Phys. Rev. D.

75. For a more detailed discussion, see (e.g.) Ref. 8 (Danburg thesis), pp. 26 ff.

76. Ref. 8 (Danburg thesis), p. 32.

77. Ref. 37 (Mettel thesis), p. 19.

78. See (e.g.) Ref. 8 (Danburg thesis), p. 36.

79. See Ref. 69 (Benson thesis), p. 13, and ref. 9 (Rader thesis), p. 25.

80. Ref. 10 (Hess thesis), p. 68.

81. Particle Data Group Review of Particle Properties, LBL Report LBL-100.

82. Ref. 67, p. 1416.

83. N. Barash *et al.*, Phys. Rev. 156, 1399 (1967), p. 1403.

84-90. These numbers were not used.

FIGURE AND TABLE CAPTIONS

TECHNICAL INFORMATION DIVISION
LAWRENCE BERKELEY LABORATORY
UNIVERSITY OF CALIFORNIA
BERKELEY, CALIFORNIA 94720